Università degli Studi di Firenze
Scuola di Ingegneria
DIEF - Department of Industrial Engineering of Florence

PhD School: *Energetica e Tecnologie Industriali ed Ambientali Innovative*
Scientific Area: ING-IND/08 - *Macchine a Fluido*

Multiphysics and multiscale numerical tool optimization for wall temperature prediction of gas turbine combustor liners

PhD Candidate: Ing. Alberto Amerini

Tutor: Prof. Ing. Bruno Facchini

CoTutor: Dr. Ing. Antonio Andreini

PhD School Coordinator: Prof. Ing. Giovanni Ferrara

XXXV PhD School Cycle - 2019-2022

Alla mia famiglia.

Ad Alessandra.

Acknowledgements

Prima di lasciarvi alla lettura della tesi vorrei ringrazionare tutte quelle persone che hanno reso possibile il raggiungimento di questo risultato.
Ci tengo particolarmente a ringraziare il Prof. Ing. Bruno Facchini per l'incredibile opportunità di crescità professionale e personale che mi ha concesso. All'inizio del mio percorso universitaro tutto avrei immaginato tranne che fare il dottorato di ricerca ma durante il percorso di studi mi ha prima fatto conoscere le turbine a gas e successivamente lo scambio termico, facendomi scoprire qualcosa di cui, ora come ora, non riuscirei a fare a meno.

L'altra persona senza la quale questo traguardo non sarebbe stato possibile è il Prof. Ing. Antonio Andreini che mi ha avviato alle tematiche numeriche, mi ha contagiato con la sua passione ed incredibile preparazione. Si è sempre dimostrato disponibile nei miei confronti fornendomi consigli e spunti di riflessione per completare al meglio il mio percorso.

Vorrei ringraziare tutte le persone coinvolte nel progetto ACROSS ed in particolar modo l'Ing. Ennio Spano sotto la cui supervisione ho avuto modo di allargare i miei orizzonti professionali interfacciandomi con una realtà enorme come quella di Avio Aero.

Infine vorrei ringraziare tutti i membri dell HTC-Group, è stato un onore poter collaborare con così tanti colleghi competenti e trasformare la stima professionale in una sincera amicizia.

Abstract

Despite the accurate prediction of heat fluxes and thus metal wall temperatures of gas turbine (GT) combustor liners is a complicated and numerically expensive task, the Computational Fluid Dynamic (CFD) support for the design of cooling systems is essential to ensure safe and proper operation of the entire gas turbine engine. In fact, it is well known how complicated and costly it is to conduct experimental campaigns inside combustion chamber operating under working conditions. The high operating pressures and temperatures coupled with the reactive environment that forms within them makes their instrumentation very complicated. When available, the data are often reduced to a few thermocouples at strategic points in the burner, which do not allow for a complete thermal characterization of the metal liners containing the flame.

The correct prediction of thermal fluxes in a CFD simulation depends on the proper modeling of all the involved phenomena and their interaction with each other. For this reason, Conjugate Heat Transfer (CHT) simulations are mandatory in gas turbine cooling system applications.

Multiphysics and scale-resolved simulations based on loosely-coupled approaches have emerged as extremely effective numerical tools as they provide enormous computational time savings as compared with standard CHT simulations. The fundamental advantage of such approaches is based on the fact that each heat transfer mechanism is solved with the most suitable numerical setup, which leads to the use of spatial and temporal resolutions following the characteristic time scales of each phenomenon to be solved.

For industrial applications, where the availability of numerical resources is limited and, at the same time, the timelines with which to obtain results are rather tight having robust and easy-to-use loosely-coupled solutions available for the design of combustion chamber cooling systems would be extremely valuable. In this context, the objective of this work is to perform an optimization for the multiphysics and multiscale tool U-THERM3D developed within the University of Florence, to revise the coupling strategy workflow to make the numerical tool faster and easier to use. A review of the data exchange management between different solvers will be carried out to reduce the time associated with these operations. To maintain the tool as flexible as possible, the interactions between the different heat transfer mechanisms and their management will be carried out in a modular way. Specifically, after an initial review and preliminary validation of the new optimized methodology on a simplified case study, the problem will be divided into two parts to focus on different heat transfer mechanisms.

The first part of the work focused on the application of the new management for the interaction between convective and conductive heat fluxes to carry out further validation of the simplified methodology and eventually be able to use the new tool in a stand-alone manner. The revised methodology is applied to the RSM gas turbine combustor model test case developed by the cooperation between the Universities of Darmstadt, Heidelberg, Karlsruhe, and the DLR. The test point of the effusion-cooled RSM combustor operating with a partially premixed flame was investigated with different high-fidelity numerical approaches. In the work, it emerged how moving from hybrid RANS/LES numerical approaches, which currently represent the state-of-the-art for gas turbine combustor industrial applications, to full-LES methods leads to better prediction of wall temperatures. The newly obtained results are compared and analyzed, both qualitatively and in terms of computational time savings, with those previously achieved with the current version of the U-THERM3D tool. Moreover, a calculation time analysis was carried out to quantify the savings achieved by the new proposed methodology for the loosely-coupled

CHT framework.

The radiative heat flux contribution and its management within the multiphysics tool were studied on a dedicated test case. For this second part of the activity, an academic Rich-Quench-Lean (RQL) combustor model is chosen to be studied with high-fidelity loosely-coupled CHT simulation. The sooting flame with which the burner is operated makes the prediction of radiative heat load a key aspect for the correct estimation of wall temperatures. For the new radiative thermal load management, the approach used in the U-THERM3d framework was retained but a reduced coupling frequency was used. Based on the results of the first part of the work, the simulation with the new loosely-coupled workflow was carried out directly with an LES approach. Comparison of numerical results with experimental data shows how a multiphysics, multiscale approach is necessary for the correct estimation of thermal loads on the walls of a gas turbine combustor. Again, the computational cost analysis allows for the quantification of the savings compared to the starting U-THERM3D framework.

Contents

Nomenclature

Acronyms

ACARE	Advisory Council for Aeronautics Research in Europe
CAEP	Committee on Aviation Environmental Protection
CFD	Computational Fluid Dynamics
CHT	Conjugate Heat Transfer
DES	Detached Eddy Simulation
DLR	Deutsches Zentrum für Luft-und Raumfahrt
FGM	Flamelet Generated Manifold
FIRST	Fuel Injector Research for Sustainable Transport
HTC	Heat Transfer Coefficient
ICAO	International Civil Aviation Organization
IRZ	Inner Recirculation Zone
LES	Large Eddy Simulation
LII	Laser-Induced Incandescence
OPR	Overall Pressure Ratio
ORZ	Outer Recirculation Zone
PAH	Polycyclic Aromatic Hydrocarbon
PDF	Probability Density Function

PID	Proportional-Integral-Derivative
PIV	Particle Image Velocimetry
$RANS$	Reynolds Averaged Navier Stokes
RMS	Root Mean Square
RQL	Rich-Quench-Lean
RR	Reaction Rate
RSM	Reaktive Strömungen und Messtechnik
RTE	Radiative Transfer Equation
$SBES$	Stress-Blended Eddy Simulation
$SIMPLEC$	Semi Implicit Method for Pressure Linked Equations-Consistent
SN	Swirl Number
SST	Shear Stress Transport
STS	Solid Time Step
$SV-CARS$	Shifted Vibrational Coherent Anti-stokes Raman Scattering
TBC	Thermal Barrier Coating
TIT	Turbine Inlet Temperature
TKE	Turbulent Kinetic Energy

Greeks

α	Absorptivity	$[-]$
α	Injection Angle	$[deg]$
α	Thermal diffusivity	$[m^2 s^{-1}]$
δ	Thermal Flame Thickness	$[m]$
ϵ	Emissivity	$[-]$
ϵ	Turbulence eddy dissipation	$[m^2 s^{-3}]$
η	Effectiveness	$[-]$
θ	Zenith Angle	$[rad]$
κ	Absorption Coefficient	$[-]$
λ	Wavelength	$[-]$
μ	Dynamic viscosity	$[kgm^{-1}s^{-1}]$

ν	Kinematic viscosity	$[m^2 s^{-1}]$
ρ	Density	$[kgm^{-3}]$
ρ	Reflectivity	$[-]$
σ	Stefan-Boltzmann constant	$[-]$
σ	Scattering coefficient	$[-]$
τ	Time Scale	$[s]$
τ	Transmissivity	$[-]$
ϕ	Azimuthal Angle	$[rad]$
χ_{st}	Scalar Dissipation Rate	$[s^{-1}]$
ω	Solid Angle	$[sr]$
ω	Turbulence eddy frequency	$[s^{-1}]$
Δ	Gradient	$[-]$
Φ	Equivalence Ratio	$[-]$

Letters

A	Area	$[m^2]$
Bi	Biot Number	$[-]$
c	Speed of light	$[ms^{-1}]$
c	Progress Variable	$[-]$
c_p	Spec. heat capacity at const. P	$[Jkg^{-1}K^{-1}]$
D	Diameter	$[m]$
Da	Damköhler Number	$[-]$
E	Emission Power	$[Wm^{-2}]$
E_a	Activation Energy	$[J]$
Fo	Fourier Number	$[-]$
G	Irradiation	$[Wm^{-2}]$
h	Heat Transfer Coefficient	$[Wm^{-2}K^{-1}]$
I	Intensity of Radiation	$[Wsr^{-1}]$
I	Momentum Flux Ratio	$[-]$
K	Equilibrium Kinetic Constant	$[-]$
k	Thermal Conductivity	$[Wm^{-1}K^{-1}]$
k	Turbulent kinetic energy	$[m^2 s^{-2}]$
Ka	Karlovitz number	$[-]$

L	Hole length	$[m]$
L	Reference length	$[m]$
M	Ratio of modelled and resolved k	$[-]$
$\dot{m}$	Mass flow rate	$[kgs^{-1}]$
Nu	Nusselt number	$[-]$
Pr	Prandtl number	$[-]$
P	Pressure	$[Pa]$
$\dot{q}$	Specific heat flux	$[Wm^{-2}]$
Re	Reynolds number	$[-]$
S_L	Laminar Flame Speed	$[ms^{-1}]$
S_T	Turbulence Flame Speed	$[ms^{-1}]$
s	Direction of the Radiation Beam	$[-]$
T	Temperature	$[K]$
t	Solid thickness	$[m]$
t	Time	$[s]$
$U/V/v$	Velocity	$[ms^{-1}]$
y^+	Non-dimensional wall distance	$[-]$
Z	Mixture Fraction	$[-]$

Subscripts

AD	Adiabatic
air	Air
c	Chemical
c	Coolant
$comb$	Combustion
$cond$	Conductive
$conv$	Convective
eff	Effusion
f	Fluid
f	Forward
$fuel$	Fuel
g	Gas Phase

h	Hole
is	Isentropic
k	Kolmogorov scale
ov	Overall
rad	Radiation
ref	Reference
t	Turbulent
TOT	Total
w	Wall
PIV	Particle Image Velocimetry
∞	Freestream
λ	Wavelength

Introduction

Nowadays, gas turbines are so technologically mature that they are a reference both for energy production applications and for aeroengine systems . Over the years, both the thermal efficiency and specific power of gas turbines have gradually increased due to the possibility of being able to raise the Turbine Inlet Temperature (TIT) and the Overall Pressure Ratio (OPR). This technological advancement has been made possible by continuous development of materials and their thermo-mechanical properties and further improved by cooling systems that allow safe and efficient operation of gas turbines at temperatures even higher than those allowed by materials, as can it be appreciated in Figure 1. This development trend has been made possible by the simultaneous increase in the performance of cooling systems required to balance the higher levels of heat flux on the metal liners of gas turbine combustors [1, 2]. Therefore, despite the increasing thermal stresses to which engines are subjected, they can work safely thanks to the strict control of operating temperatures for which cooling systems have been designed [3, 4].

Especially in propulsion, the development of the cooling system plays a key role in the design of the entire engine. The emission regulations for aircrafts are established by the International Civil Aviation Organisation (ICAO) and its Committee on Aviation Environmental Protection (CAEP). For the new targets set by the Advisory Council for Aeronautical Research in Europe (ACARE) with Flightpath 2050 [6] in reducing noise and pollutant emissions great efforts on new combustion processes are being studied. The emissions produced by engines are the combustion

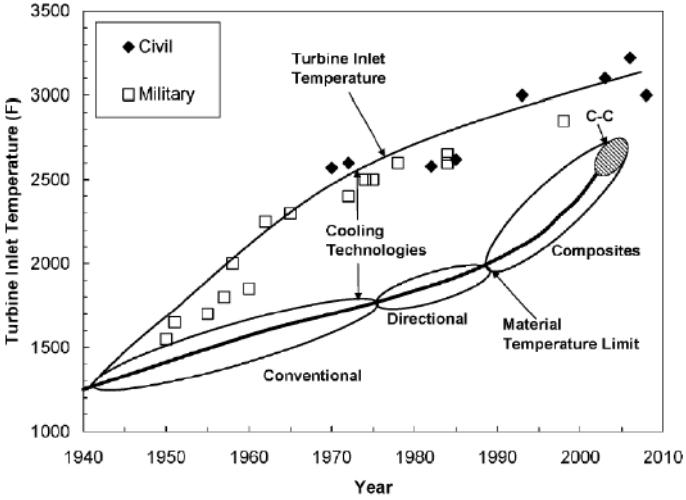

Figure 1: Turbine Inlet Temperature evolution due to the material technology development and cooling systems [5]

products that, as in the case of CO and NO_x, are dependent by the temperatures and the equivalence ratio (Φ) achieved in the combustion chamber, Figure 2. Furthermore, reducing emissions by acting only on temperature would produce a negative effect in terms of cycle efficiency as it would reduce TIT and OPR, so it is easy to understand how complex these issues are.

Several gas turbine combustor architectures have been developed over the years in order to reduce emissions by acting simultaneously on both combustion chamber temperature, residence time and local equivalence ratio values. Since the maximum temperature is achieved in the areas where stoichiometry conditions are reached, the Rich-Quench-Lean (RQL) combustor concept have been developed to reduce the time in which these conditions are actually present. These combustors are characterized by a well-defined oxidation process in the combustion chamber. They present a primary rich zone ($\Phi = 1.2 - 1.6$) in which the chemical reaction is

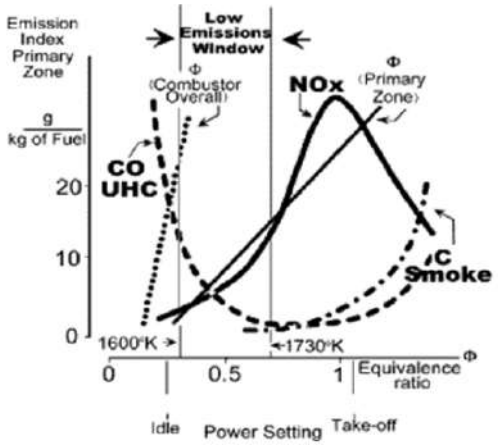

Figure 2: Turbine Inlet Temperature evolution due to the material technology development and cooling systems [7]

promoted, then a large amount of air is injected called "quenching zone" in which the equivalence ratio is rapidly lowered and ending with the third "lean" zone ($\Phi = 0.5 - 0.7$) where the reaction is completed. Although this technology represents the state-of-the-art in aeroengine combustors it has the criticality of a low control over the locally stoichiometric zones that are formed during mixture quenching and consequently on the reduction of NO_x due to thermal peaks.

Gas turbine combustor concepts for lean combustion have been developed in recent years. Compared with the previous ones, there is a strong redistribution of air as shown in Figure 3. In this concepts in fact, the large amount of air is supplied through the injection system to reach a lean combustion process and thus, contain temperature peaks associated with locally stoichiometric zones within the combustion chamber. Although these systems have critical aspects in terms of operability and safety that require further development this technology represents the starting architecture to achieve future legislative emission limits and at the same time even more efficient gas turbine systems.

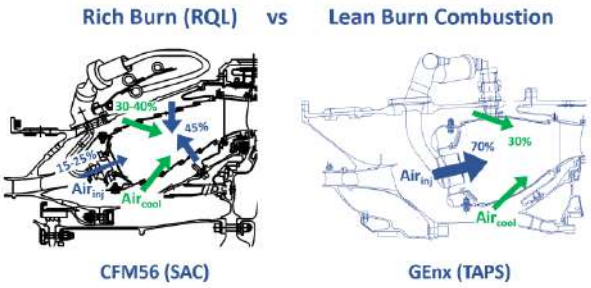

Figure 3: Rich burn (on the left) and lean burn (on the right) combustor concepts. [8]

As visible in Figure 3, the two combustor concepts described above have different availability of cooling air as they have to ensure their own methods of reducing emissions. Moreover, since the development trend is towards lean combustion the air destined for the cooling system is likely to be even less in the future. With this in mind, a cooling system capable of removing large amounts of heat flux with relatively low amounts of available cooling air is mandatory for the proper durability of hot metal components [9].

As a direct consequence, great efforts have been made to study and develop advanced cooling solutions to ensure thermal levels within safe parameters for the metal parts of gas turbine combustors [10]. Over the years, technology based on effusion systems for multi-perforated liners has proven to be the most efficient so as to become the state-of-the-art for combustor cooling [11]. This technique provides a uniform coolant air layer to protect the flame-exposed sides of metal liners together with a non-negligible heat sink effect due to the convective heat transfer related to the passage of coolant air through the holes [12, 13].

In this context the computational fluid dynamics is particularly attractive as it allows to have a complete understanding of the results with a rather low cost compared to the equivalent experimental test. Taking into account the operating conditions of gas turbines combustors, it is

extremely complicated and expensive to carry out experimental tests. For the study and design of effusion cooling systems interesting experimental measurements, although conducted under nonreactive conditions, are those of adiabatic effectiveness capable also to quantifying the effect due to the interaction between swirl flow and coolant coverage [14, 15, 16, 17, 18].

On the other hand, numerical modeling of these cooling systems is computationally expensive since it requires the discretization of a large number of holes with a low length-to-diameter ratio [12], which exponentially increases the number of computational grid elements to be used for a good resolution of the flow fields and turbulence structures. To reduce the computational effort associated with multi-perforated liner simulations, several simplified approaches have been developed to model film cooling injection [19, 20, 21]. In any case, most of the works in the literature are based on the application of uniform velocity and turbulence profiles that do not allow the correct prediction of the jets in cross-flow structure [22, 23, 24]. A more advanced modeling method for effusion cooling holes was proposed by Paccati et al. [25] but, at the moment, the procedure has never been applied for reactive simulations.

Low-fidelity numerical computational methods such a Reynolds-Averaged Navier–Stokes (RANS) simulation can be exploited in the preliminary stages of the combustor design but do not allow accurate solution for heat transfer problems, which are dominated by the turbulent interaction between aerothermal field, combustion, and heat removal due to cooling systems. It should be kept in mind that the flow conditions that are established in gas turbine combustors are highly turbulence-dependent so that for the proper solution of the velocity and turbulent structures a Scale-Resolving numerical approach (SR) is necessary which requires additional computational effort [26, 27, 28, 29, 30]. The recent technological development of super-computing infrastructure has allowed increasing use of Large Eddy Simulation-based approaches (LES) [31, 32], or at least hybrid Detached Eddy Simulation (DES) approaches in which only the unguided flow is solved in an unsteady manner while in near-wall region RANS strategy is adopted [33, 34, 35], which currently represent

the state-of-the-art methods for industrial application.

Moreover, a multiphysics strategy is required in order to take into account the interaction of hot gases with combustor walls and thus the conductive thermal loads. Given the characteristic times associated with the conductive phenomenon and the thermal inertia of solid components, which are significantly higher than those of convective phenomena, simulating conduction with the same time-step adopted for turbulent flows as in standard Conjugate Heat Transfer (CHT) simulations is an extremely computationally onerous solution due to the long thermal transient of metal parts. In contrast, radiative phenomena have extremely low characteristic times scales with respect to other heat transfer mechanisms. From this point of view, loosely-coupled approaches are particularly advantageous as they allow a temporal decoupling between each heat transfer mechanism and thus a desynchronization in time by permitting the most suitable numerical setup to be adopted for the individual modeling and, above all, minimising calculation costs.

Several tools based on loosely-coupled strategy for solving unsteady conjugate heat transfer problems have been proposed in literature [36, 37] and developed specifically for aero-engine combustor applications [38, 39, 40].

Aim of the work

The objective of the present research activity is to perform an optimization of the pre-existing loosely-coupled multiphysics and scale-resolved framework named "U-THERM3D". The tool was developed by Bertini [41] for the accurate prediction of heat fluxes and wall liner temperature inside combustors exploiting the commercial CFD solver ANSYS Fluent [42].

The proposed optimization will focus on managing the interaction between convective, conduction and radiative heat transfer. Starting from the original U-THERM3D, a complete revision of the workflow was carried out for the interaction-logic between the different heat transfer

mechanisms in order to make the tool simpler in its use and suitable for the design of cooling systems for gas turbine combustors for industrial applications and finally, no less important, to reduce the computation time associated for updating operations of coupled interfaces between each solver.

The optimized workflow will be developed and validated on a simplified numerical test case. A second and more thorough validation will be carried out on two different gas turbine combustor model. The first part will focus only on managing the interaction between convective phenomena and conduction heat transfer, will be carried out on an effusion-cooled combustor operated with a swirl stabilized partially premixed flame. The presence of the cooling system makes the validation extremely challenging since the estimation of heat fluxes is totally dependent by the correct prediction of turbulent convective mixing near the liner walls. To assess the impact of numerical turbulence modelling, two different simulations based on the optimised workflow will be performed: for the former a hybrid RANS/LES approach, currently the state of the art in industrial gas turbine applications, will be employed, while the latter will be carried out using a full LES approach.

The second test case has been used to validate the entire optimized workflow of the multiphysics and multiscale framework. Also in this case an academic gas turbine combustor model have been used. The sooting flame with which the burner operates makes the estimation of radiative heat flux essential for the correct assessment of wall temperatures. A Comparison with reference experimental data will be made for both test cases under study for full validation of the numerical procedure, in addition for each of them an assessment of the computational savings achieved with the optimized workflow will be made. The eparate verification of the interactions between the different heat transfer mechanisms was carried out with the aim of keeping the instrument as flexible and robust as possible so that it could be used in different application areas and not only in the field of gas turbines.

Thesis outline

During this research activity, in order to wisely optimize the current workflow of the U-THERM3D numerical framework, a review of the main heat transfer mechanisms within gas turbine combustors was conducted to ensure proper modeling of different phenomena and their interaction with each other. These aspects are mandatory for the robust estimation of heat fluxes and wall temperatures. A large effort was spent on studying the operating principles and coupling management logic between the different solvers of the U-THMER3D tool. After employing the current version of the multiphysics and multiscale framework for the complete understanding of the strengths and critical issues to be improved with optimization, the new workflow was developed. Finally after preliminary validation of the new coupling management between the several involved solvers, the new procedure was applied to two different academic, but well-representative, of gas turbine combustors operating conditions. The optimized numerical procedure was validated with benchmark experimental data and analyzed in terms of computational savings obtained.

The structure of the manuscript is described as follows:

- **Chapter 1**: the principle heat transfer mechanisms present in gas turbine combustors are here described. The purpose of the chapter is to highlight the main characteristics of each, in accordance with the time-scales that characterize them and the parameters to which they are most sensitive, to be able to treat them in the most effective way within the loosely-coupled approach;

- **Chapter 2**: this chapter will focus on the advantages of loosely-coupled approaches for unsteady CHT simulations and provide a description of the U-THERM3D tool, detailing the reference workflow and the different variants previously employed in the literature. The key points to be maintained and the critical aspects of the procedure to be improved through optimisation will be highlighted. The optimised workflow will be presented, the discussion will first focus on a simplified version of the tool that handle only the inter-

action between convection and conduction by carrying out an initial validation on a simplified test case. Subsequently, the radiative heat transfer mechanism will also be included and the preliminary validation will be repeated;

- **Chapter 3**: a simplified version of the optimized tool will be applied for the first time to an academic gas turbine combustor model. In this first numerical application only the interaction between convection and conduction will be taken into account. The main features of the experimental test rig will be provided and all aspects of numerical modelling will be described. All preparatory numerical activities for the use of the baseline U-THERM3D tool will be shown. Finally, the simplified optimized workflow will be employed and a detailed comparison of the results obtained with the several methods will be carried out. After the complete validation of the workflow the computation cost analysis will be performed and the benefits obtained will be highlighted;

- **Chapter 4**: in this chapter, the complete optimised workflow will be applied on a second academic combustor. Also in this case, a detailed description of the experimental apparatus will be provided together with numerical modelling aspects. The numerical evidence obtained on the first test case will be reused here for the simulation with the optimised workflow. The results achieved with the new optimized approach will be compared with those obtained with the baseline tool and the experimental reference data. A comparison of the computational effort of the two approaches will be made to highlight the impact of the radiative heat transfer treatment on the whole multiphysics and multiscale tool procedure for accurate prediction of heat fluxes and wall temperatures;

The last part of the manuscript will summarize the main outcomes of the research activity and provide recommendations for further future development.

Chapter 1

Heat transfer mechanism in gas turbine combustors

The gas turbine combustor is definitely the component subject to the most critical operating conditions of the entire machine. The metal parts of the combustor, in addition to being subject to high operating pressures they are also exposed to high thermal fluxes. Moreover, under normal operating conditions, a reactive environment is established that leads to high thermal gradients and strong instabilities of various kinds, including thermo-acoustic vibrations and additional thermomechanical loads. A Correct heat flux estimation is fundamental to design the cooling system and ensuring proper functioning of the combustor and thus of the entire gas turbine system in terms of working cycle efficiency, durability, cost payback and safety. As already anticipated, the heat fluxes and temperature distributions that are established within the combustion chamber depend on several factors, such as convective phenomena that dominate the flow fields, conduction and radiation that can take a greater impact for specific fuels with high pollutant production during their combustion. To further complete the discussion, the mutual interaction of the different heat transfer mechanisms cannot be neglected as each leads to a change in thermal conditions. Therefore, to take into account all the

aspects just introduced, it is essential to use a multiphysics approach for the correct solution of the conjugate heat transfer problem.

1.1 Conduction

The diffusive process that occurs at the molecular level in a solid by vibration, fluid or in gas by collision, that leads to energy transfer between interacting particles is called *conduction* [43]. The complex submicroscopic mechanisms that are involved during the atomic interaction leads to a heat transfer between the most energized region at high temperature to the region with less energy content and lower temperature. Although conduction also occurs in liquids and gases, in the latter the convective contribution takes on significantly greater weight such that conduction can be neglected in estimating heat fluxes.

For the scale magnitudes achieved in a gas turbine combustor, that is, at the macroscopic level, conduction is characterized by Fourier's law.

$$\vec{q} = -k\nabla T \tag{1.1}$$

The amount of heat exchanged within the solid depends on the thermal gradient ∇T established in the body as well as its thermal conductivity k and the geometry of the body itself. Thermal conductivity is a material property that, when the assumption of homogeneous material is applicable, depends only on temperature. In general, for gas turbine applications this hypothesis is always applicable. After this necessary premise, looking at the Fourier equation it is easy to understand that the amount of thermal energy exchanged is directly proportional to the temperature gradient established within the body. This vector represents the direction in which the temperature grows. Applying the principle of energy conservation to an infinitesimal volume, shown in 1.1 it is possible to derive the conduction equation.

Taking into account only the direction in which heat exchange develops, the energy balance can be expressed as follows to compute the $\dot{q}_G$ terms,

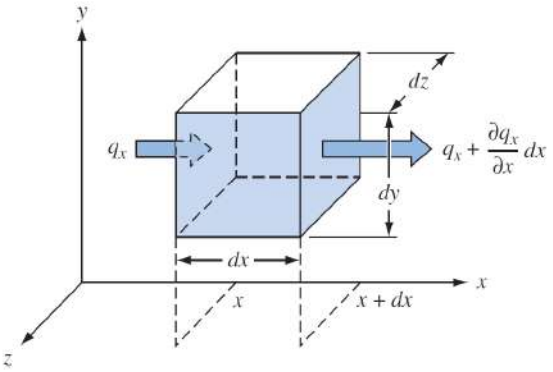

Figure 1.1: Conductive energy balance applied on an elemental volume of material [44].

that represents the energy generation of the unit volume [44]:

$$-kA\frac{\partial T}{\partial x}\bigg|_x + \dot{q}_G A\Delta x = -kA\frac{\partial T}{\partial x}\bigg|_{x+\Delta x} + \rho A\Delta x c\frac{\partial T(x+\Delta x/2,t)}{\partial t} \quad (1.2)$$

The two terms on the left side of the equation represent the heat transferred by conduction inside the volume and the thermal source term within it. While the two right-hand terms are respectively the heat transferred by conduction out of the volume plus the energy gain due to the heat storage. By dividing both members by the control volume and performing some mathematical operations, not showed in the text for the sake of brevity, it is possible to express the conduction equation as follows:

$$k\frac{\partial^2 T}{\partial x^2} + \dot{q}_G = \rho c\frac{\partial T}{\partial t} \quad (1.3)$$

This equation equalizes the increase in internal energy of the volume, on the right side, with the net heat energy exchanged by the solid by conduction and the energy generated within the body itself. This formulation allows the calculation of the one-dimensional temperature distribution along the direction in which heat transfer occurs. Generalizing the problem in three-dimensional space, introducing the α parameter

as the thermal diffusion of the material defined by the ratio of $k/\rho c$ the conduction equation becomes:

$$\frac{\partial^2 T}{\partial x^2} + \frac{\partial^2 T}{\partial y^2} + \frac{\partial^2 T}{\partial z^2} + \frac{\dot{q}_G}{k} = \frac{1}{\alpha}\frac{\partial T}{\partial t} \tag{1.4}$$

Referring now to temperature, time, and distance as dimensionless quantities by dividing each by a reference value T_r, t_r and L_r:

$$\theta = \frac{T}{T_r} \quad \xi = \frac{x}{L_r} \quad \tau = \frac{t}{t_r} \tag{1.5}$$

it is possible to express the previous Equation 1.2 in dimensionless terms:

$$\frac{\partial^2 \theta}{\partial \xi^2} + \frac{\dot{q}_G L_r^2}{k T_r} = \frac{L_r^2}{\alpha t_r}\frac{\partial \theta}{\partial \tau} \tag{1.6}$$

In this form, the *Fourier number Fo* that represents the ratio between the heat transfer rate by conduction and the rate of energy storage in the system, can be recognized as:

$$\mathrm{Fo} = \frac{\alpha t_r}{L_r^2} = \frac{(k/L_r)}{(\rho c L_r/t_r)} \tag{1.7}$$

This number provides an estimate of the rate at which conductive heat transfer occurs, in fact for high values of the Fourier number the thermal transient undergone by the solid is rapid, in contrast, for low Fourier numbers the transient behavior is slower until quasi-steady conditions are reached.

To take into account the mutual influence between conductive and convective heat transfer, that are usually always present inside gas turbine combustors, it is convenient to define another dimensionless quantity: the *Biot number, Bi.* Introducing conductive and convective thermal resistances respectively as $R_k = r_o/k$ and $R_c = 1/\bar{h}_c$ in which the $\bar{h}_c$ term is the mean HTC on the body surface is used, the Biot number can be defined as:

$$\mathrm{Bi} = \frac{R_k}{R_c} = \frac{\bar{h}_c r_\alpha}{k} \tag{1.8}$$

As a consequence when the Biot number is small associated with an extremely low thermal resistance for the solid or, in other words high thermal conductivity, the heat transfer will occur mainly by convection and it will be possible to treat the solid as an isothermal body. Conversely, for cases identified by high Biot numbers, the solid domain will be subject to long and intense thermal transients with respect to the adjacent convective phenomenon.

1.2 Convection

The heat flux exchanged between a generic fluid in motion and a solid surface is governed by convective phenomena and is generated by the flow of the fluid itself. When the movement is caused by the buoyancy phenomenon alone, activated by a density gradient in the fluid, it is called *natural convection*, whereas when the motion is generated by a strong pressure gradient or in general by a mechanical organ, it is defined as forced convection *forced convection* [43, 45].

As already explain in the previous section a fluid can be characterised by being subject to both convective and conductive heat flow, depending respectively on the presence or not of moving particles within it. In any case, conduction in a fluid has a kind of exciting effect on convective phenomena, which will therefore have a much higher intensity and proportion to the fluid's velocity. This heat transfer process can be modelled with *Newton's law of cooling*:

$$q'' = h(T_w - T_\infty) \tag{1.9}$$

where T_w is the surface temperature of the plate and h represents the local heat transfer coefficient, also indicated with HTC, meanwhile the T_∞ is a characteristic temperature of the fluid. In general, there is no unique definition for this quantity, but it is defined as that temperature which is not affected by wall effects.

The HTC is the key parameter to model the convective heat transfer since is influenced by the surface characteristics of the considered plate, by the velocity as well as the fluid properties i.e. dynamic viscosity μ, thermal conductivity λ, density ρ and specific heat c_p. As a consequence, its value is not generally constant, varying from point to point.

Discussing about the fluid velocity, it is important to keep in mind the viscous stresses that occur at the wall due to the non-slip condition. At fluid-solid interfaces, since the fluid is stationary, heat is transferred by conduction. Given thermal gradients and thermal conductivity at the interface, it is possible to apply the previously introduced Fourier's law for

the determination of conductive heat flow at the solid surfaces in which the thermal gradient is still subject to the heat exchange that takes place within the fluid:

$$q'' = -k_{\mathrm{f}} A \left| \frac{\partial T}{\partial y} \right|_{\text{at } y=0} \tag{1.10}$$

By combining the Newton and Fourier equations, it is possible to find a new formulation for the heat transfer coefficient:

$$h = \frac{q''}{T_w - T_f} = -\frac{k(\partial T/\partial y)|_{y=0}}{T_w - T_f} \tag{1.11}$$

In the field of application covered by this research, the case in which the working fluid is in a gaseous state with a high energy content is particularly interesting. In this case, convective heat flux can be expressed as a function of *adiabatic wall temperature* or also called *recovery temperature* (T_{aw}):

$$q'' = h(T_w - T_{aw}) \tag{1.12}$$

This quantity represents the equilibrium temperature reached by the surface absence of heat exchange with the wall [43], generally it's a function of both the properties of the fluid and of the bounding wall.

The dimensionless parameter governing convective heat transfer, the Nusselt number, can be obtained by dimensionalizing the heat transfer coefficient h:

$$Nu = \frac{h\delta}{k} \tag{1.13}$$

where δ is the characteristic length of the investigated system and k is the fluid thermal conductivity. From a physical point of view, this number is defined by the ratio of heat exchanged by convection to heat exchanged by conduction when a temperature gradient is present in the working fluid. Considering a portion layer of height δ of the fluid, the following can be demonstrated:

$$\frac{q_{conv}}{q_{cond}} = \frac{h\Delta T}{k\frac{\Delta T}{\delta}} = \frac{h\delta}{k} = \mathrm{Nu} \tag{1.14}$$

From the above formula, it is easily understood that as the Nusselt number increases, there is also an increase in convective heat flow.

Again, there are several dimensionless parameters with which it is particularly convenient to express the Nusselt number for gas turbine applications: the *Reynolds* and the *Prandtl* numbers defined as follow:

$$\mathrm{Re} = \frac{\text{inertia forces}}{\text{viscous forces}} = \frac{\rho U_\infty \delta}{\mu} \tag{1.15}$$

$$\mathrm{Pr} = \frac{\text{molecular momentum diffusivity}}{\text{thermal diffusivity}} = \frac{\mu c_p}{k} \tag{1.16}$$

The Reynolds number characterises the motion of the fluid by indicating whether it is laminar or turbulent flow through the ratio of inertia and viscous forces. Prandtl's number, on the other hand, gives an indication, from a different perspective to Nusselt's number, of the relative impact of convective compared to conductive heat flow. This number is in fact defined as the ratio of momentum diffusivity to thermal diffusivity.

For heat transfer applications several correlations have been developed for estimating the Nusselt number starting from the Reynolds and Prandtl number, under varying operating conditions, that in general they all assume the following form [46, 47, 48, 49, 50, 51]:

$$Nu = CRe^m Pr^n \tag{1.17}$$

where C, m and n vary according to the flow conditions and the properties of the working fluid.

Particularly interesting for gas turbine combustors is the behaviour of turbulent flows. When the Reynolds number exceeds a critical value, i.e. when the inertia of the flow is much greater than the viscous phenomena, it assumes an irregular and chaotic behaviour characterised by a large number of small coherent vortex structures. These randomly generated three-dimensional flow structures lead to a strong increase in mass, momentum and heat transport phenomena.

The Reynolds decomposition provides an analytical representation of turbulence. From this it is possible to define the instantaneous velocity as

the sum of its average component plus a fluctuation of a stochastic nature responsible for turbulent structures, as shown in the following equation.

$$u_i(\mathrm{x}, t) = \bar{u}_i(\mathrm{x}) + u_i'(\mathrm{x}, t) \tag{1.18}$$

The fluctuating velocity component can be considered in statistical terms as the standard deviation $u_{i,rms}$ of the population sample under investigation. This quantity, along the three dimensions of the flow field development, allows to gives an estimation of the turbulent kinetic energy (TKE) contained in the moving flow.

$$k = \frac{1}{2}\left(u_{x,rms}^2 + u_{y,rms}^2 + u_{z,rms}^2\right) = \frac{3}{2}u_{rms}^2 \tag{1.19}$$

Different sizes of eddies can be found within turbulent flows, in fact, depending on their energy content, they can have a more or less characteristic size. Starting from the largest scales, similar to those of the domain under consideration, the vortices begin to dissipate energy by breaking down from a strongly anisotropic situation to increasingly smaller and isotropic characteristic scales. The process is aided by the sub-inertial range that carries turbulent kinetic energy down to the smaller scales until the eddies are completely dissipated. The largest eddies are called *integral scales* and have a dimension comparable with the characteristic scales of the flow in which are present ($l_0 = o(L), u_0 = o(u_{rms}), \tau_0$) and for this reason are influenced by the boundary conditions. On the other hand, the smallest scales, also known as *Kolmogorov scales* for which the dissipation process takes place, have viscous forces comparable with those of inertia. A key parameter to model the turbulent kinetic energy dissipation is the *turbulent dissipation rate*, ϵ, defined as follow:

$$\epsilon \approx \frac{u_0^3}{l_0} \approx \frac{u_0^2}{\tau_0} \tag{1.20}$$

which shows how turbulent dissipation only depends on integral scales when the equilibrium conditions between turbulent energy transfer and turbulent energy dissipation are satisfied. By substituting in the equation

just defined the relation $k \approx u_0^2$ it is possible to define the integral turbolent length scale as a function of k and ϵ:

$$l_0 \propto \frac{k^{1.5}}{\epsilon} \tag{1.21}$$

From which it is understandable how the lower scales have even smaller characteristic velocity and residence times.

1.3 Combustion

In gas turbines, combustion has the fundamental role of increasing the energy content of the working fluid before it is transformed into mechanical energy by the turbine. Usually the exothermic oxidation reaction takes place between a hydrocarbon-based fuel (C_xH_y) and oxygen O_2 as oxidant produces, together with the reaction products a high energy release in the form of heat and flame brightness. Since the reaction occurs only after molecular mixing has taken place between the reactant species, for liquid fuels the complete evaporation is necessary. The oxidation reaction consists of several elementary reactions with the production of highly reactive intermediate species that promote and accelerate the main reaction. This results in extremely high reaction speeds for which residence times are shorter than those needed to ensure chemical equilibrium is reached and thus complete the main oxidation reaction. As a result, chemical kinetics play a key role in the correct design of gas turbine combustion system.

To estimate the characteristic times of a chemical process, consider the following general reaction:

$$aA + bB \leftrightarrow cC + dD \tag{1.22}$$

The *Rate of Reaction* (or *Reaction Rate*, *RR*) that represents the velocity for which the chemical reaction takes place can be defined as the variation in time of each chemical species. In other words, represents the time required for the reagent to decrease its concentration and simultaneously for the products to increase their concentration [52]. Using the law of mass action, the reaction rate for the reactant species of the previous chemical reaction can be expressed as a function of the reactants concentrations as follows:

$$RR_f = K(T)C_A^{\alpha}C_B^{\beta} \tag{1.23}$$

where K is the temperature-dependent *kinetic constants* of the chemical processes. The effect of temperature on this constant can be modelled

using the Arrhenius equation reported below [53].

$$K(T) = A_f T^{\beta} e^{-\frac{E_a}{RT}} \tag{1.24}$$

The A_f term is called *collision frequency*, the T^{β} with $(0 < \beta < 1)$ it the *Boltzmann factor* meanwhile the E_a is the *activation energy*, which must be provided to the reactants for the reaction to begin.

It has already been mentioned that the chemical reaction only takes place after molecular mixing of the species, i.e. when local stoichiometric conditions are reached. This suggests that the turbulence of the flow in which the reaction takes place has a strong impact on the reaction rate. For laminar flames, mixing only occurs via molecular diffusion, which is why this type of reaction is characterised by low reaction rates. In gas turbine combustors, however, turbulent flames always occur. In these cases, turbulence favours mass transport and thus encourages the transport of fresh reactants to the area where the reaction actually takes place, accelerating the reactive process. Compared to laminar flames, the flame front is distorted by the vortices, generating a greater flame front surface area and promoting mixing.

One of the fundamental parameters for the study and characterisation of premixed flames is the *laminar flame speed*, s_L, that represent the speed of the flame front moves compared to the fresh reagents [54]. The flame front characterised by the the *flame thickness*, δ_L, in which the reaction occurs and moves with the laminar flame speed is called *flame brush*. Whereas the motion of laminar flames is characterised by a direction orthogonal to the flame front, for flames in a turbulent regime this is not the case, for these flames in fact the flame brush is not cohesive and well delineated due to the presence of the eddies that wrinkle the flame front and increase its surface area. As for laminar flames, for turbulent flames it is also possible to define a speed for the flame brush, named *turbulence flame speed*, defined as a function of the laminar flame speed and flame front surface ratio for turbulent and laminar regimes:

$$S_T = S_L \frac{A_T}{A_L} \tag{1.25}$$

The relationship allows to also highlight the direct impact of turbulence, and thus of velocity fluctuations, on turbulent flame speed [55]:

$$\frac{s_T}{s_L} = \frac{A_T}{A} \approx 1 + \frac{u'}{s_L} \tag{1.26}$$

To recognise the different regimes of turbulent premixed flames and thus be able to carry out a careful analysis of characteristic time scales it is convenient to introduce two fundamental dimensionless parameters the *Damköhler* and the *Karlovitz* numbers that allow a comparison of turbulent and chemical characteristic scales. The former is employed for large turbulent length scales and is defined as the integral time scale to chemical time scale ratio, meanwhile the second it's used for the smallest eddies and it's a sort of inverse of the Damköhler number, and for this reason defined as the ratio between the chemical time scale to the Kolmogorov time scale. The equations of the two numbers just introduced is given below:

$$\text{Da} = \frac{\text{turbulent mixing}}{\text{chemistry}} = \frac{L_T s_L}{\delta_L u'} \tag{1.27}$$

$$\text{Ka} = \frac{\text{chemistry}}{\text{turbulent micromixing}} = \left(\frac{\delta_L}{L_k}\right)^2 \tag{1.28}$$

Depending on these two dimensionless numbers, several regimes of turbulent premixed flames can be identified, by means of Borghi's diagram the different behaviors of turbulent flames can be visualized in a 2D manner in Figure 1.2.

Through the Damköhler number, two borderline conditions can be highlighted. For $Da >> 1$ chemical reactions are characterized by smaller time scales than those of turbulent mixing, or in other words, they have a higher velocity than turbulent velocity. In this case, the flame front is only slightly distorted by turbulent phenomena but prefectly laminar in the core regions. This operating conditions is called *flamelets regime* in which the chemical reaction can be modeled with a single-step reaction because it occurs with very high speed (*fast chemistry*). In contrast for $Da << 1$ the chemical reactions are extremely slower than the turbulent mixing

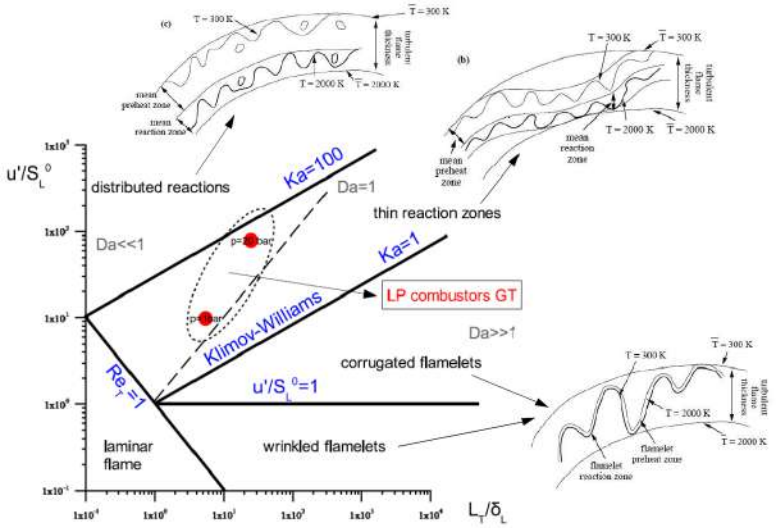

Figure 1.2: Borghi's diagram for premixed turbulent flame according to the classification proposed by [56] (adapted from [57]).

process and the system can be modeled with the Arrhenius equation (already shown in Eq.1.24), and dependent only on the temperature and concentrations of the species.

Several zones can be identified from the diagram in Figure 1.2. Starting with the regimes identified by low Karlovitz numbers, for $Ka < 1$ the *flamelets regime* already described in the Damköhler analysis. It is characterized by a quasi-laminar regime in which all chemical time scales are smaller than the turbulent time scales associated with the lower scales of Kolmogorov. This regime can also be divided into two families depending on the u'/S_L ratio: for values less than unity, the impact of turbulence on the chemical reaction is reduced meanwhile for values greater than one the larger turbulent scales tend to form corrugated flame fronts.

As the Karlovits number increases, turbulent contributions on the chemical reaction start to have a greater impact. The most interesting

region for gas turbine combustion chambers is without doubt the one identified as the *thin reaction zone* for $1 < Ka < 100$. In this region microscopic turbulent scales produce a thickening of the preheating zone but no change in the reaction zone which remains nearly laminar with only some wrinkling effects. Moving at higher Karlovitz numbers $Ka > 100$ turbulent fluctuations lead to complete destruction of laminar structures.

The discussion becomes more complicated by moving the study to non-premixed flames. For these flames, in fact, the mixing between fuel and reactants assumes a main role and does not allow easy separation of the times characteristic of mixing phenomena from the chemical characteristic scales. The treatment is always by analysis of the Damköhler number but the definition of its critical values becomes complex as it depends by the local mixing conditions. However, even for these types of flames, laminar flame behavior can be obtained for high values of the Damköhler number because the reaction zones are not affected by turbulent eddies. As the Damköhler number decreases, unsteady effects increase until a limiting operating condition is reached beyond which the chemical characteristic scales become too slow or turbulent structures are too high until flame extinction is reached.

1.4 Radiation

Electromagnetic radiation emitted by a body due to the heat of the body itself is called *Thermal radiation*. Differently from the previously described heat transfer mechanisms, this can occur even in the absence of a material medium. This mechanism is present in each body with a temperature above $0K$ due to the continuous energy emission due to vibration and rotation of molecules, atoms and electrons. Since the temperature of a body has a direct impact on entropy and thus on atomic interactions, a rise in temperature will correspond to a strong increase in the radiation emitted by the body. This behavior can be modelled by Stephen-Boltzmann's generalised law that defined the energy emitted by a surface in the whole wavelength spectrum.

$$E = \sigma_0 \epsilon T^4 \tag{1.29}$$

where $\sigma_0 = 5.67 \cdot 10^{-8} \left[W/\left(m^2 K^4\right)\right]$ is the Stefan-Boltzmann constant and ϵ is the emissivity of the material. The emissivity property is bounded between 0 and 1, where only ideal bodies, called *blackbodies* have the highest emissivity as they are perfect radiator at any given wavelength. Even for surfaces approximating as grey bodies, the emissivity is not a function of wavelength but is fixed and constant ($\epsilon = 0.6$); for all real surfaces the emissivity is a fraction of the ideal emission and is therefore related to that of the blackbody and defined as follow:

$$\varepsilon = \frac{E(T)}{E_b(T)} = \frac{E(T)}{\sigma T^4} \tag{1.30}$$

To better understand this concept it is worthwhile to introduce the monochromatic emissive power for a blackbody, E_λ, so called because it defines the power emitted per unit wavelength at a fixed temperature, that is defined by the following *Planck's law*:

$$E_{b\lambda}\left(T\right) = \frac{C_1}{\lambda^5 \left(e^{C_2/\lambda T} - 1\right)} \tag{1.31}$$

where C_1 and C_2 are the first and the second radiation constants.

In Figure 1.3 trends of the monochromatic emissive power for a blackbody for different temperature values are shown.

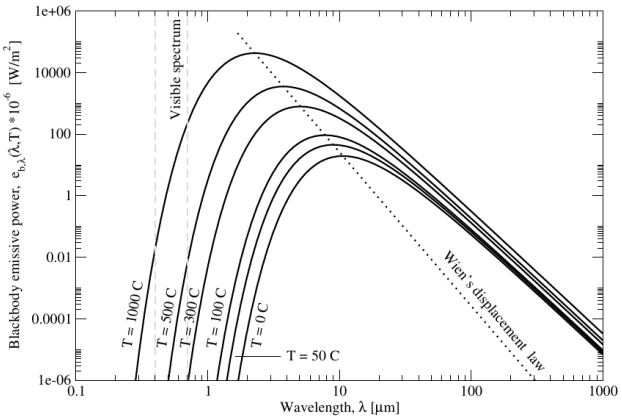

Figure 1.3: Spectral blackbody emissive power and the Wein's displacement law (dash line) [58].

At this point is clearly to understand that the Eq. 1.30 represents the area under each curve of Figure 1.3, since the total emissive power represents the total thermal radiation emitted over the entire wavelength spectrum:

$$\int_0^\infty E_{b\lambda} d\lambda = \sigma T^4 = E_b(T) \tag{1.32}$$

To characterize the behaviour of a surface when a radiation is incident on it, it's necessary to introduce the *absorptivity*, *reflectivity* and *transmissivity* that describe how the total incident radiation is split by means of the following relationship:

$$\alpha + \rho + \tau = 1 \tag{1.33}$$

In other words, it could be stated that a fraction of the total energy emitted will be fraction will be absorbed by the surface, another will be reflected and a part will be transmitted. When all the energy is

transmitted ($t = 1$) the material is trasparent, meanwhile if no part of the radiation is transmitted, the material is opaque ($t = 0$). It is important to underline that a blackbody is both a perfect emitter and a perfect absorber, so in this case the previous relation reduces to $\alpha = \epsilon = 1$ for each wavelength. Also in this case the three properties are dependent by the radiation wavelength and by the direction of the radiation with the exception of grey bodies for which the properties are constant over the entire wavelength spectrum, furthermore the portion of reflected radiation is emitted equally in each direction (*diffuse* surfaces).

According to Eq. 1.30, when two arbitrary surfaces exchange heat by radiation in vacuum, the net heat exchange is proportional to the difference of the temperature to the fourth power. The net heat exchanged released by the hotter surface and absorbed by the colder one, Q_{net}, is influenced by the radiative properties of the involved materials but also the geometrical characteristics of the considered surfaces. In general the heat exchanged can be defined as follow:

$$Q_{\text{net}} = A_1 \mathcal{F}_{1-2} \sigma \left(T_1^4 - T_2^4\right) \tag{1.34}$$

where $\mathcal{F}_{1-2}$ is the *transfer factor* which allows to take into account all the geometric factor as the areas, the shapes, the orientation and the spacing of the considered surfaces.

In gas turbine application, the treatment of heat exchanged by radiation is much more complex than the way it has been presented, in fact materials differ greatly from having a blackbody or greybody behaviour, the space around the surfaces considered can also have an impact emitting or absorbing radiation for certain wavelength. Additionally, the amount of radiation that is emitted by a surfaces trough another one is dependent by the direction of the radiation itself and not only by temperature and wavelengths. Moreover, the radiating beam during its transit can interact with the participating media, particles or surfaces that modify the direction and the intensity of the beam itself. For this reason, for the radiating problems it's convenient to perform the discussion in a spherical coordinates system and introduce the *intensity of radiation*, $I_\lambda(\theta, \phi)$. This

quantity is defined as the amount of the radiation emitted by the single wavelength λ, in the center of a solid angle centered in the direction (θ, ϕ) by a surface of unit area normal to the direction considered. From the definition just provided, it can be deduced that the intensity of radiation emitted for the entire wavelength spectrum is given by the following equation:

$$I(\theta, \phi) = \int_0^\infty I_\lambda(\theta, \phi) d\lambda \tag{1.35}$$

In order to be able to carry out an energy balance, it is essential to take into account not only the amount of radiation emitted by a surface but also the radiation incident on the surface itself. The *incident spectral intensity*, $I_{\lambda,i}$ is defined as the previous quantity with the different that in this case is not the emitted radiation but the radiant energy that is which is reached by the surface. The quantity *irradiation* is introduced to consider all directions through which radiator beams can reach the generic surface.

In order to obtain the spectral irradiation of a single wavelength reached by the surface under examination from all spatial directions, it will be necessary to integrate the spectral intensity incident on the entire space identified by the cylindrical reference system in the unit solid angle, as follow:

$$G_\lambda = \int_0^{2\pi} \int_0^{\pi/2} I_{\lambda,i}(\lambda, \theta, \phi) \cos\theta \sin\theta d\theta d\phi \tag{1.36}$$

At this point, to obtain the total irradiation for the whole spectrum of wavelength it will also be sufficient to integrate over all wavelengths.

$$\begin{aligned} G &= \int_0^\infty G_\lambda(\lambda) d\lambda \\ &= \int_0^\infty \int_0^{2\pi} \int_0^{\pi/2} I_{\lambda,i}(\lambda, \theta, \phi) \cos\theta \sin\theta d\theta d\phi d\lambda \end{aligned} \tag{1.37}$$

As already introduced, during the radiation passes through, it can interact with the medium and alter its intensity by gain or loss energy as well as change his direction due to scattering by the interaction with solid particles. The attenuation suffered by the radiation beam during its

passage is proportional to the incident energy intensity and the distance covered by the beam in the medium. By indicating the travel direction in which the beam passes as $\hat{s} = (\theta, \phi)$, the following can be defined:

$$(dI_\lambda)_{att}(\hat{s}) = -\beta_\lambda I_\lambda(\hat{s})ds \tag{1.38}$$

where β_λ represent the energy attenuation of the beam and it is called *extinction coefficient* where the negative value indicates that a decrease in intensity occurred. This coefficient permits the consideration of both the absorbed and the scattered energy contribution described by the following relationship:

$$\beta_\lambda = \kappa_\lambda + \sigma_\lambda \tag{1.39}$$

in which compares the linear *absorption* and *scattering coefficients* constants that represents the main attenuation factors. In particular, the first is associated with true energy attenuation while the second, scattering, involves a change in the direction of the radiant beam. Again, the contribution of scattering is not unique as it can propagate in any direction, so to obtain the contribution for a specific direction, it will be necessary to integrate over all solid angles. So all the energy contribution due to scattering effects in a specified direction, $\hat{s}$, is given by:

$$(dI_\lambda)_{\text{sca}}(\hat{s}) = ds\frac{\sigma_{s\lambda}}{4\pi}\int_{4\pi} I_\lambda(\hat{s}_i)\,\phi_\lambda(\hat{s}_i, \hat{s})\,d\Omega_i \tag{1.40}$$

The ϕ_λ term is a probability function, that is called *scattering phase function* and define the probability for a beam from the generic direction $\hat{s}_i$ to be scattered into an other fixed direction $\hat{s}$ [59].

The last term to take into account for the complete characterisation of an energy transfer by radiation is the contribution of the medium within which the radiation propagates. For this purpose, the *emission coefficient* j_λ for the generic medium is introduced. With this term it's possible to quantify the medium emission in a proportional way to the length of the medium.

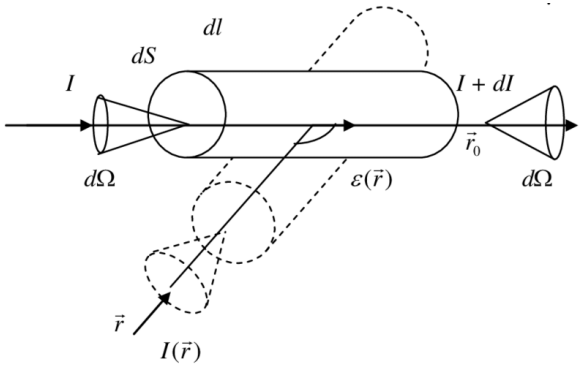

Figure 1.4: Representation of the different contributions to the conservation of radiative heat transfer equation [60].

Looking at Figure 1.4, it is finally possible to apply the complete spectral intensity of radiation $I_\lambda(\vec{r}, \hat{s}, t)$ balance in a certain position $\vec{r}$ along the direction $\hat{s}$ trough the *Radiative Transfer Equation (RTE)*.

$$\frac{1}{c}\frac{\partial I_\lambda}{\partial t} + \frac{\partial I_\lambda}{\partial s} = j_\lambda - \kappa_\lambda I_\lambda - \sigma_{s\lambda} I_\lambda + \frac{\sigma_{s\lambda}}{4\pi}\int_{4\pi} I_\lambda\left(\hat{s}_i\right)\phi_\lambda\left(\hat{s}_i, \hat{s}\right) d\Omega_i \quad (1.41)$$

All the source/sink effects previously introduced compare in the RTE equation which, to be solved, needs all the proper boundary conditions for the definition of radiation properties of the bodies. In addition, a time-dependent term appears. Considering that for gas turbine combustors applications the characteristic spatial and temporal scales are much larger compared to the speed of light c, this contribution can often be neglected. Whenever radiation is not the only heat transfer mechanism affecting the generic system, the impact that radiation has on temperature distribution must be taken into account as it then influences the other phenomena present. To couple the RTE with the energy equation, the volumetric source term is defined $\dot{\omega}_{rad}$ as follow:

$$\dot{\omega}_{rad} = \int_0^\infty \kappa_\lambda \left[4\pi I_{b\lambda}(T) - G_\lambda\right] d\lambda \quad (1.42)$$

This volumetric term, defined from the spectral intensity of radiation (I_λ) must be integrated over the entire wavelength spectrum and the entire solid angle in order to obtain the entire radiation contribution.

1.5 Time scale analysis in gas turbine combustors

The heat transfer mechanisms occurring inside a gas turbine combustor have been presented and described through their mathematical models in the previous sections. The analysis revealed that each of the above has its own characteristic time scale. This consideration highlights how complicated a numerical transient analysis for the correct evaluation of heat fluxes can be. The aim of this section is to analyse in detail all the characteristic time scales of the phenomena previously introduced in order to bring out clearly the challenges in numerical modelling of heat transfer.

As already mentioned, flows within gas turbine combustors are dominated by turbulent phenomena with consequent impact on convective heat transfer. Both spatial and temporal characteristic scales of turbulence cover a wide range. Indeed, considering the energy cascade process already introduced, the integral scales associated with large anisotropic vortices are known to dissipate energy and turn into smaller isotropic vortices linked to Kolmogorov scales. Although the smallest scales have a huge impact in the mass and heat transport phenomena within the fluid they have a reduced effect on wall temperatures. On the other hand, near-wall regions are affected more by strong thermal gradients caused by the larger eddies associated with integral scales. Trying to express these considerations into a mathematical form, a law for defining characteristic convective time scales can be found with the following relationship:

$$\tau_{conv} = \frac{L}{U} \tag{1.43}$$

where L and U are respectively the reference values for length and velocity. Keeping in mind that the integral scales have a comparable spatial size with those of the areas where they occur and velocities similar to those of the flow, estimates can be made for the convective characteristic scales that are formed inside gas turbine combustors. Considering a characteristic length equal to that of a combustor $L = o(0.1m)$ and a typical flow-through velocity of $U = o(100m/s)$ the characteristic time of the generic convective phenomenon is in the order of $\tau_{conv} \approx 1ms$.

Combustion is the other phenomenon that has a strong impact on the flow that develops inside the combustor, which in turn depends greatly on the turbulence. Depending on the rate at which the chemical reaction occurs extremely different time scales may be present. For low reaction rates in fact, the times are in the order of magnitude of $(o(1s))$, meanwhile for fast reactions is $(o(10^{-9}s))$. As already seen in Figure 1.2, for gas turbine combustor applications the flame is established in the regime of a Damköhler number between $o(10) - o(100)$ and a Karlovitz number within the range of $o(10^{-1}) - o(10)$.

Again it is convenient to formulate the problem from a mathematical point of view. Assessments of the characteristic times of chemical reactions can be carried out by means of the reference quantities of velocity and length relative to the flame and so, define the time as the ratio of the laminar flame thickness (δ_L) to laminar flame speed (s_L) of the flame brush.

$$\tau_{comb} = \frac{\delta_L}{S_L} \tag{1.44}$$

For gas turbine combustors, typical laminar flame speed values vary in the range between $o(10^{-1}) - o(1)m/s$ while for the flame thickness values are within the interval of $o(10^{-5}) - o(10^{-4})m$. At this point it can be concluded that the characteristic time scales order for combustion within gas turbine combustors changes between $o(10^{-5}) - o(10^{-3})m$.

Moving to conductive problems, the fundamental parameter that defines the ability of a material to heat more or less quickly is the thermal diffusivity α/L. As a consequence, the characteristic conductive time scale for conductive heat transfer will be a function of the thermal diffusion and the thickness of the body t in which the heat exchange takes place. Therefore, the characteristic time scale for conduction can be estimated through the following relationship:

$$\tau_{cond} = \frac{t^2}{\alpha} \tag{1.45}$$

Since the thickness of metal liners of gas turbine combustors is in the range of $t = o(0.001\ m)$ and the thermal diffusivity of the materials employed is

about $\alpha = o(10^{-6}\ m^2/s)$ it is possible to conclude that the characteristic time scale for conductive problem in combustors is $\tau_{cond} = 1\ s$.

Regarding radiative heat transfer, on the other hand, it has already been introduced that the speed at which radiation occurs in the medium is in the order of the speed of light ($c = 3 \cdot 10^8$). This quantity, in general, is not affected by the material properties and is not dependent by the spectrum wavelength. Since combustor liners are composed of special metal alloys, it is possible to treat surfaces as opaque. This assumption makes it possible to consider the characteristic length scale of the combustor, since it allow to consider the radiation only present in the gas phase. As a result of the above, the characteristic time scale of radiative heat transfer can be defined as follows.

$$\tau_{rad} = \frac{L}{c} \tag{1.46}$$

For the values considered, the characteristic time of the radiative phenomenon is in the order of 1 ps.

It is evident from the analysis that each characteristic time scale of the heat transfer mechanisms treated is profoundly different from each of the others. In particular, the convective time scale is at least two orders of magnitude lower than the conductive characteristic time, meanwhile the difference with the radiation scaling time is even more pronounced, enough to model the latter as a steady-state process.

Chapter 2

Unsteady Conjugate Heat Transfer modelling

It has been emphasized previously how important the estimation of the correct heat fluxes in a gas turbine combustor is to ensure the correct design of the cooling system and thus guarantee that the entire machine operates at high efficiency and under safe conditions. Experimental tests on combustors in representative conditions of normal gas turbine operation are often impractical. The reactive environment which is formed inside the combustion chambers combined with the high operating pressures makes experimental campaigns extremely complex and expensive. In fact, experimental tests are often reduced to final verifications to check the correct functioning of the gas turbine combustor. It must also be taken into account that combustion chamber, as well as other components of industrial gas turbines, are extremely complex and it becomes even more challenging to instrument the machine in order to acquire data during operation. However, even if experimental measurements were carried out on industrial gas turbines combustors, they can hardly provide complete information on the conditions inside the combustion chamber since are often reduced to temperature values over a small number of critical points in the combustor.

From this perspective CFD simulations result in a winning solution as they allow a complete understanding of the results with reduced effort compared with experimental tests. Given the strong impact of turbulence on heat transfer problems, steady-state RANS simulation or hybrid approaches, that represent the standard for industrial application, do not seem to be the correct CFD solution for obtaining accurate results. In fact, these numerical methods present limitations in the prediction of turbulent structures and since the flow inside the combustion chambers is typically fully-turbulent the numerical results could be affected by significant underestimation of the heat fluxes. The estimation of heat fluxes is therefore also critical due to the strong interaction between the swirl flow, the walls and when present also with the coolant flow.

Figure 2.1: Characteristics time and length scales in gas turbine combustors.

The continuing development of computational infrastructures has enabled increasingly commonplace use of more scale-resolved and accurate numerical approaches. LES models, or at least hybrid RANS-LES approach, have now become the standard in research and development fields. In any case, from the previous Chapter 1 it became clear that it is necessary not only to correctly solve the different heat transfer mechanisms but also the mutual influence on each other and furthermore, showed how these are driven by different characteristic time scales, as also shown in

Figure 2.1. This aspect makes the selection of the time discretization step to solve the unsteady CHT simulation particularly critical. For the correct solution of turbulence-driven convective phenomena a small time-step is necessary but at the same time solving the conduction with the same time-step would lead to a heavy increase in the computational cost since the simulation would have to be carried out for such a time that the thermal transients in the solid parts would be correctly solved.

Unsteady CHT simulations with the direct, or so called *strong*, coupling of the different heat transfer mechanisms would involve computationally unfeasible costs for industrial applications so, alternative methods for their numerical modeling will be presented in the following paragraphs.

2.1 Loosely coupled approaches for CHT simulation

In 3D CHT simulations, multiphysics phenomena affecting different regions characterised by a specific state of matter are analysed. In this sense, the purpose of simulation could be to study the interaction that takes place between a fluid phase and a solid body, and specifically in CHT simulations, to evaluate the heat transfer between the two zones driven by different physical phenomena. Compared to standard CFD calculations in conjugate heat transfer simulations, the objective is to evaluate the heat fluxes at the interface surfaces where the coupling between the different physics under study occurs. These surfaces, known as *coupling interfaces*, play a key role in solving the thermal problem. In fact, all multiphysics approaches have to guarantee the continuity of energy-based quantities between the different physical domains considered, hence through the coupling surfaces placed on the interfaces within the calculation domain.

In gas turbine combustors three thermal phenomena are usually considered, which are convection, conduction and radiation. The coupling interfaces between the fluid domain dominated by convective phenomena and the solid parts subject to conductive heat transfer are the surfaces identifying the metal walls of liners, components for which thermal ver-

ification is mandatory. As far as introduced, there will be a constraint condition on these coupled interfaces that imposes the equality of the heat fluxes flowing in and out of the surfaces themselves.

Concerning the fluid/radiation interaction, it is not possible to identify a proper coupling surface as the interface consists of the entire fluid volume. In this case, in fact, energy continuity is imposed through source/sink effects resulting from radiative heat flux, which in turn will be affected by the pressure, temperature and chemical species distributions developed in the fluid domain.

Similar considerations can be made for the interaction between radiation and the solid parts of the calculation domain, again the coupled interfaces will be the metal liner surfaces that will be affected by the radiative source terms, which in turn will be subject to a certain thermal distribution of the solid walls.

Depending on how the characteristic equations on the different coupled interfaces of the CHT simulations are solved, two approaches can be defined. A *strongly coupled* approach is defined when, at each iteration/step of time, all equations of the multiphysics problem are solved. In this case, as long as the convergence condition is not reached for all equations on the coupling interfaces, the simulation does not proceed to the next iteration/time-step. It is worth emphasising that, since the entire CHT problem is solved by a single solver, the compliance of the energy continuity condition is intrinsically achieved, i.e. no special simulation requirements need to be fulfilled.

On the other hand, loosely coupled approaches are defined as all those methods in which the convergence energy criterion on the coupled interfaces only occurs at specific iterations/time-steps and at the end of the multiphysics simulation. These approaches are based on dividing the initial CHT problem into several sub-domains, in each of which only a specific physical phenomenon involved within the problem is solved. Each sub-domain therefore is characterised by a single heat transfer mechanism that is solved by a dedicated solver. Once the solution is reached, the sub-domains must be coupled together in order to exchange the quantities

required to verify the energy balance on the interface surfaces [61]. The coupled interfaces of the strongly-coupled problem, in a loosely-coupled framework are different surfaces or volumes, each belonging to a dedicated sub-domain that have to communicate with each other to satisfy the energy balance by updating specific boundary conditions as shown in the simplified flowchart in Figure 2.2.

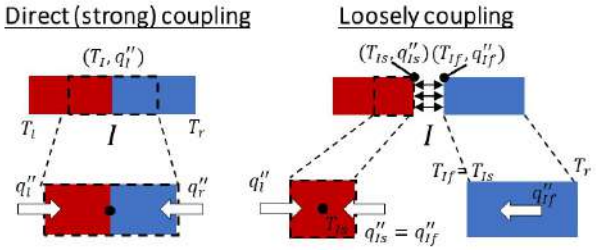

Figure 2.2: Outline of coupling approaches for CHT problems.

Loosely-coupled approaches can be adopted for solving both steady-state and unsteady-transient problems. Generally, steady-state approaches adopt sequential coupling. In this case, the coupling occurs only after that the convergence energy conditions have been reached: one solver passes the data to the second solver and then the one after it, and so on until the loop for finishing single iteration of the whole multiphysics approach. This loop is repeated through to the end of the simulation. For scale-resolved CHT simulations, the update of the different sub-domains is more efficient through parallel management. In this case the different solvers run in parallel and exchange data with a given coupling frequency.

For gas turbine combustors applications loosely-coupled approaches are particularly advantageous as they allow a temporal decoupling between each heat transfer mechanism and thus a desynchronization in time by permitting the most suitable numerical configuration to be adopted for the study of each individual phenomenon under investigation.

2.2 State of the art of loosely coupled approaches for CHT problem

In recent years, several algorithms based on loosely-coupled approaches for solving conjugate heat transfer problems have been developed by various research institutes. This development trend is due to the high efficiency of loosely-coupled approaches in solving CHT problems, compared to the direct coupling methods, guaranteed by the opportunity to use the most suitable time discretisation for each heat transfer mechanism involved in the problem. Although the workflow of loosely-coupled approaches is generally more complex, as it requires the use of several solvers that must communicate with each other, the gain in terms of computational savings is such that they have become state-of-the-art for conjugate heat transfer problems. It deserves to be emphasized, however, that once the coupling logic between the different solvers is defined and fine-tuned, the solvers used do not require any particular changes from the existing original codes [62].

It is clear from the above that the crucial part of loosely-coupled approaches are the algorithms that handle the coupling between different solvers. Implementing an effective algorithm for data exchange is not simple due to the two constraints that the procedure requires: the verification of the energy balance on the coupled interfaces of the problem and have stable behavior to ensure the correct and accurate CFD simulation solution. In fact, the type of boundary conditions applied to the coupling interfaces combined with the specific quantities exchanged between the different solvers has a strong impact on the stability of the whole procedure [63, 64].

Furthermore, the use of different time-steps for the several involved domains also introduces constraints on the frequency to be used for data exchange for the consistency of the final solution.

Given the general character of heat transfer problems, loosely-coupled approaches can be used for a wide variety of applications [37, 65], however, they are particularly successful when employed to model heat transfer

mechanisms with very different time scales. In gas turbine applications, they have been used to model the heat transfer of secondary flows [66] and for the study of different geometric configurations of film cooling holes on linear ducts [67].

In literature, many applications of loosely coupled approaches concern conjugate heat transfer on turbine blades [61, 68, 69, 70, 71].
In particular, Duchaine et al. [61] use a loosely coupled approach for the solution of a CHT simulation with a LES model. In the cited work, a parallel calculation infrastructure is developed [72] in which the AVBP code is used as the CFD solver meanwhile the solid solution is achieved by the AVTP solver, both managed by a third software, OpenPALM [73], developed as a computational framework for high-performance parallel computing. In this work, the stability of the numerical process was ensured through the use of a relaxation factor applied to the Dirichlet/Neumann mixed boundary conditions on heat flux and temperature at the coupled interfaces. It is important to emphasise that this type of approach allows the steady-state metal temperature to be obtained with a reduced computational cost, but in common with all loosely-coupled approaches, it does not allow for the temporal reconstruction of the temperature fluctuations on the coupled walls. In [61] a study of the stability of the multiphysics procedure is also proposed that highlighted the strong impact of two parameters: the Biot number, dependent on the spatial discretisation of the solid domain and the thermal diffusivity of the material in question. This coupling strategy was later extended with the introduction of the radiative solver in [38] for the solution of the CHT problem in an aero-engine RQL combustor.

He et al. in [71] proposed a time-scale decomposition for the near-wall region. The mean value of the wall temperature obtained by the fluid domain is passed to a steady-state conduction solver, meanwhile a Fourier transform is employed to decompose the unsteady fluctuation. The harmonics thus obtained are used to compute the wall temperature in the spectral domain by a semi-analytical interface. This data is then coupled with the heat flux from the fluid domain with a one-dimensional solver to

respect the energy conservation. Finally, the wall temperature obtained is transformed into the time domain and added to the steady-state contribution provided by the solid solver, thus reconstructing the temperature time signal to be applied to the interface surface of the CFD solver. An unsteady conduction solver is needed when it is necessary to reconstruct thermal fluctuations in the solid domain.

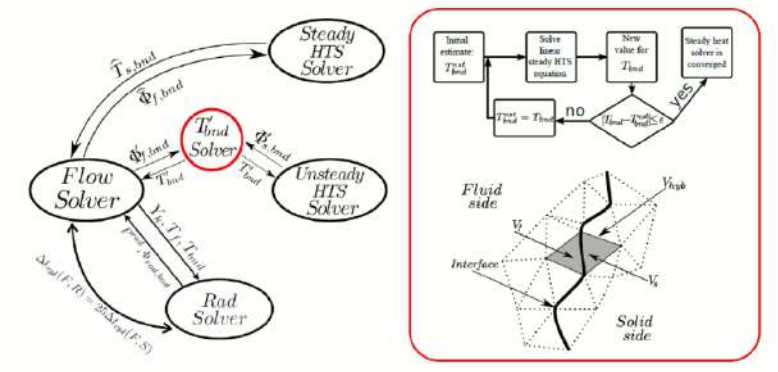

Figure 2.3: Representation of Koren et al. coupling strategy. The red box highlight the interface fluctuating temperature model (adapted from [40]).

A different coupling strategy is employed by Koren et al. in [40, 74] that is based on the utilization of the already cited OpenPALM software for coupling the different solutions, a sketch of the workflow is shown in Figure 2.3. In this solution the energy conservation is ensured by a Hybrid-Cell interface around the first layer cell of both meshes by the resolution of a dedicated ODE solver. The interface temperature thus obtained is imposed as a Dirichlet boundary condition on both the domains. Moreover a proportional–integral–derivative (PID) controller dynamically adjusts the coupling time-step to contain the integration error. In order to obtain the transient development of the wall temperature with an affordable computational cost, two conduction solvers are used, one for the steady problem that calculates the mean value and the second for

the unsteady problem to calculate the fluctuations. This method permit an acceleration of the transient temperature behavior to a staedy-state regime due to the filtering behavior of the average magnitudes during the first couplings, which will always be strongly influenced by fluctuations but not allow the desynchronization of the time-step between the solvers.

Zhang et al. [75, 76] employed a loosely-coupled approach to solve the CHT problem characterise by hypersonicflows. In the cited work, the authors exploits an adaptive coupling time-step with a PID controller showing a significant improvement in computational efficiency compared with using a fixed time-step.

2.3 U-THERM3D tool

This section will be dedicated to the description of the in-house 3D multiphysics and multiscale CHT strategy of which an optimisation will be proposed in the next sections. The aim of this paragraph is to highlight both its strengths and critical issues to optimize the workflow as efficiently as possible.

The original 3D U-THERM3D tool allows different heat transfer mechanisms within gas turbine combustors to be solved by separate solvers due to the loosely coupled approach with which it is managed, that allows the use of the most efficient modeling for each phenomenon involved. The key aspect of the U-THERM3D tool is the desynchronization of the time-steps for each involved heat transfer mechanism, which generally for gas turbine applications are convection, conduction in solid parts, and radiation. The feasibility of using the desired time-step for each heat transfer mechanism is ensured by the fact that each is solved in a dedicated simulation, all performed in parallel with a coupling strategy and exchanging instantaneous values at run time. The multiphysics and multiscale U-THERM3D tool has been developed in the department of industrial engineering of the University of Florence within the ANSYS Fluent solver [42]. The tool previously created for steady simulations

by Mazzei et al. [21, 30] has been updated by Bertini et al. [77, 78] to handle coupling between unsteady simulations and finally adopted in a LES framework for the prediction of wall temperatures in a RQL combustor model operating with sooting flame [79] in which the results are compared with those obtained with the stationary version of the tool.

The U-THERM3D procedure is shown in Figure 2.4 and structured as follows.

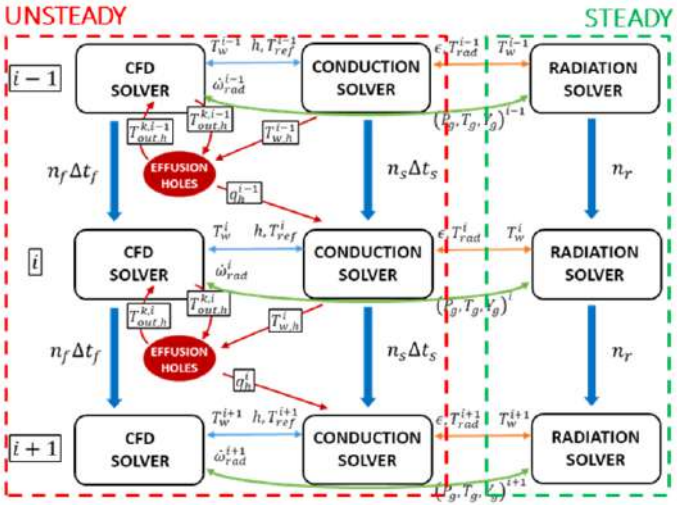

Figure 2.4: Workflow of the U-THERM3D parallel coupling strategy (adapted from [41]).

As already introduced, the CHT framework is based on a loosely coupled approach and each heat transfer mechanism is solved in a dedicated solver. Convective phenomena, given their similar characteristic time-scales and their strong influence on each other, are solved in a single ANSYS Fluent session. In this case *CFD solver* in Figure 2.4 refers to the one in which the fluid domain of the gas phase together with the combustion process is solved.

The different solvers interact each other with a parallel coupling strat-

egy. Both CFD and conduction solvers perform unsteady simulations, using their own time step highlighted in the sketch of the workflow by the symbols Δt_f and Δt_s respectively. According to the outcomes of Chapter 1, given the extremely low characteristic time scales of radiation phenomena this is solved in the dedicated solver with a steady-state manner.

The solvers interact with mutually synchronising each other at well-defined time instants to update special boundary conditions on the coupling interfaces. CFD and conduction unsteady solvers write the required data whenever they have simulated a user-defined time and equal to $n_f \Delta t_f$ and $n_s \Delta t_s$ respectively, meanwhile the steady-state radiation solver update the boundary conditions every n_r iterations.

Each solver exchanges well-defined quantities to verify the energy balance on the desired coupling interfaces. More in detail, for the 2D coupling interfaces by means the fluid/solid and the solid/radiation coupling surfaces the heat fluxes and the wall temperature distribution are exchanged. Thermal interaction between convection in fluid and radiation occurs in the entire volume under study, within which an exchange of a 3D aero-thermal distributions must be provided.

To ensure the stability of the entire simulation during the updating of boundary conditions at the 2D coupling interfaces, relaxation factors are used. In particular the convective wall heat flux calculated by the CFD solver is transformed in a Robin boundary condition before to be applied to the solid coupling surfaces with the following formulation.

$$q''_{\text{conv}} = h \left(T_{ref} - T_w \right) \tag{2.1}$$

This heat transfer coefficient h does not represent the real physical value resulting from the flow field established in the proximity of the coupled walls but is a numerical relaxation term fixed by the user. Even the term T_{ref} has no real physical meaning as it is that temperature value that allows the convective heat flow calculated within the CFD domain to be respected.

The same procedure is applied for the solid/radiation interface with the difference that the radiative heat flux is transformed. Within the black-body model, emissivity ϵ is the relaxation factor meanwhile T_{rad} is the reference temperature to respect the radiative heat flux calculated by the appropriate solver, thus the Robin boundary condition is obtained by the following equation. More detail on stability conditions of the U-THERM3D framework is covered in Bertini's reference study [41].

$$q''_{\text{rad}} = \epsilon\sigma_0 \left(T_{rad}^4 - T_w^4\right) \tag{2.2}$$

Moving on 3D data quantities the fact that CFD gas phase distributions, in particular pressure, temperature and species composition, are exchanged has already been introduced. These data are interpolated over the radiative domain in which only the RTE is solved. Instead, to take into account the impact of radiative energy within the CFD solver, a source/sink term is added to the energy transported equation. The source term resulting from the radiation solver takes into account all the RTE contributions previously described in the section 1.4.

The procedure thus defined allows the use of a different time advance for each solver in the simulation. Although this aspect is the biggest source of computational savings compared with a directly coupled CHT simulation the advantages of using the U-THERM3D tool are not ended. The capability to solve radiative heat transfer in a domain of its own allows for additional advantages. The resolution of the RTE, even though not at the level of the CFD domain, is particularly onerous. For this reason, the capability of being able to use a numerical setup optimized for this specific aspect is a factor that should not be underestimated. In addition to solving the radiation by steady-state approach, it is possible to limit the computational domain only where it plays a key role, such as in the flametube of a gas turbine combustor, and not consider the contribution of other areas where it has a negligible impact, i.e. the supply lines of cooling systems or inner and outer annulus, where generally the coolant temperature is almost constant and therefore the net radiative heat load will also be not relevant. In addition, a coarser computational grid can

be used for the parts of the computational domain under consideration because it is not necessary to solve turbulent momentum structures.

Although not directly addressed within this research work, in order to emphasize the modularity and adaptability of the U-THERM3D tool, it deserves to be introduced the effusion holes solver. As already mentioned, the complete modelling of effusion cooling would require the discretization of a large number of holes, resulting in a large increase in the size of the calculation grid on which the CFD simulation is to be carried out, and thus a high computational increase. For this reason, a simplified solver for effusion cooling has been developed since the earliest versions of the loosely coupled CHT framework analysed here. This model is based on the use of an imprinting technique, the holes are not discretized, but only a pair of inlet and outlet boundary conditions are present within the calculation domain, for the inlet inside the high-temperature combustion chamber and the outlet from the effusion hole supply system respectively [22]. The model was further developed to establish the coolant mass flow rate released by the several rows of effusion holes as a function of the local pressure drop across the perforated plate [80]. In addition, a correlative approach was developed for modelling the thermal phenomena occurring inside the holes, mainly the heating of the coolant flow as it passes through the holes due to the sink effect [20, 81]. A new machine learning-based model improvement is being developed by Paccati et al. [25] to apply velocity profiles that are functions of the flow field conditions inside the combustion chamber and no longer flat velocity profile for inlet cooling flow boundary conditions. The interested reader in effusion cooling systems and their related numerical modeling is referred to the following work [82].

2.4 U-THERM3D workflow optimization proposal

In the previous section, the working principle of the U-THERM3D procedure was described. The purpose now is to go into even more detail

about the core part of the CHT loosely coupled framework, which is the of data exchange management between different solvers. The data exchange is managed automatically by a series of User-Defined Functions (UDFs) that allow the correct definition of quantities on the coupling surfaces and automate the procedure. To better understand how to optimize the updating of boundary conditions on the coupling interfaces, it is necessary to comprehend what happens at execution level within the U-THERM3D framework.

Focusing on the interaction between the fluid and solid domains of Figure 2.4, the loop will be described in more detail. The CFD domain is chosen because it is the most onerous to solve as both spatial and temporal discretization must be ensured for the correct solution of both the turbulent structures and the chemical reaction. From a practical point of view, the fluid domain provides convective thermal flux at the interface surfaces with the solid domain, while the latter, after conductive heat transfer has been resolved, will provide a wall temperature distribution that will be applied to the coupled surfaces of the fluid domain as Dirichlet thermal boundary condition. As already said, the convective wall heat flux is first converted in the Robin boundary condition for stability reasons and then imposed on the coupled solid surface. This coupling cycle is repeated throughout the multiphysics and multiscale simulation and solvers interacting with each other only when the boundary conditions are updated and progressing in time with their own time-step. Coupling between the different simulations and thus updating the boundary conditions occurs whenever the fluid domain has performed 10 time-steps. The updating of boundary conditions on the coupled interfaces between different computational domains is achieved through write and read operations that result in increased simulation times without actually being associated with computation times. Since this operation is performed with high frequency throughout the whole CHT simulation, input/output (I/O) operations related to updating boundary conditions have a non-negligible impact on the overall simulation time and for this reason, the management of data exchange between different solvers is the bottleneck of the described

procedure. Of course, what has been stated for fluid-solid interaction also occurs with 3D data for updating conditions on coupled interfaces for fluid-radiation interaction.

Another aspect to take into consideration is the difficulty of using the multiphysical and multiscale instrument. Although the simulation coupling is handled autonomously through specific ANSYS User Defined Functions (UDFs) the procedure has some constraints including preparing three or more simulations, one for each heat transfer mechanism to be solved and the definition of a large number of boundary conditions, at least two for each interface surface between the coupled domains. In addition, increasing the number of simulations to be performed also raises the risk of unexpected errors. It is worth to underline that an unexpected shutdown of even one of the three solvers causes the whole simulation to stop because the boundary condition update loop on one or more of the coupling interfaces is no longer possible, resulting in the freezing of the entire loosely coupled procedure.

The proposed optimization will aim to simplify the multiphysics procedure and reduce the time associated with data exchange between solvers. This will be achieved through the built-in feature of the ANSYS Fluent solver called *Solid Time-Step* (STS) to manage the interaction between fluid and solid heat transfer mechanisms. This method allows a specific time-step size to be used for the solid zones of the computational domain thus maintaining a multi-domain architecture for solving the energy equation but in a single session of ANSYS Fluent. As described above, the goal is to use a larger time-step for solid parts to lower thermal inertia and thus reduce the cost of computation compared with a strongly coupled CHT simulation. This solution eliminates the time to update the boundary conditions of the current U-THERM3D version by solving the multiphysics and multiscale problem in a single Fluent session and thereby reducing the computational effort. Furthermore, it considerably simplifies the use of the numerical tool, as the new approach does not require the coupling of multiple simulations solved in parallel.

Regarding radiative heat transfer, the treatment is more complex. In

that, to the author's knowledge at the time the work was carried out a possible solution that could allow the internalization of the RTE within the CFD domain while maintaining the enormous advantages previously mentioned is not achievable. For this reason, it was decided to keep the management of radiation, from a conceptual point of view, unchanged compared to the original U-THERM3D tool but, taking into account the characteristic time scales of the two phenomena involved: convection and radiation, it was decided to operate on the frequency with which the coupling with the CFD domain occurs. As already introduced, in the original loosely-coupled CHT framework the coupled interfaces of the fluid domain are updated every 10 time-steps. In this sense considering that the two phenomena have a difference between orders of magnitude of the characteristic time scale by a factor up to $o(1000)$, as can be easily deducted from Chapter 1, it is possible to conclude that the coupling frequency can be reduced while maintaining the correct solution of the interaction between convective and radiative heat transfer mechanisms.

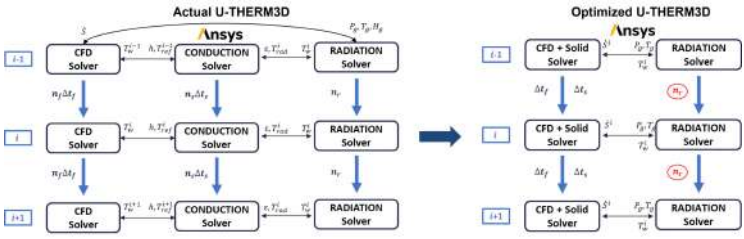

Figure 2.5: Workflow comparison between the actual and the optimized U-THERM3D parallel coupling strategy

In conclusion, the optimized workflow of the U-THERM3D tool, shown in Figure 2.5, is based on the internalization of the interaction between convective and conductive heat transfer which allows the complete elimination of the time related to the execution of write/read operations for updating the coupling interfaces. This solution led to the simplification of the workflow itself by moving from running two simulations in parallel, one for the CFD domain and one for the solid domain in which the conduction

is solved, to a single one while maintaining the parallel architecture of loosely-coupled approaches using the ANSYS Fluent built-in feature called Solid Time-Step method by allowing desynchronization of the two heat transfer mechanisms solution. With regard to the integration of radiative heat flux, on the other hand, it was decided to maintain the same handling as the current U-THERM3D tool and only act on the coupling frequency of the CFD solver's coupling interfaces. Although this management does not completely eliminate the operations for updating the boundary conditions of the two different sub-domains involved, it reduces their impact on the overall simulation time and at the same time allows the current advantages of the pre-existing loosely coupled procedure to be maintained.

2.4.1 Preliminary assessment of the optimized U-THERM3D workflow

In this section a first validation of the proposed workflow is carried out on a simplified test case. With the aim of keeping the tool as flexible and modular as possible, the audit will be divided into two parts. The procedure of only the interaction between convection in the fluid domain and conduction in the solid will first be analysed and validated, and only then the radiative heat flow will be introduced. This procedure was preferred to generalise the tool's usability not only for heat transfer applications in gas turbine combustors. In fact, although thermal radiation is constantly present, it is not always necessary to considerate its impact, especially when the temperatures involved are not very high, or when the temperatures of the bodies under examination are not significantly different from those of the surrounding environment, or even when the phenomena of conduction and convection dominate the heat transfer and have a significantly greater impact [83].

The first part of the validation will compare the simplified version of the U-THERM3D tool, to study just the interaction between convection and conduction, with the STS method with the aim to validate the new

management for the fluid-solid interaction. To better visualize the workflow a block diagram of the simplified U-THERM3D approach is shown in the figure below.

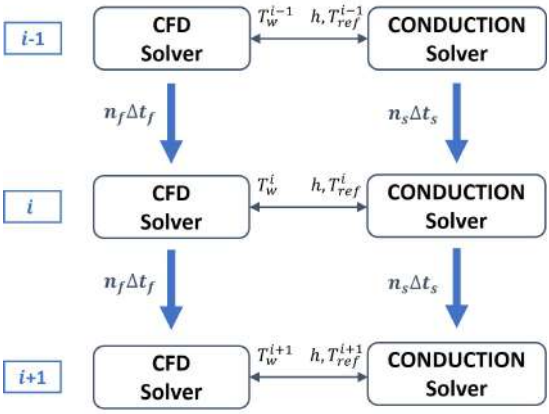

Figure 2.6: Simplified U-THERM3D diagram to consider only convective and conductive heat transfer phenomena

The test case considered for this preliminary validation is the backward-facing step that besides being well known in the literature for many experimental [84, 85], numerical [86, 87, 88] and heat transfer studies [89, 90, 91, 92] was used for the first development of U-THERM3D by Bertini [78].

For the first validation a non-reactive simulation of the quasi-2D computational domain, shown in Figure 2.7, was examined. The test case features a channel coupled with a solid plate having a thickness of 1.5 mm. To better force the oscillatory behavior of the flow, a sinusoidal velocity condition was imposed at the inlet of the duct. The set of boundary conditions consists of a constant inlet temperature and a convective heat flow condition on the bottom surface of the solid foil, meanwhile, a pressure condition is imposed at the outlet section. The lateral surfaces of the computational domain are treated as symmetrical. A hexahedral

grid consisting of 800K elements was used for the fluid domain while 20K elements were used to discretize the solid domain. Compared with the simulations performed by Bertini [78], in which a Scale-Adaptive Simulation (SAS) approach was used for turbulence modeling, a Stress-Blended Eddy Simulation (SBES) method is used [35] in this new numerical campaign. This hybrid approach for turbulence modeling ensures an LES solution in regions where flow is not well driven while it applies the kω-SST model [93, 94] in near-wall regions providing a numerically affordable boundary layer modeling. For the CFD solver a $5 \cdot 10^{-5} s$ time-step is used to ensure the proper resolution of the larger turbulent length scale, meanwhile, a $5 \cdot 10^{-2} s$ is used to solve the energy equation in the solid domain.

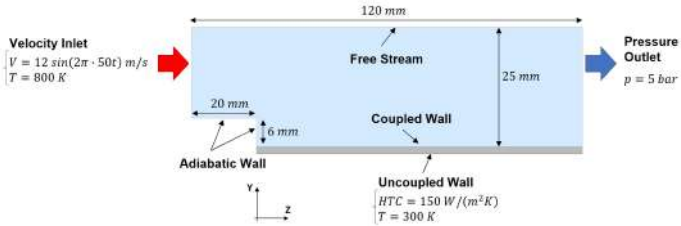

Figure 2.7: Calculation domain and imposed boundary conditions of the backward-facing step

Table 2.1: Solid properties for the backward-facing step plate.

Name	Symbol	Value	Unit
Density	ρ	100	kg/m^3
Specific Heat	c_p	50	kJ/kgK
Thermal Conductivity	λ	5	W/mK

To validate the Solid Time-Step method, a numerical experiment was performed on this test case. The two loosely-coupled approaches, simplified U-THERM3D and Solid Time-Step, are compared with a strongly-

coupled conjugate heat transfer simulation using the same mesh and numerical setup. To reduce the computational effort of the numerical test, solid domain properties were adopted to reduce the thermal inertia and are summarized in Table 2.1. This assumption is even more legitimate since with loosely-coupled conjugate calculation procedures the temporal development that the solid components undergo is not temporally synchronized with the convective phenomena occurring in the fluid domain. Therefore the instantaneous heat fluxes are not the actual ones undergone by the walls during thermal transients but only the average heat load will be the same.

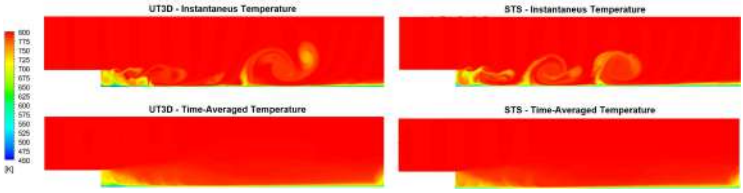

Figure 2.8: Instantaneous and time-averaged temperatures maps from U-THERM3D (left) and Solid Time-Step simulations (right)

The instantaneous and time-averaged temperature distributions in the CFD domain obtained by the two loosely-coupled methods are shown in Figure 2.8. As anticipated, the numerical approach used allows the correct prediction of the major turbulent scales, as can be seen from the instantaneous temperature distributions downstream of the step where several vortical structures are formed. The intensity of these vortices is even more emphasized by the sinusoidal velocity profile imposed. By comparing the average temperature fields, it can be seen that the two methods provide qualitatively the same result. Only slight differences near the edge of the step and in the middle of the recirculation zone are visible.

The time-averaged wall temperature distributions along the axial development of the plate, shown in Figure 2.9, also reveal no particular differences highlighting the good agreement between the loosely-coupled

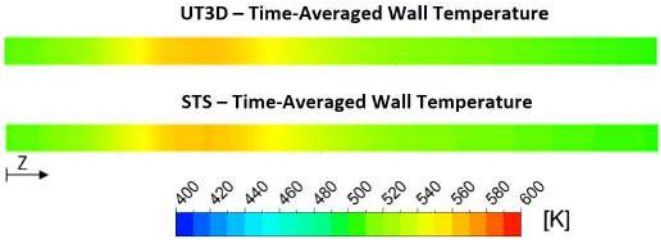

Figure 2.9: Time-averaged wall temperature distributions from U-THERM3D (top) and Solid Time-Step simulations (bottom)

methodologies analyzed. Comparing the results obtained more quantitatively, the time-averaged one-dimensional wall temperature trends for both the U-THERM3D and STS simulations are shown in Figure 2.10. The graph also shows the values obtained with the strongly-coupled simulation (CHT). What was highlighted above is even clearer by comparing the one-dimensional temperature profiles of the solid surface coupled with the fluid. The agreement among the three numerical methods is total and it allows to conclude that the STS approach enables the achievement of the same results as the simplified U-THERM3D simulation while performing a single simulation and eliminating the requirement to couple two simulations solved in parallel.

After this initial validation, the same calculation domain was used to verify the optimised workflow including radiative heat flux. Again, the numerical results obtained with the two approaches shown in Figure 2.5 will be compared with a directly coupled CHT simulation in order to have the correct reference result. To solve the RTE the Discrete Ordinate model (*DO*) has been employed. With this model, radiation is solved for a discrete number of solid angles each relative to a vector direction projected in cartesian space as shown in Figure 2.11. In this case, an angular discretisation was used on a 4x4 matrix while a 3x3 pixel array was considered for each direction as has been validated in [95] and applied in previous works [77, 78, 79, 96]. The only additional boundary condition required is the emissivity of the metal sheet, which is set equal to 0.8.

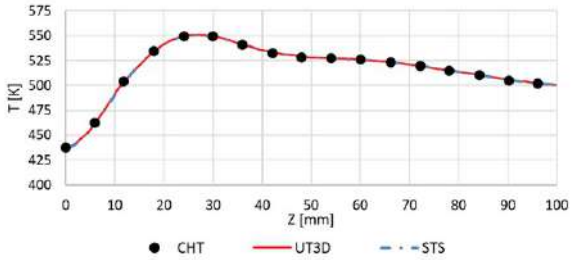

Figure 2.10: Axial profile of the time-averaged wall temperature on the solid plate for the three conjugate heat transfer methods analyzed to validate the convective-conduction interaction

In order to completely validate the numerical procedure of the opti-

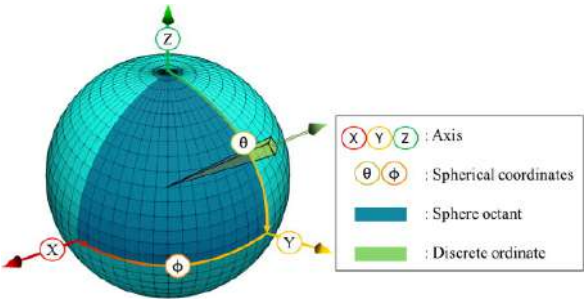

Figure 2.11: Graphical representation of the discretization of the angular space (Adopted from [97])

mized workflow several coupling frequency have been tested during the preliminary activity. The first frequency analyzed is equal to that used also in the U-THERM3D framework, in which the update of the boundary conditions on the coupling interfaces takes place every 10 time-steps of the fluid domain. In addition, two further coupling frequencies were evaluated: every 50 and every 100 fluid time-steps. The results are shown in term of time-averaged profile of the wall temperature along the solid plate in Figure 2.12, in which, with the name *oU-T3D* are indicated the tempera-

ture profiles obtained with the full optimized U-THERM3D framework. Before going into the analysis of the different curves, a comparison with the wall temperature profiles shown in Figure 2.10 highlights how the results vary with and without the radiation contribution. The associated heating causes the flow in the recirculation zone to behave differently due to the increased diffusivity, which causes more turbulent mixing and thus brings the peak temperature closer to the trailing edge of the step.

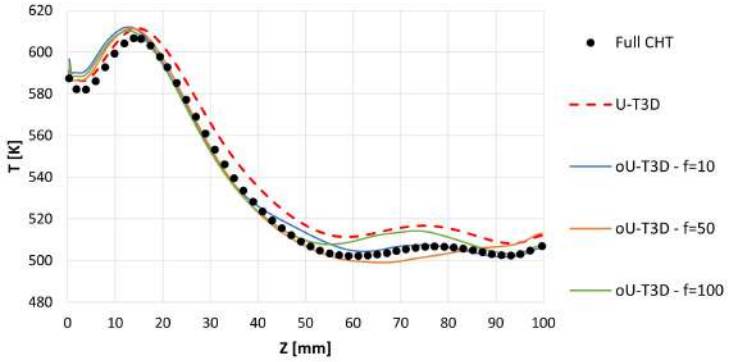

Figure 2.12: Comparison of axial profile of the time-averaged wall temperature on the solid plate for the three conjugate heat transfer methods analyzed to validate the full optimized U-THERM3D workflow tested with three different coupling frequency

The results show that all loosely coupled procedures for solving the conjugate heat transfer problem adopted are in agreement with the strongly coupled *Full CHT* simulation. The pattern of the trends for the different curves is in line with what could be expected. As the coupling frequency increases, and thus performing the updating of the boundary conditions of the coupled interfaces more often, the results tend to coincide with those produced by the strong coupled simulation. Indeed, remembering that in strong coupled simulation the equations are solved at each time-step on the coupling interfaces, it is normal that as the update frequency increases, the results tend towards those obtained with the full CHT

standard approach.

The simulation conducted with the current workflow of the U-THERM3D tool shows a maximum difference to the reference simulation, near the axial dimension at about 75mm from the step, of 1.5%. A similar trend but with an even smaller error is achieved with the optimised approach with updating of boundary conditions every 100 fluid time-steps. The agreement between the results makes it possible to validate the new data exchange management for updating the boundary conditions on the coupled interfaces of the calculation domain where the conjugate heat transfer problem is solved with a loosely coupled approach.

It is worth underlining that the purpose of this first numerical campaign was to validate the numerical approach and to confirm that the different loosely-coupled methodologies provided the same results. The test case under investigation does not permit the proper evaluation of the computing savings of the optimized loosely-coupled approach with respect to the actual U-THERM3D one because the amount of data exchanged between the computation domains involved is limited, so the execution times of the write and read phases are almost zero. In any case, the elimination of I/O operations for data exchange to update fluid-solid coupling interfaces and the reduction of the frequency with which fluid-radiation interface updates are performed by a factor of 10 is considered to contribute to a net saving in computational costs. Moreover, the proposed new workflow considerably simplifies the current U-THERM3D framework by reducing the number of simulations to be carried out in parallel from three to two.

2.4.2 Concluding remarks

This chapter describes the current development of the various loosely coupled numerical tools for solving conjugate heat transfer problems. Special attention was dedicated to the U-THERM3D tool developed within the University of Florence whose advantages and critical aspects of its functioning were presented. In order to reduce the execution time

for updating the boundary conditions on the coupled surfaces of the multiphysics problem a new handling of thermal loads managements was proposed. The optimised procedure is based on the employment of the built-in feature of the commercial ANSYS Fluent solver called 'Solid Time-Step'. This concept allows the two fluid and solid domains to be solved within a single simulation while maintaining a loosely coupled approach that allows desynchronisation between the two domain solutions. Moreover, this optimized workflow allows simplifying the workflow of the pre-existing tool and thus facilitate its use. As far as the contribution of radiative heat transfer is concerned, the handling of data exchange is unchanged, but the impact of the update frequency of the coupled interfaces on the final result was studied. In particular, the use of a lower coupling frequency between the coupled interfaces, every 100 fluid time-steps, makes it possible to predict the wall temperature with good accuracy and at the same time limiting the time associated with update operations. The proposed procedure was validated on a simplified test case. First the handling of the fluid-solid interaction was verified and then RTE was introduced to repeat the validation with the new thermal contribution. This double validation makes it possible to keep the new workflow as flexible and modular as the original one but with the above-mentioned advantages. In the following chapters, the new U-THERM3D tool model will be applied to two academic but well representative case studies of industrial gas turbine combustor models with the aim of stress-testing the proposed framework for a second validation and a detailed study on the savings achieved in terms of computational cost.

Chapter 3

RSM effusion-cooled combustor model

This chapter will highlight the capabilities of the optimized workflow of thesimplified loosely-coupled unsteady multi-physics tool (U-THERM3D) developed at the University of Florence within ANSYS Fluent solver. As already anticipated, this first application will focus on the interaction between convective and conductive heat transfer mechanisms alone by neglecting the radiation heat transfer to repeat a similar validation as done on the simplified non-reactive test case analyzed in the previous chapter. The coupling strategy will be employed for the numerical analysis of the RSM effusion-cooled swirl burner, an academic test rig well representative of the working conditions of a partially premixed combustion chamber equipped with an effusion cooling system, developed by the collaboration of the Universities of Darmstadt, Heidelberg, Karlsruhe, and the DLR. The highly detailed numerical results obtained from the unsteady multi-physics and multi-scale simulation will be compared with experimental data to validate the numerical procedure.

From the author's knowledge, it does not appear that this academic test case has ever been studied by CFD simulations so after a description of the experimental rig, a whole series of preliminary numerical activities will be

carried out to validate the numerical model, ending with the employment of the simplified loosely coupled procedure U-THERM3D. This preliminary assessment is conducted with the aim to obtain a reference solution with which compare the novel and optimized oU-THERM3D tool. Several aspects emerged during the numerical activity that had to be improved for the correct prediction of wall temperatures. Therefore, during the course of the numerical activities, boundary conditions were changed based on the results obtained. Part of the numerical effort was made to evaluate the impact of turbulence modeling within the loosely coupled unsteady simulations performed. In particular, the hybrid RANS/SBES approach will be compared with the full LES approach for estimating wall heat fluxes.

To facilitate the interpretation of the results obtained, an initial analysis of the preliminary results will be carried out with the simplified baseline version of U-THERM3D. Next, the actions required to set up the simulation with the Solid Time-Step, the core of the new optimized workflow, will be presented, and then the results will again be compared with the experimental data and the U-THERM3D reference simulation.

Due to the large number of reactive simulations performed a summary of the computational cases is given in Table 3.1 in order to clarify and highlight the differences. In this activity, only the interaction between convection and conduction is simulated, so when the term U-THERM3D is used, reference is made to the simplified procedure, while STS means that the multi-physics simulation is carried out using the Solid Time-Step method previously introduced.

Table 3.1: Simulations Summary of the RSM test case.

Case	Simulation Type	Turbulence Model	Conduction Solver
1	RANS CHT	Realiz. k-ϵ	Enabled
2	Adiabatic SBES	Dyn. Smagorinsky + k-ω SST	Disabled
3	U-THERM3D SBES	Dyn. Smagorinsky + k-ω SST	Enabled
4	STS SBES	Dyn. Smagorinsky + k-ω SST	Enabled
5	STS LES	Dyn. Smagorinsky	Enabled

3.1 Experimental test case description

In the present work an unsteady, multi-scale and multi-physics simulation is carried out on a single sector effusion cooled swirler burner developed and tested by the cooperation between the universities of Darmstadt, Heidelberg, Karlsruhe, and the DLR, named *RSM* combustor. The main objective of the experimental investigations was a detailed quantitative characterization of the confined swirling diffusion flames stabilized in a gas turbine combustor model under close-to-reality operating conditions and fueled with natural gas.

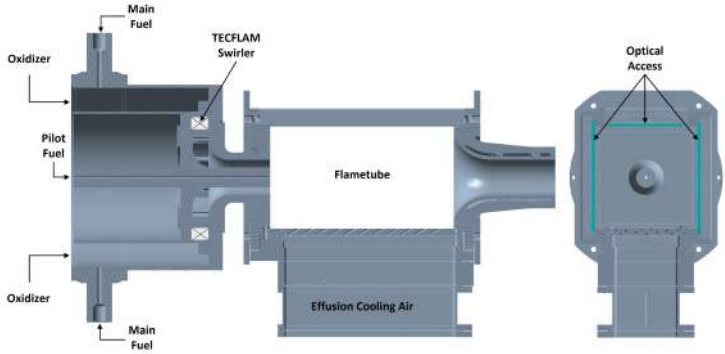

Figure 3.1: Rearranged double cross-section of the RSM combustor, tested in [98, 99]

The single-sector RSM combustor, shown in Figure 3.1, which takes its name from the research institute (Reaktive Strömungen und Messtechnik) within the University of Darmstadt led by professor A. Dreizler, will be the test case on which the advantages introduced by the new optimized loosely-coupled methodology will be analyzed. This academic burner has several interesting features that make it a very representative model of industrial combustors. It operates under pressure and not under ambient conditions, it also can work with both premixed and partially premixed methane-air flame conditions and finally has an effusion-cooled plate. The RSM combustor is also equipped with a mobile block swirler to control

the geometric swirl number based on the TECFLAM design [100] widely studied in literature both experimentally [101] and numerically [102] in its unconfined version.

The rig presents a central duct for fuel supply so that it can operate with a fully premixed or partially premixed flame. The flametube has a square cross-section and features three quartz optical access windows. The liner has an effusion cooling system with 145 circular holes, with a diameter of 2mm and an angle of 30 degrees to the direction of flow. A sketch of the effusion cooling pattern geometry is shown in Figure 3.2.

The combustor was tested under several operating points and detailed

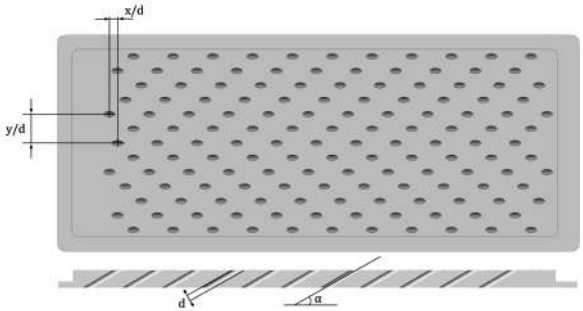

Figure 3.2: Rearranged effusion-cooled plate scheme installed on the test rig, tested in [98, 99]

measurements were carried out with different techniques. The flow field was measured under both reactive and non-reactive conditions using Particle Image Velocimetry (PIV) in [98] whereas, the temperature profiles were obtained using the Coherent Anti-Stokes Raman Spectroscopy (CARS) technique. In [99, 103] a flame structure study is performed with the Planar Laser-Induced Fluorescence of OH (OH-PLIF) to investigate the flame-cooling air interaction. In the above-mentioned work, the thermal maps on a portion of the effusion cooled liner are obtained by 2D Thermographic Phosphor Thermometry (TPT). The different measurement zones analysed in the combustion chamber can be seen in Figure 3.3.

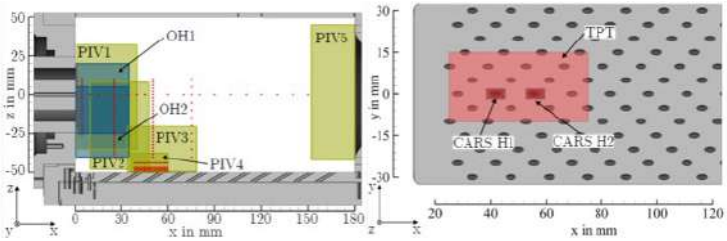

Figure 3.3: graphical summary and regions on which data acquisition was carried out in the experimental campaigns of [98, 99]

For further details on measurement techniques and the experimental apparatus, please refer to the above-mentioned works.

Only one operating condition of those analyzed by Hermann and Greifenstein et al. in [98, 99] has been investigated in the framework of this work, the details are highlighted in table 3.2. In this study only the partially premixed flame is analyzed where the combustor works in lean conditions with a pilot fuel percentage of 10% of the total, indicating with the name *staging ratio*.

Table 3.2: Test points analyzed.

Name	Symbol	Value	Unit
Operating pressure	P	0.25	MPa
Swirl number	S	0.7	–
Oxidizer mass flow	$\dot{m}_{ox}$	30	g/s
Oxidizer temperature	T_{ox}	623	K
Eff. cooling mass flow	$\dot{m}_{eff}$	7.5	g/s
Eff. cooling temperature	T_{eff}	623	K
Fuel mass flow	$\dot{m}_f$	1.128	g/s
Pilot fuel temperature	T_{pf}	333	K
Staging ratio	SR	10%	–
Equivalence ratio	Φ	0.65	–

3.2 Numerical details

All numerical analyses were carried out with the 2019R1 version of the commercial CFD solver ANSYS Fluent [104]. In the following sections, the employed numerical models will be described.

3.2.1 Turbulence modelling

The hybrid RANS/LES approach named Stress-Blended Eddy Simulation (SBES) [35, 104], was used to carry out most of the simulations. This model belongs to the family of DES methods in which wall stresses are solved using a RANS approach whereas, regions subjected to massive separations and unguided flows are solved using a LES approach. With this approach, kω-SST model [93, 94] is employed to solve near-wall regions whereas the flow field is solved in an LES manner in the freestream. The transition between RANS and LES behaviors is handled internally by a blending function [104] that defines the SBES sub-grid stress tensor. For the modeling of the sub-grid stresses in the LES part the Dynamic-Smagorinsky model is adopted [105]. This numerical method allows optimal handling of turbulence models as a function of the local flow field, improving the quality of the solution that would be provided by a fully RANS simulation but at the same time reducing the computational efforts for boundary layer modeling that would be mandatory with a pure LES simulation. The switch between RANS and LES behaviors is uniquely controlled by means of a blending (or also called *shielding*) function f_{SBES}, which is defined as in Equation 3.1.

$$\tau_{ij}^{SBES} = f_{SBES} \cdot \tau_{ij}^{RANS} + (1 - f_{SBES}) \cdot \tau_{ij}^{LES} \tag{3.1}$$

Where τ_{ij}^{LES} and τ_{ij}^{RANS} are, respectively, the LES and RANS parts of the sub-grid stress tensor. As already said, the RANS sub-grid stress is modeled with the kω-SST model [93, 94], while the LES part is calculated with the Dynamic-Smagorinsky model [105] for the closure of the sub-grid stress tensor. In this approach, eddy viscosity is a function of the resolved

strain rate $\bar{S}$ computed as follow:

$$\mu_t = \rho L_s^2 |\bar{S}| \tag{3.2}$$

wherein $\bar{S}$ is the symmetric part of the square of the velocity tensor gradient without trace.

$$|\bar{S}| = 2\sqrt{\bar{S_i}j\bar{S_i}j} \tag{3.3}$$

Meanwhile, L_s is the characteristic subgrid-scale (SGS) mixing length defined as follow.

$$L_s = min(kd, C_s V^{1/3}) \tag{3.4}$$

In this quantity compared the Kolmogorov constant k, the distance of each cell from the nearest wall d as well as the cell volume V and the Smagorinsky constant C_s that depend by the resolved turbulent scales.

3.2.2 Combustion modelling

The Flamelet Generated Manifold (FGM) combustion model has been considered to describe the reactive behavior of the flame. This flamelet-based approach is widely used for combustor CFD gas turbine simulations [27, 28, 78, 79, 106], in which a lookup table is created from the resolution of a set of 1D laminar flamelets (opposed jets). In this framework, the reactive flow behaviors depend only on two quantities, i.e. the mixture fraction Z and the progress variable c [107], which is a dimensionless index of how far the chemical combustion reaction has advanced toward the products, and through which it takes into account the ignition and quenching phenomena. The progress variable is defined as the ratio of the mass fractions of CO and CO_2 to their values at local equilibrium [108] as follow.

$$c = \frac{(Y_{CO} + Y_{CO2})}{(Y_{CO} + Y_{CO2})_{eq}} \tag{3.5}$$

The manifold $\Phi\ (Z, c)$ was generated with 64x64 points using the ANSYS Fluent built-in tool in which the turbulent interaction is included by assuming a priori a β-Probability Density Function (β-PDF) for the two

control variables Z and c [109]. The integrated value of a generic turbulent variable Ψ (Z, c), assuming Z and c to be statistically independent of each other, results in

$$\tilde{\psi} = \iint \psi(c, Z) PDF\left(\tilde{c}, \tilde{c}''^2\right) PDF\left(\tilde{z}, \tilde{Z}''^2\right) dZdc \tag{3.6}$$

where $\tilde{c}$, $\tilde{Z}$ are the mean values and $\tilde{c}''^2$, $\tilde{Z}''^2$ the variances values of mixture fraction and progress variable that are obtained by the resolution of two additional transport equations. The turbulent-chemistry interaction is modeled using the finite rate closure for the $\tilde{c}$ source term [104]. As a result, is required a 4-D tabulation for all the manifold quantities.

The same natural gas mixture as used in the experimental reference work conducted by Greifenstein et al. [99] was used for the simulations, adopting the GRImech 3.0 [110] reaction mechanism with 325 reactions and 53 species.

3.2.3 Simplified U-THERM3D simulation numerical setup

As already introduced, The objective of this preliminary phase of the numerical activity is to carry out the simulation with a simplified U-THERM3D approach in order to have a reference simulation with which to compare the optimised workflow. The simplified version of the described approach will be used, since the contribution of radiative heat transfer will be neglected due to the typical small luminosity of methane flames and due to the lean condition in which the burner is operated. Therefore, only the interaction between the fluid and the solid domains will be modeled as previously shown in Figure 2.6.

As mentioned in the previous chapter 2.3, CFD and conduction solvers advance in time with their own and proper time-step, while data on the coupled surfaces of the two simulations are exchanged regularly with a user-defined frequency to update the boundary conditions. In this work, the coupling between the two simulations occurs every 10 fluid and 30 solid time steps. For numerical stability reasons, the heat flux of the CFD simulation is firstly converted in an equivalent Robin boundary condition

and then transferred to the solid simulation.

The simplified U-THERM3D approach requires the setup of two different simulations to solve convective and conductive heat transfer problems. For the SBES CFD simulation, the pressure-based algorithm SIMPLEC was used, all equations were solved with a second-order upwind scheme and a second order implicit formulation for time discretization were employed. Regarding the fluid time step, it has been set to $1{\cdot}10^{-6}$s to ensure a Courant-Friedrichs-Lewy (CFL) condition almost equal to 1 over the entire calculation domain. The CFD domain is shown in Figure 3.4 (solid plate and effusion plenum are deliberately shifted to highlight the coupled walls). Regarding the coupled boundary conditions, in addition to the two faces of the plate shown in Figure 3.4, the lateral surfaces of the cylindrical effusion holes were also coupled. For each inlet, the corresponding mass flow rate value and temperature indicated in Table 3.2 was set, while for the outlet the operating pressure is imposed. The temperature of the pilot jet was set at 333K, following what was declared by Greifenstein et al. in the reference works [98, 99].

Concerning the duct pilot fuel modeling, the length of the pipe has been reduced with respect to the original dimension after a first SBES simulation carried out on the complete domain. This first simulation showed a RANS-like solution within the pilot duct and next to the tube outlet due to a SBES shielding function equal to 1, resulting in an underestimation of turbulence and mixing levels in these regions, as highlighted in Figure 3.5. To improve the quality of the simulation in these areas it was decided to reduce the pilot duct extension according to the geometry reported in Figure 3.4 and to model the inlet with a fully developed velocity profile defined by means of the power law [111] and a mean value of 12.73 m/s to match the experimental fuel mass flow rate. To ensure a level of turbulence required for a LES-like solution, a synthetic turbulence generation [104] at the fuel pilot inlet was also imposed with integral values for turbulence quantities. No further assessments of the impact of pilot fuel jet boundary conditions were conducted in this first analysis due to the unavailability of additional supporting experimental data and

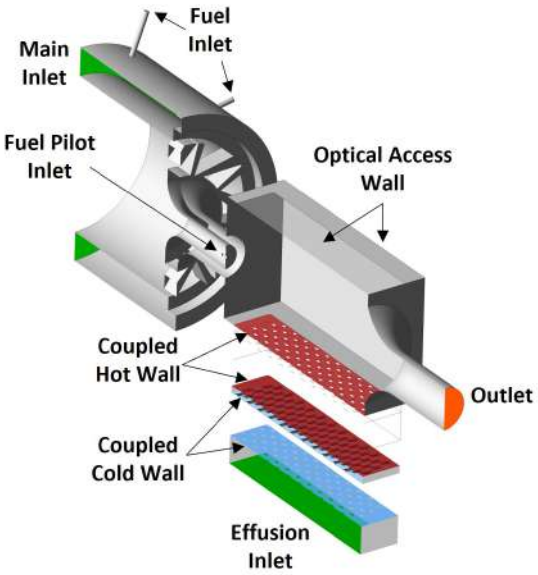

Figure 3.4: Computational domain and boundary conditions applied. Solid plate and effusion plenum are deliberately shifted to expose the coupled interfaces belonging to the two different domains

because the focus was on ensuring a solution in line with the numerical approach used. As will be shown in the following sections, this boundary condition will then be updated for the simulations conducted with the Solid Time-Step method for the optimised workflow.

The properties of the reactive mixture were imposed temperature dependent and derived from dedicated calculations carried out in Cantera [112].

As discussed above, radiative heat transfer was neglected in this first study of the RSM burner, due of an assumed insignificant emissivity of the gaseous methane-air flame. On quartz surfaces, it was decided to impose a fixed temperature for the three optical accesses with which the flametube is equipped. Since in Greifenstein et al. work [98, 99] there is no informa-

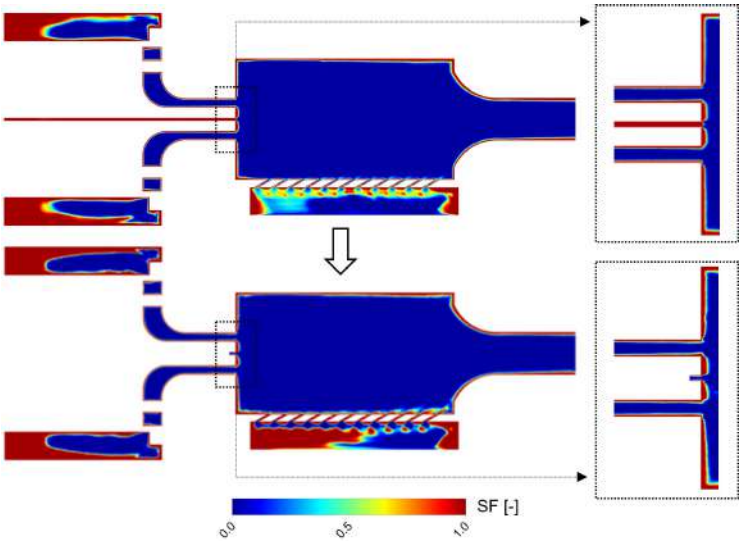

Figure 3.5: Shielding Function [104] comparison between the original CFD domain (top) and new one (bottom), employed for the numerical activities

tion about the thermal characterization of quartz windows, a numerical campaign based on directly coupled CHT RANS simulations was carried out in order to study the effect quartz walls temperature on the behavior of the simulated combustor. Three simulations were carried out: the first one with adiabatic quartz walls whereas the other two imposing a uniform temperature of 1300K and 1500K respectively. The results obtained were compared with the experimental temperature profile on the combustor centerline in Figure 3.6. For the subsequent unsteady simulations, the actual objective of the work, a uniform temperature of 1300K on the three optical accesses was chosen as the reference condition for the quartz as it is the condition that approximates most closely the experimental result. This value is also comparable to the typical operating temperatures of the quartz employed for this type of laboratory application.

Concerning the solid domain simulation, only the energy equation

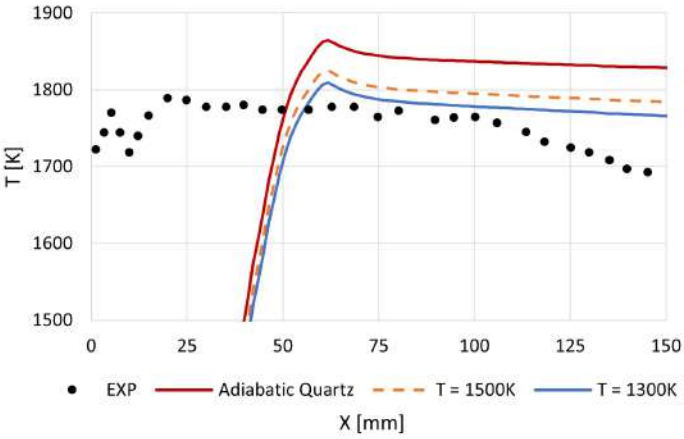

Figure 3.6: Gas-phase temperature sensitivity analysis results along the centerline of the combustion chamber as the imposed quartz temperature varies

is solved as only heat transfer by conduction is present. Due to the temporal desynchronization of the loosely coupled approach, the solid domain simulation could adopt a time step of $1{\cdot}10^{-3}$s consistent with the characteristic timescales of the conductive phenomenon. The solid was modeled as an alloy metal with polynomial temperature-dependent properties.

Both computational grids were generated in ANSYS Meshing. A mesh of 146M tetrahedral elements with 5 prismatic layers in the near-wall region was generated for the CFD simulation and converted to 42M polyhedral elements [113], as shown in Figure 3.7. Several local refinements have been introduced to ensure correct resolution of turbulent structures. Compared to the nominal mesh sizing of 1mm, the swirler and primary zone have been discretized with elements of 0.45mm. For the pilot jet duct and the area immediately downstream, an additional thickening has been inserted, using in this area a size of 0.1mm. An element size of 0.15mm was employed for the discretization of the effusion holes, whereas

in the area near the hot wall a sizing of 0.75mm was adopted.

Mesh sizing was defined according to [114] which suggests to adopt a

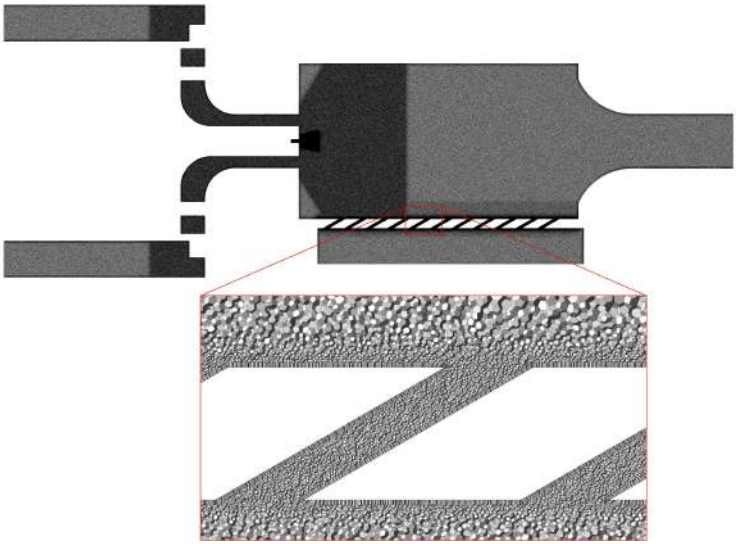

Figure 3.7: Calculation grid employed for the CFD simulation of the gas-phase domain of the simplified U-THERM3D approach

grid resolution based on the local values of turbulence Reynolds number and of Kolmogorov length scale for a proper scale resolving simulation. The calculation grid defined in this way allows the resolution of the 80% of the turbulent kinetic energy, thus satisfying the Pope criterion [115] which gives an indication of the good quality of the obtained LES solution. The above criterion is widely used in applications involving reactive flows within combustion chambers [116, 117] and it is often reported in terms of M, the ratio of modelled to resolved turbulent kinetic energy as shown in Figure 3.8. As can be seen, the resolved turbulent kinetic energy is well above the 80% threshold, resulting in M values less than 0.2 over a large part of the calculation domain.

Regarding the conductive simulation, a mesh grid with a uniform tetrahedral element size of 0.75mm has been generated with a total num-

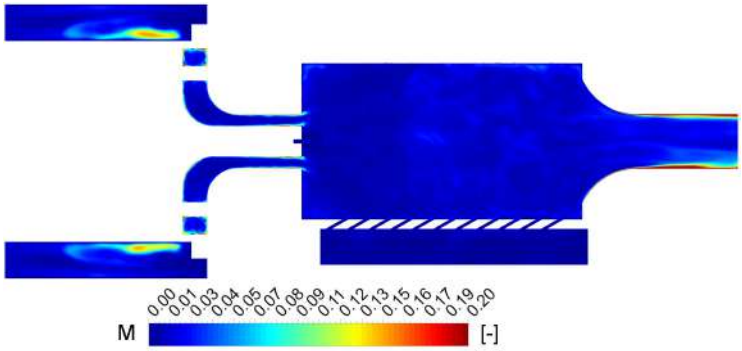

Figure 3.8: Pope criterion

ber of elements equal to 7M.

3.3 Preliminary Results

As already mentioned, results will first be analysed to validate the numerical model of the RSM combustor and to analyse the results obtained with the multiphysics and multiscale procedure U-THERM3D. These will then serve as a reference for comparison and validation of the new optimised workflow of the U-THERM3D tool, based on the Solid Time-Step method. In particular, this section presents and discusses the results obtained from the simplified U-THERM3D procedure. The achieved multi-physics results will be compared with the experimental data and with two simulations, a steady-state RANS CHT and a SBES fluid simulation with adiabatic walls. These preliminary results have already been discussed by the author of the manuscript in [118].

The aim is to verify what has been stated in the previous chapters: namely that for the correct prediction of wall heat fluxes, steady state RANS approaches do not allow a good prediction of wall temperatures, due to the limitations already discussed on turbulence modelling, and that multiphysics scale-resolving approaches are necessary since the heat

transfer between the gas-phase and metal parts has a strong impact on the entire behaviour of the combustion chamber and not only in the near-wall regions.

To verify what has just been introduced, the preliminary results will be discussed as follows: firstly, the results of the velocity field within the combustor will be discussed both qualitatively and quantitatively by employing profiles of velocity components along the radial direction. Subsequently, the temperature maps will be presented and finally, the effusion system will be studied by analyzing the wall temperature maps.

3.3.1 Aerothermal fields

The typical velocity structures of a swirling flow are well evident in all the contours shown in Figure 3.9. In the lower-left corner of the flametube the Outer Recirculation Zone (ORZ) vortex is well developed. As expected, the experimentally measured vortex structures are predicted quite accurately by the unsteady simulations compared to those obtained with the steady state approach. This can also be seen in the proximity of the pilot jet injection within the Inner Recirculation Zone (IRZ).

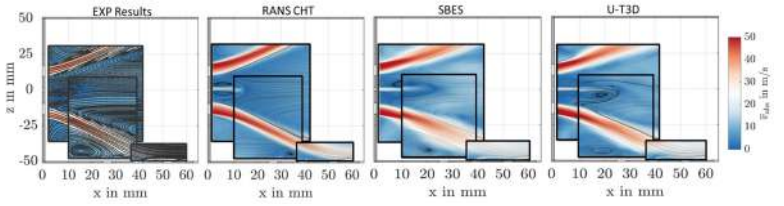

Figure 3.9: Reactive flow field comparison of the RSM combustor primary zone between experimental data, form [99] and different numerical approaches adopted

Comparing the two unsteady simulations, it is possible to note some differences in the behavior near the effusion-cooled wall. This is because in the SBES simulation the adiabatic wall is considered, while in

the U-THERM3D simulation the coupling with the solid plate provides greater temperature variations that affect the local velocity field. These considerations can also be confirmed by considering the one-dimensional radial profiles of the velocity components at 5mm from the bluff body, reported in Figure 3.10, which scaling the distance with respect to the diameter of the pilot fuel line corresponds to X/D = 2. The numerical approaches predict a higher axial velocity for the pilot jet about twice to the experimental data, whereas for the other radial positions the agreement is within 10% of the experimental reference value. As will be described in the following section, the modeling of the fuel pilot jet will have a strong impact on the whole behavior of the flame as it will vary the local mixture fraction conditions, influencing therefore the local reactivity. Moving the discussion to the next axial sections it is possible to observe the axial, radial and tangential velocity components profiles at two different axial locations, respectively at 25mm from the bluff body and before the combustion chamber exit, at 170mm. The comparison of tangential velocity components is only computed on the last two axial locations as not experimentally measured in the first section.

In Figure 3.11 the improvement introduced by unsteady numerical approaches in terms of velocity field and swirling flow prediction is clearly visible especially in the radial component velocity prediction. At the same time multi-physics simulations predict excessive penetration of the pilot jet that is also evidenced in the axial velocity profiles at 25mm that in dimensionless term correspond to X/D = 10, confirming what has already been discussed about the profiles in Figure 3.10. Concerning again the axial velocity profiles, there is a slight shift in terms of position of the bottom swirl jet interacting with the cooled wall. Near the flametube outlet, the numerical velocity profiles overestimate about 20% the experimental ones. In this zone, however, the experimental velocity profiles are subject to greater variability, as can be seen from the graphs in Figure 3.12 which show the comparisons between the radial profile of the root mean square (RMS) velocity components. Both unsteady simulations are reasonably in agreement with experimental RMS so turbulent fluctuations

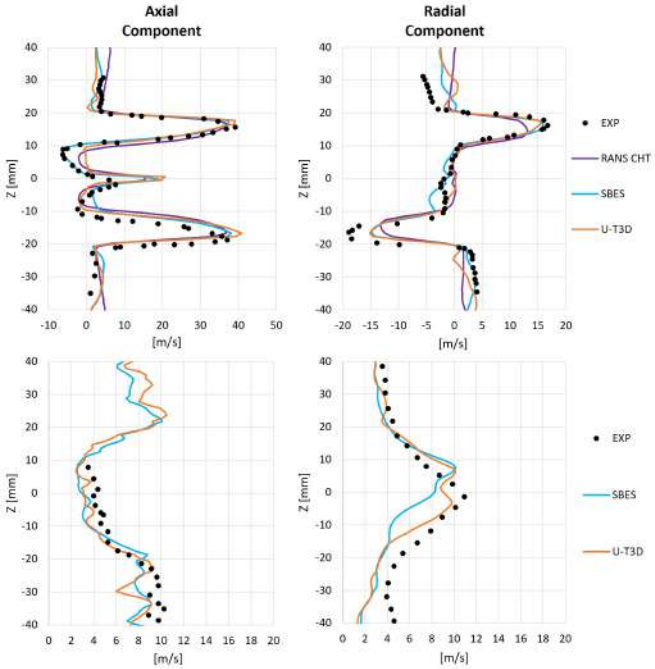

Figure 3.10: Radial distribution of axial and radial velocity components (top) and RMS at 5mm compared with experimental data from [98]

are correctly predicted by the SBES approach. In the primary zone, the main differences between experiment and numerical results are in proximity of the effusion plate, where the turbulent contribution of the interaction between main swirling flow and effusion jets is observed to be underestimated by the numerical approaches.

Focusing on the thermal fields obtained in this first numerical campaign of the RSM combustor operating with partially premixed flame, in Figure 3.13 it's possible to view the temperature maps of the flametube of the three different numerical approaches on the symmetry plane of the combustor; for the two unsteady simulations, the time-averaged maps are shown. The temperature maps obtained from the three simulations

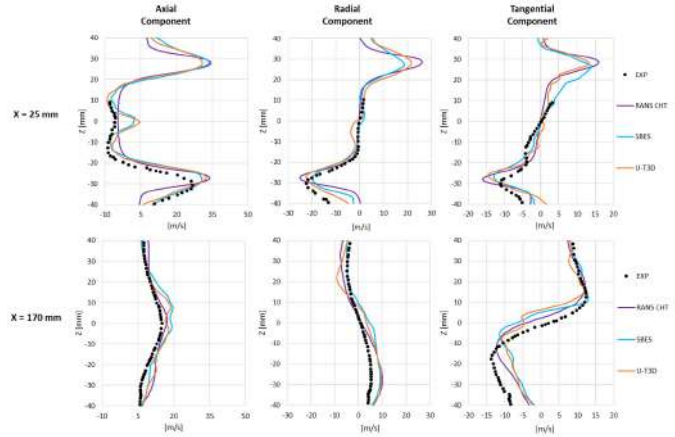

Figure 3.11: Radial distribution of axial, radial, and tangential velocity components at 25mm from the bluff body (top) and at 170mm (bottom) compared with experimental data from [98]

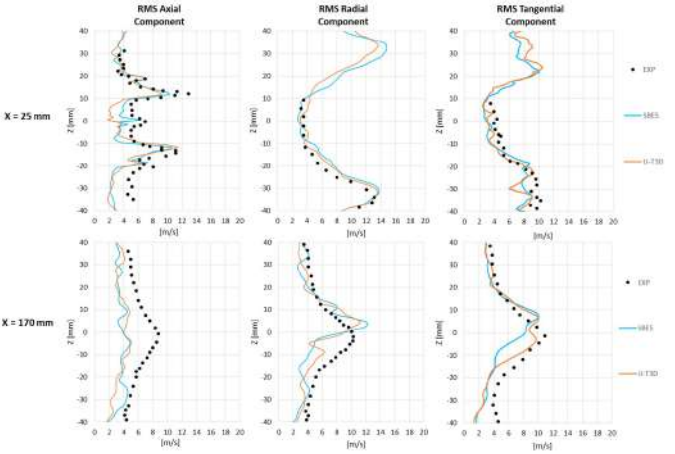

Figure 3.12: Radial distribution of axial, radial and tangential RMS velocity components at 25mm from the bluff body (top) and at 170mm (bottom) compared with experimental data from [98]

Figure 3.13: Temperature maps on XY midplane of the combustion chamber: RANS CHT (left), adiabatic SBES (Middle) and simplified U-THERM3D (right) simulations

are consistent with each other. While for the multi-physics simulations (RANS CHT and U-THERM3D) a rather symmetrical flame structure is recognizable this is not the case for the SBES simulation where only the aerothermal field is resolved. Furthermore, it is possible to notice a reduction in temperature inside the combustion chamber due to an accurate resolution of turbulence and thus of mixing which increase heat transfer combined with increased diffusion of the fuel pilot jet.

For the U-THERM3D simulation, this aspect is even more evident, but it is important to remember that in this simulation the temperature of the quartz optical accesses has been imposed to consider the heat loss towards the outside calculation domain. This boundary condition combined with the heat removed by the effusion cooling system leads to strong cooling of the flame which then causes a lower temperature in the entire combustion chamber. The penetrating behavior of the pilot fuel jet can be observed for all simulations. For the SBES simulation, the strong IRZ near the bluff body, visible in Figure 3.9, leads to an increase in temperature, due to a higher predicted mixing between fuel and oxidant and so to a higher reaction rate.

This phenomenon is also present in the U-THERM3D simulation, but it is of lesser magnitude since the recirculation vortex at the sides of the pilot jet is weaker, whereas it is almost absent in the steady simulation due to the underestimation of turbulence typical of RANS approach. For a deeper understanding from a quantitative point of view, radial temperature profiles are shown for different axial locations of the combustor in

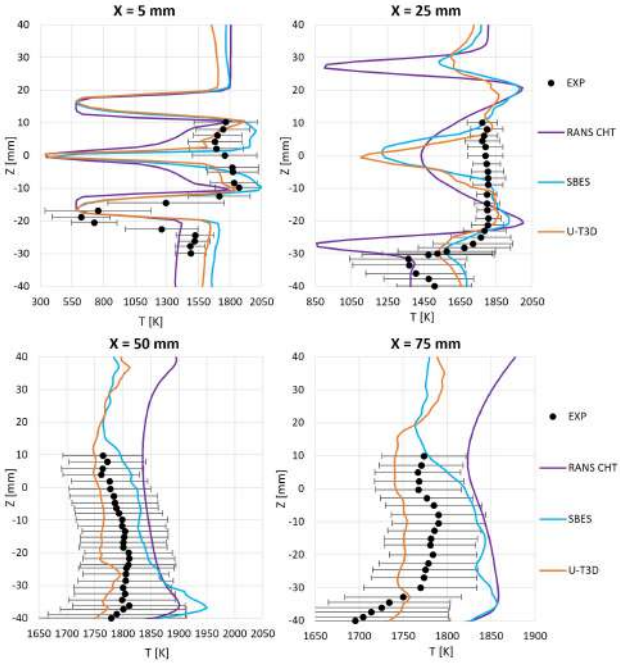

Figure 3.14: Temperature radial distributions at four axial sections of the combustion chamber compared with experimental data from [98]

Figure 3.14. The black bars referring to the experimental profile indicate the uncertainty of the measurement itself. It is evident from the temperature profiles, that the numerical procedures are not fully in agreement with the experimental measurements near the pilot jet area but at the same time for the axial sections located downstream in the combustion chamber, the simulations tend to predict the same temperature as the experimental one.

Although the test rig under consideration is academic, it is affected by an extremely complex aerothermal field, and the conditions in the primary zone are highly dependent on the behavior of the pilot jet. In fact, the modeling of a partially premixed flame is particularly critical,

moreover, the uncertainties linked to the thermal boundary conditions (not taking into account the pilot fuel heating that may occur during the passage through the swirler system) can have a significant impact on the reactivity of the mixture in the primary region.

To further highlight the criticality related to a proper fuel pilot modeling, temperature profiles on the combustor centerline are reported in Figure 3.15 In this case, the black bars relative to the experimental result indicate the minimum and maximum measured values.

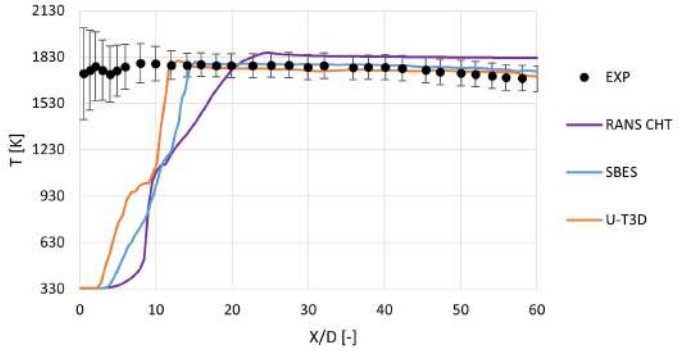

Figure 3.15: Gas-phase temperature profile along the combustion chamber centerline compared with experimental data from [98]

According to the CARS experimental measurements, a very high temperature was found to be that of unreacted fuel close to the bluff body for this reason a second data post-process i proposed in Figure 3.16. In this case, the data are obtained by an average over a circular sector with the same diameter of the pilot fuel supply pipe. Although with the second post-process the agreement with the experimental data tends to improve, the gap between the measured and predicted temperature in the pilot jet zone is still high. This is probably related to underpredicted turbulence mixing in the region next to the pilot inlet due to the imposed boundary conditions. This aspect could be improved by using profiles also for the turbulent quantities instead of the integral values currently

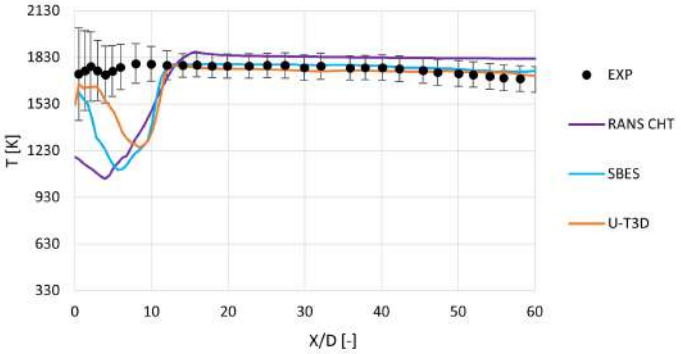

Figure 3.16: Gas-phase temperature profile averaged along a circular sector on the centerline of the combustion chamber compared with experimental data from [98]

used and derived from the fully developed velocity profile as previously described and will be applied for the next simulations. After the mixing zone and the complete reaction of the pilot fuel (about 10 times the pilot duct diameter), the numerically predicted temperatures agree with the experimental values. This agreement between the results allow to conclude that in terms of gas-phase temperature in the second zone of the combustion chamber, the temperature boundary condition imposed on the optical accesses permits to take into account the heat dissipated by radiation to the external environment through the quartz windows without the resolution of the RTE within the CFD simulations.

On the contrary, the differences between the two unsteady simulations in the primary zone can depend on the excessive heat removal by the quartz walls of the U-THERM3D simulation. Support of this thesis is seen in Figure 3.17, which shows the temperature maps of the XY midplane of the flametube. Focusing the attention on the primary zone it is possible to see the influence of the boundary condition imposed on the quartz walls of the U-THERM3D simulation compared to an adiabatic walls condition as imposed in the SBES simulation, leading to a good prediction for the

loosely coupled simulation, while the simulation of the gaseous phase only leads to an inevitable overestimation of the temperatures along the combustor centerline. Finally, the impact that the thermal boundary

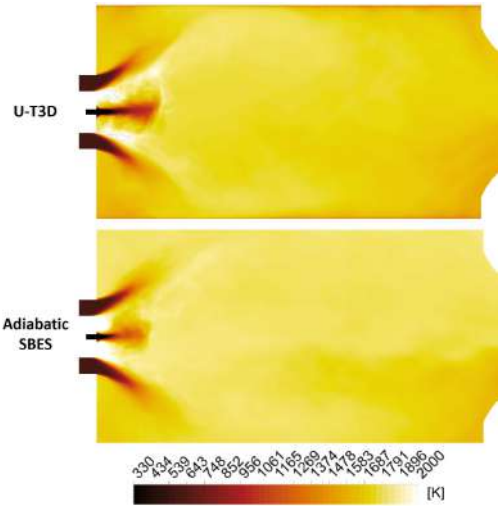

Figure 3.17: Time-averaged gas-phase temperature distributions on XY midplane of the combustion chamber for the simplified U-THERM3D (top) and the adiabatic wall (bottom) simulations

condition on the quartz walls has on the entire primary combustor zone is further emphasized by focusing on the ORZ. It is observed that the U-THERM3D simulation is significantly cooler than the same zone in the SBES simulation. This leads to excessive cooling of the flame with consequent change of the local reactivity of the flame and therefore flow characterization inside the IRZ.

3.3.2 Effusion-cooled plate temperature analysis

In this section the wall temperature maps on the hot side of the effusion cooled plate obtained for the two multi-physics simulations, respectively

the steady-state and the scale-resolved ones are shown in Figure 3.18. The maps have an extension of 20 mm in spanwise direction centered symmetry plane of the effusion plate while having an axial development. The

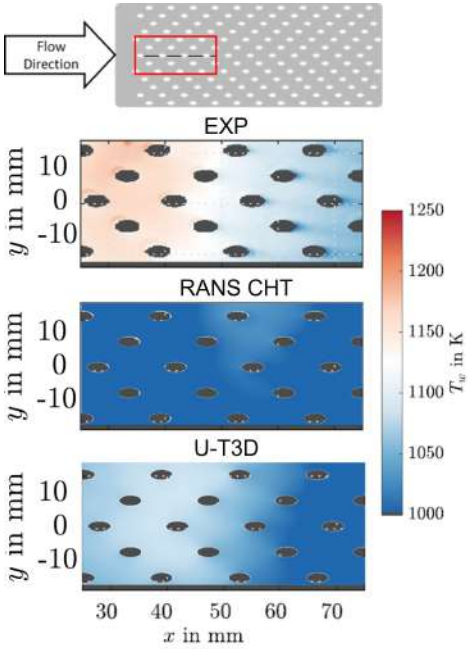

Figure 3.18: Wall temperature maps comparison: experimental data (adapted from [99]), steady-state CHT (middle) and simplified U-THERM3D (top) simulations

numerical distributions underestimate the values obtained experimentally. Whereas the RANS CHT simulation fails to predict experimental data, the U-THERM3D approach allows partial agreement with reference results. The wall temperature map achieved with the unsteady simulation is similar, at least in shape, to the experimental one and correctly predicts the thermal gradient in the axial direction.

A quantitative comparison of the wall temperature profiles is shown in Figure 3.19. Also, in this case, the black bar relative to the experimental

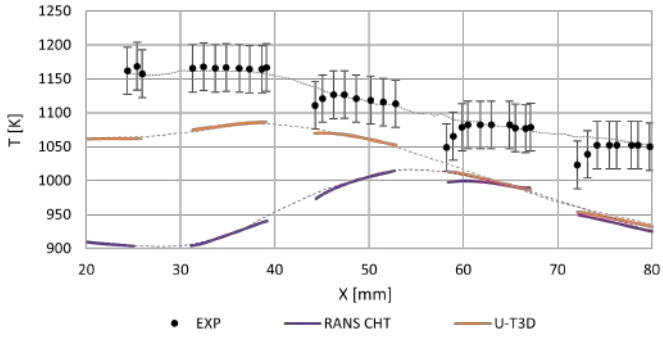

Figure 3.19: Wall temperature profile along the centerline of the effusion-cooled plate in the highlighted portion visible in Figure 3.18 and compared with experimental data from [99]

data indicates the measured uncertainty. For each case two curves are reported, the continuous lines represent the wall temperature along the liner centerline intercepting four effusion holes rows: these parts are masked. The dotted lines, on the other hand, represent the wall temperature between one row and the next in the spanwise direction without intercepting any holes. As previously said, the simulations tend to underpredict the wall temperatures. Although the underestimation is on the order of 100K, the U-THERM3D simulation is able to qualitatively predict the experimental temperature trend, showing a great improvement with respect to the steady simulation in the first region. The better predicted flame-wall interaction and turbulence lead to a more reliable computation of the local heat fluxes. The fact that both numerical simulations predict the same wall temperature after 60mm partially agrees with what has been reported in [99]. In fact, several parameters, including the swirl number and flame type, are varied parametrically in the experimental work, and the author concludes that after this axial distance from the bluff body the wall temperature only depends on the injected coolant flow rate.

To highlight these aspects, the velocity magnitude and radial component velocity contours at the exit of the centerline of the second and

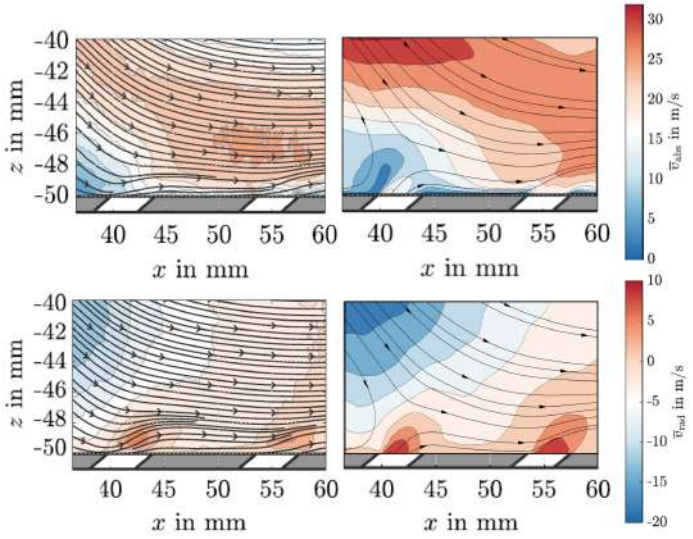

Figure 3.20: Magnitude (top) and radial (bottom) velocity distribution comparison at second and third rows exit of effusion holes. Experimental maps (left) adapted from [99]

third rows of effusion holes are shown in Figure 3.20. As it can be seen from the velocity fields, the radial component of the swirling flow seems less intense than that measured experimentally, this causes a locally lower interaction between the main swirling flow and the coolant coming from the first effusion holes, which therefore limits the mixing between the two streams. This fact could justify the lower predicted wall temperatures in the first part of the effusion plate.

Focusing on the cooling system a possible cause could be the underprediction of the penetration of the jets exiting the effusion cooling holes, leading to a mass adduction regime that does not occur. The low mixing between coolant and main flows could generate a well-defined protective film that limits wall temperatures and at the same time, tends to raise the temperature of the gas phase before the zone of interaction between hot gas and coolant, as understandable from the first two graphs

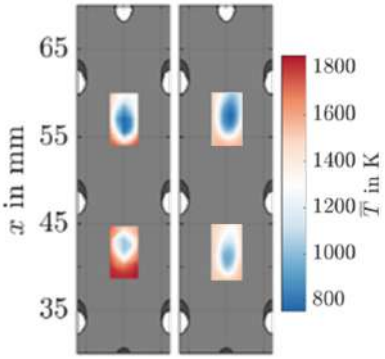

Figure 3.21: Gas-phase temperature distribution 0.5mm above the cooled liner: experimental maps adapted from [99] (left) and simplified U-THERM3D simulation (right)

of Figure 3.14. To deeply understand the behavior of the cooling system, the gas phase temperature comparison at 0.5mm from the cooled wall is shown in Figure 3.21 to highlight the shape of the central effusion jets of the second and third rows (flow direction from bottom to top). Qualitatively, a good agreement with the experimental measurement is achieved. Comparing the bulk outlet velocity magnitude on the centerline of the second effusion row by estimating it with overall time-averaged quantities, the simulation predicts a different distribution of the coolant mass flow exiting the holes. In detail, the bulk velocity is 16 m/s, while for the numerical simulation it is 12.5 m/s. This data not only indicates that the simulation predicts a different wall coolant distribution from the experimental one but also confirms what was previously anticipated, i.e. that there is an overestimation of the heat removed from the cooling system.

3.3.3 Concluding remarks

The main objective of the present preliminary work was to carry out the first reactive simulation of the RSM gas turbine combustor model operating under close-to-reality conditions, with a partially premixed flame and an effusion cooled liner. The numerical models and assumptions made are described. Several numerical approaches were compared, including a simplified version of the U-THERM3D multi-physics tool. In this first numerical study, it was decided to neglect the radiative heat transfer due to the assumption of the low emissivity of methane flames, whereas a uniform temperature was imposed to simplify the modeling of the quartz walls. The results obtained were compared with available experimental data, both in terms of aerothermal fields and solid wall temperatures. SBES approaches have been shown to predict the velocity, turbulence, and temperature fields accurately compared to the steady-state approach, except for the area where the fuel pilot jet develops. A significant improvement with respect to a RANS calculation is obtained thanks to the resolution of the largest scales of the turbulence spectrum with an affordable computational cost. Moreover, a more accurate prediction of the reactive flow field thanks to a scale resolving approach permits an improvement of the prediction of flame-wall interaction and so of the wall heat fluxes and temperatures. The effectiveness of the loosely coupled strategy is highlighted since it allows to properly take into account the heat losses related to the solid heat transfer. Therefore, it is evident how it is mandatory employing a multi-physics approach for a reliable prediction of the combustor aerothermal fields are since an adiabatic simulation leads inevitably to an overestimation of the temperatures. The wall temperature map obtained with the simplified version of the U-THERM3D approach correctly predicts the experimental pattern, although an underprediction of approximately 100K is computed.

Considering the purpose of the entire research work i.e. to optimise the procedure for managing data exchange between the different solvers for updating the boundary conditions on the coupled interfaces of the multiphysics problem, it is considered that the test case lends itself effectively to the verification of the new optimised workflow for the U-

THERM3D tool, which will be based on the internalisation of the solid domain in the CFD solver while maintaining a parallel architecture that allows temporal desynchronisation between the convective and conductive phenomena involved.

3.4 Application of STS method for U-THERM3D optimisation

As mentioned extensively above, the objective of the work is to compare the Solid Time-Step approach versus the simplified U-THERM3D tool for an initial optimization step of the latter. The results provided by U-THERM3D have already been analyzed in the previously section. To be as consistent as possible with the results already discussed, the numerical setup was not varied except for changes to improve agreement with the reference experimental data. The following paragraphs will highlight in detail the few changes made from the baseline simplified U-THERM3D simulation. In this part of the activity the impact of the near-wall region turbulence subgrid model on heat fluxes will be evaluated. In particular, the results obtained with the hybrid Stress-Blended Eddy Simulation (SBES) numerical approach will be compared with full LES ones. The results will firstly focus on the analysis of the flow and temperature fields within the combustion chamber and then focus on the wall temperature maps. After verification of the results, the calculation times of the different simulations will be analyzed, highlighting the critical issues of the U-THERM3D procedure and the savings obtained with the STS method. For complete contextualization of the data, a brief description of the supercomputing center used will also be provided.

3.4.1 Updating the numerical setup

In the previous section it was extensively discussed that the behavior of the pilot fuel jet has a strong impact on the whole combustion chamber. Since an overestimation of the pilot jet penetration ascribable to the use of integral values for the turbulent boundary conditions imposed on the inlet

was observed in the previous numerical campaign, in this new numerical task, profiles were also imposed for the turbulent quantities to improve the agreement with the experimental data. The opportunity to be able to change boundary conditions to improve agreement with the experimental data directly in the Solid Time-Step (STS) simulation was made possible by the complete validation of the methodology described in Section 2.4.

Concerning other numerical aspects, the same assumptions made in the previous Section 3.2 are also adopted in this new simulations. As already motivated the impact of radiative heat flux was neglected given the low brightness of methane flames. The same treatment was adopted for the quartz surfaces, meaning they were imposed at a fixed temperature of 1300K based on the preliminary RANS campaign conducted on the test case, Figure 3.6, due to the good agreement in term of gas phase temperature in the post-flame section of the combustion chamber, Figure 3.16.

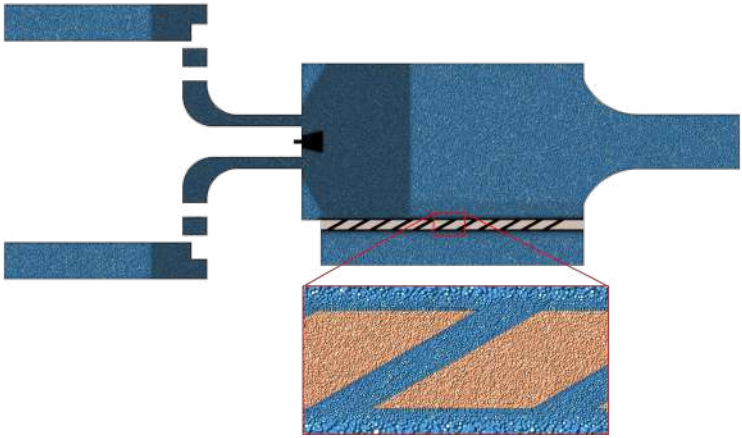

Figure 3.22: Computational grid exploited for the fluid domain in light blue and for the solid plate in orange

The STS method allows a specific time-step to be set for both the solid

parts and the gas phase, eliminating the problem of having to perform multiple simulations in parallel that exchange information with each other to update the coupling interfaces by permitting to simulate each domains in a single Fluent session [104].

To be able to use this methodology, it is thus necessary to create a new calculation grid that, compared to the previous one used (Figure 3.7), have to include the effusion-cooled plate within the CFD simulation. For the new mesh, exactly the same sizing was used as described in the previous Section 3.2. The mesh obtained has globally 66 million of polyhedral elements of which 42M are related to the fluid domain, the same size also obtained previously, while the 24M remaining belong to the solid domain, visible in Figure 3.22. Compared to the mesh generated for the U-THERM3D simulation of the solid domain used in of 7M the new one is much fine but should not be surprising, as it is affected by the refinements performed on the fluid domain in the near-wall regions. In any case, as will be discussed in the following sections this increase in grid elements will have no impact from a computational cost point of view.

The *index of quality*, LES_{IQ}, for LES simulation proposed by Celik et al. [114] is shown in Figure 3.23, on this one is also superimposed on the line identifying the unit value of the *Shielding Function*, f_{SBES}, already introduced in Section 3.2 for the similar simulation carried out using the SBES approach. As can be seen, the mesh employed achieves an index of more than 90% over the entire calculation domain.
By linking the index quality data with the shielding function, it can be seen that the SBES simulation fails to guarantee a full LES solution within the effusion holes so an underestimation of turbulent kinetic energy can be expected. In this sense, although the mesh employed guarantees a maximum y^+ equal to 1 on the effusion-cooled plate, the advantages of using the full LES approach are to be found downstream the holes, directly in the combustion chamber where the LES simulation will not underestimate the turbulent mixing between coolant and hot gases.

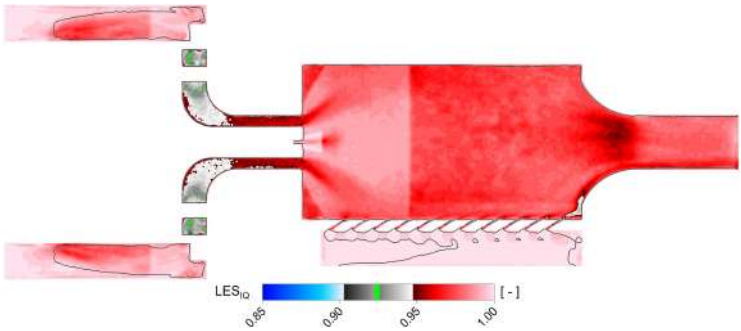

Figure 3.23: Time average of the quality index for LES proposed by [114] with the superimposition of shielding function = 1 identified by the black isoline for the similar simulation carried out with hybrid SBES approach

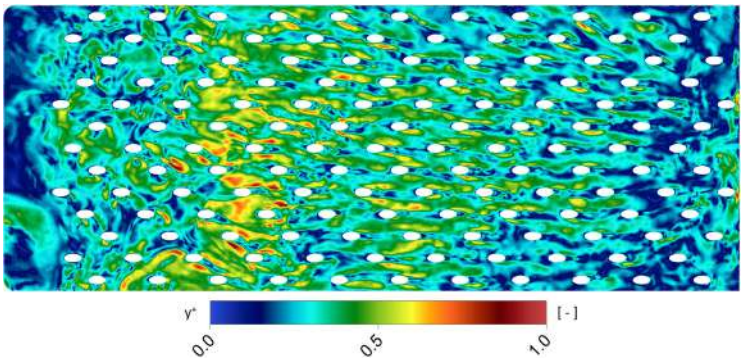

Figure 3.24: y^+ distribution on the hot side of the effusion-cooled plate

3.4.2 Gas phase velocity fields

From the comparison of the velocity fields in the primary zone of the combustion chamber in which the swirl flow is present, shown in Figure 3.25, it is noticeable how all simulations provide an accurate prediction of the swirling flow structures. The vortex in the Outer Recirculation Zone (ORZ) of the swirled flow is well predicted by both simulations with STS and very similar to that measured experimentally in [98]. The less

contracted shape of ORZ vortices predicted by STS simulations compared with the U-THERM3D simulation could be due to the less invasive handling of thermal boundary conditions between the gas phase and plate wall. It is worth mentioning that at each update of the U-THERM3D simulation, new wall temperature values are set for the coupled surfaces of the CFD domain while new convective heat flux is fixed on the solid surface of the effusion-cooled plate, operations that inevitably lead to discontinuities of the local thermal fields in the near-wall regions. Although the two simulations with STS are very similar in proximity to the effusion-cooled plate, it is possible to see a more intense recirculation for the LES simulation in which higher velocities are reached implying more interaction between swirled flow and the effusion-cooled wall.

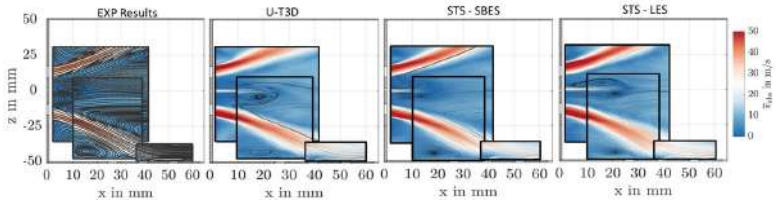

Figure 3.25: Comparison of primary zone reactive flow fields among experimental PIVs [98], simplified U-THERM3D simulation and numerical approaches carried out with the Solid Time-Step.

Well-developed vorticity structures can also be observed for the Inner Recirculation Zone (IRZ), but they appear to be shifted forward with respect to experimental PIVs. Despite the imposition of turbulent profiles at the pilot jet inlet, simulations with STS predict jet behavior that is still too penetrating. For the LES simulation, it can be noted that the vortices triggered by the shear layer of the pilot fuel jet are closer to the bluff body than for the two SBES approaches, an indication of more intense mixing.

From the radial profiles of the velocity components, it is possible to confirm the above considerations. In Figure 3.26 the velocity profile of the

axial and radial velocity components are shown together with the Root Mean Square (RMS) values at a distance of 5mm from the bluff body and equivalent to two diameters of the pilot fuel supply duct. From this detailed comparison, it is possible to observe that there is an overestimation regarding the pilot fuel jet penetration, since the velocity predicted by the simulations is about twice the experimental one. Concerning the swirl jets these are well reconstructed in terms of both axial and radial velocity, only a slight displacement of the swirl jet interacting with the effusion-cooled plate can be seen, identified by the negative Z coordinate. That obtained by the simulations is a swirl flow almost symmetrical with respect to the axis of the combustor chamber. Whereas from the experimental evidence, the latter seems more open toward the plate. This is confirmed by the fact that the minimum radial velocity value is not equal in absolute value to the maximum. Since only the part of the swirl jet interacting with the coolant air is not correctly predicted this could be due to a different behavior of the first rows of effusion holes between numerical and experimental results. Moving to the radial RMS distributions of the two velocity components it can be seen that the proposed numerical approaches can correctly capture turbulent fluctuations. In fact, both in terms of shape and numerical values, the predicted numerical profiles are very close to the experimental ones.

Moving far from the bluff body, the agreement between simulations and experimental data improves. Figure 3.27 shows the velocity profiles of all three components at 25mm and 170mm of the burner axial coordinate. What can be immediately noticed in the first section is that the axial velocity profiles of the STS simulations are no longer affected by the presence of the pilot fuel jet as in the U-THERM3D simulation, due to the change in the turbulent boundary condition imposed on the fuel pilot inlet which promotes a faster mixing within the combustion chamber. Also in this section, it is possible to see a slight difference in terms of the shape of the lower swirl jet predicted by the simulations, resulting in a modestly more closed flow, compared with the experimental data. In addition, the velocity profiles in this section confirm that the LES simulation has a

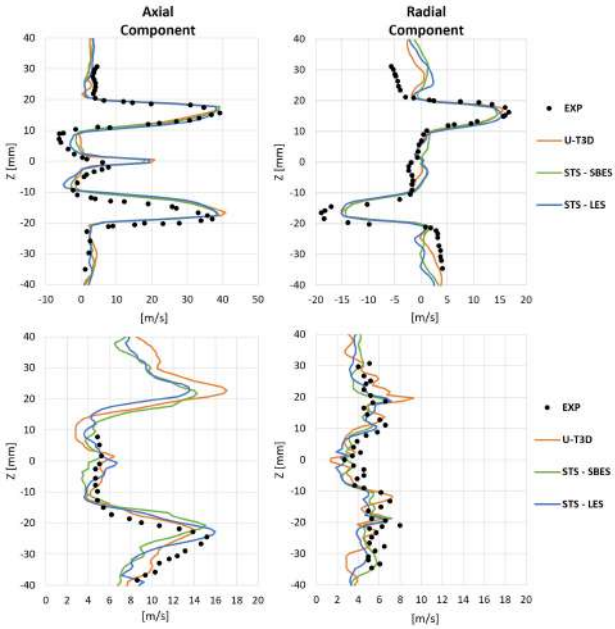

Figure 3.26: Radial distribution of axial and radial velocity component (top) and RMS (bottom) at X = 5mm

slightly faster swirled flow than the SBES calculation so more interaction between swirl flow and coolant air can be expected. Analyzing the profiles before the beginning of the converging section at the combustion chamber outlet, it can be seen that the agreement is almost total for the axial and radial velocity components, while there is an underestimation of the tangential component in the lower part of the combustion chamber for all numerical approaches reported. This trend could be due to excessive coolant accumulation in near-plate regions, which tends to dampen the tangential swirl flow wakes against a slight overestimation of the other two velocity components, which may be more affected by jets exiting the effusion holes. Unfortunately, no visualizations of the flow field in the zones near the plate are available for this axial quota, and at the

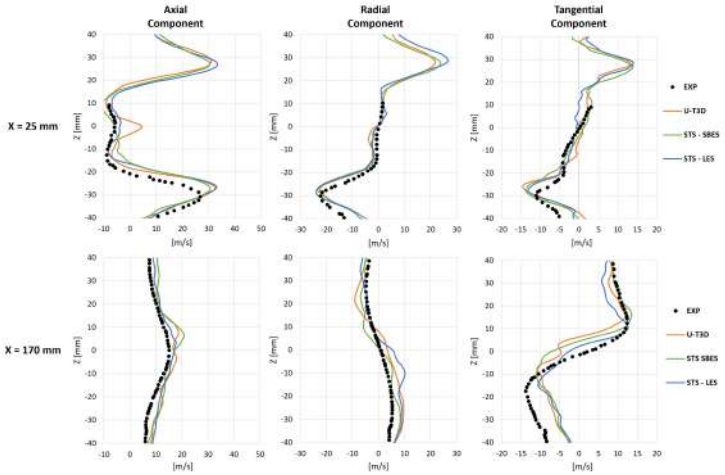

Figure 3.27: Radial distribution of axial, radial and tangential velocity component at X = 25mm (top) and X = 170mm (bottom)

same time, all experimental data stop at 10mm from the effusion-cooled plate so it is not possible to better contextualize the numerical results. Moving the analysis to the radial distributions of the RMSs of the three velocity components, shown in Figure 3.28, it can be seen that in the central region downstream of the pilot jet, i.e., 25mm from the burner, the agreement improves by passing from the SBES approach to the LES approach. This trend confirms what has been analyzed previously, namely that the application of turbulent profiles to the pilot jet inlet not only promotes mixing but also moves the numerical results closer to the experimental ones; thus confirming what previously discussed in Section 3.3 in which it was stated that the excessive penetration of the pilot jet could be partly due to underestimation of turbulent structures. Focusing attention on the portions closest to the perforated plate, i.e. in the RMS profile of the axial velocity component at 25mm, again confirms what has already been said for the velocity profiles that is, a more closed swirl flow predicted by numerical simulations leads to an underestimation of

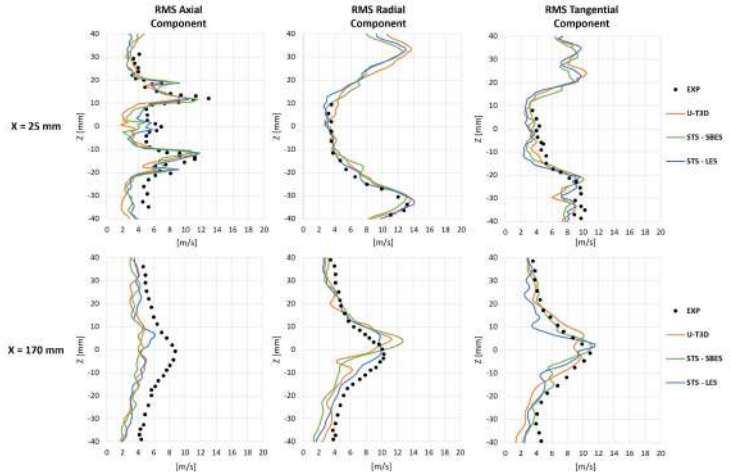

Figure 3.28: Radial distribution of axial, radial and tangential RMS velocity component at X = 25mm (top) and X = 170mm (bottom)

vortex structures. For the other two components, instead, total agreement with the experimental data can be noted. For the sections near the combustion chamber outlet there is an underestimation in terms of RMS of the axial component but of rather limited magnitude. For the other two components, the same conclusions can be drawn as for the velocity profiles, namely that the underestimation near the effusion-cooled plate could be due to an overly cohesive layer of coolant.

3.4.3 Gas phase temperature fields

The time-averaged temperature maps obtained by STS method and the one obtained by U-THERM3D simulation from the previous section 3.3 are shown in Figure 3.29. It can be seen that the three simulations are in agreement with each other, but by focusing on the IRZ, it is evident once again the impact that the behavior of the pilot fuel jet has on the entire combustion chamber. The temperatures in the flametube are higher in the simulations conducted with the STS than in the U-THERM3D

Figure 3.29: Time-averaged gas temperature at combustor chamber midplane for the simplified U-THERM3D simulation (left), the STS method obtained with SBES approach (middle) and LES approach (right)

simulation. From these, it can be observed that the pilot jet of fuel, although it has a penetrating behavior, has a greater diffusion within the primary region increasing the reactive process rate. Comparing the two STS simulations, it can be observed that a more intense reaction occurs near the shear layers of the swirled flow in the LES calculation favored by the increased mixing near the bluff body already described by the analysis in Figure 3.25.

To better quantify the differences between the three simulations analyzed, the radial temperature profiles in four relevant sections are shown in Figure 3.30. The graphs also present the minimum and maximum temperature bars acquired during the experimental test.

From the 5mm profiles, the temperature underestimation in the central region of the combustion chamber in which the pilot fuel jet is present is evident. In fact, in this section the presence of unburned fuel is no longer detected by the experimental tests while numerically there is a temperature value close to its injection value of 333K. From this profile, the slight shift in the prediction of the swirled jet discussed earlier in the velocity profiles analysis can be observed again. The section at 25mm from the bluff body is particularly interesting to better understand how far the pilot jet is penetrating within the combustion chamber. While for the U-THERM3D simulation, the unburned jet is evident in the central area, the STS simulations show instead a reacted flow, in which only a small part related to the pilot jet remains visible for the LES simulation.

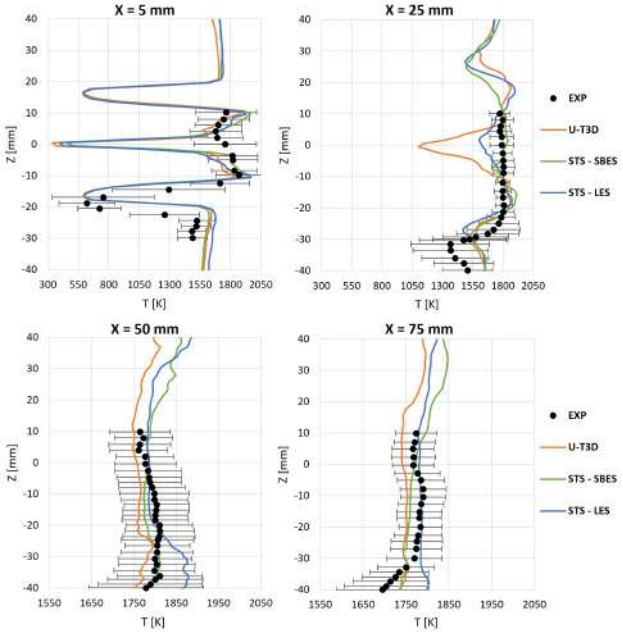

Figure 3.30: Time-averaged of the gas phase temperature radial profiles comparison with experimental results from [98]

Moving closer toward the cooled plate, the gap between experimental and numerical results increases, probably due to less interaction between swirl flow, which is slightly more closed, and cooling air leading to less turbulent mixing.

Moving downstream the radial temperature profiles tend to have an excellent agreement in the central areas of the combustion chamber. Even if LES simulation shows a slight overestimation of temperature in the region closer to the plate compared with the experimental values but is still within the range of measured data.

The goodness of temperature prediction in the central part of the combustor is well evidenced once again in Figure 3.31. To better understand the results, these are plotted along the axial abscissa scaled with respect

to the diameter of the pilot fuel jet. The profiles shown are obtained by averaging over a circular sector with a diameter of 2.5mm, the same as the duct fuel pilot. Based on what was discussed in the precious Section 3.3, this approach was preferred because experimentally an extremely high value is measured near the bluff body, which is typical of an already reacted mixture, even where pilot fuel injection occurs. This behavior is particularly strange unless experimentally the mixture reacts directly within the duct or there is some pulsating effect that may have affected the measurement. Within the first ten through diameters, the simulations severely underestimate the temperature because in this zone the mixing of the fuel is taking place that will only later bring it into the condition to be able to react. Please note that the pilot fuel injection temperature is set to 333K according to the data given in [98, 99] but it must be specified that possible heating effect of the pilot fuel in crossing the duct was neglected in the simulations due to lack of further data to estimate it. In any case, it is considered improbable that this effect would lead to the full match of the experimental data in the zones closest to the bluff body. After this region the numerically obtained profiles coincide with the experimental values, so the rective conditions inside the combustion chamber are well predicted by all numerical approaches.

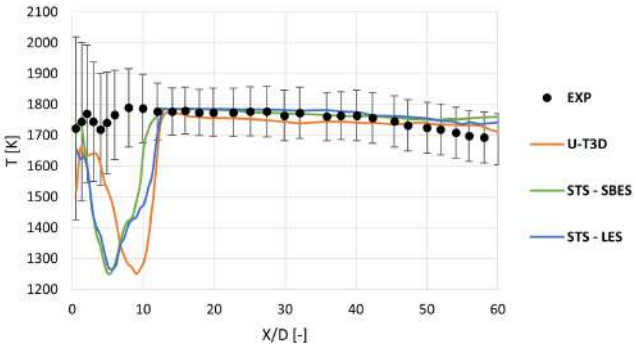

Figure 3.31: Time-averaged profiles of the gas phase temperature along the combustor centerline

3.4.4 Effusion-cooled plate wall temperature

Figure 3.32 shows the temperature maps obtained through different multiphysics and multiscale approaches used and are limited to the portion highlighted of the effusion-cooled plate experimentally investigated by Greifenstein et al. [99]. Although there is a gradual improvement in agreement with the experimental data, the wall temperature maps obtained by the STS method continue to underestimate the experimental value obtained in [99]. Reminding that the U-THERM3D simulation carried out in Section 3.3 was performed with the same computational grid and with the same SBES numerical approach it becomes evident how the behavior of the pilot fuel jet also impacts the wall heat transfer and how critical its modeling is since it strongly influences the reaction in the primary region. Specifically between the two central maps in Figure 3.32 only the boundary condition related to the turbulence imposed on the pilot fuel jet inlet changes and the latter was derived from the previous simulation U-THERM3D. As it was also observed in detail from the analysis of Figure 3.29, the different modeling of the jet leads to a non-negligible change of the entire temperature pattern within combustion chamber. Although the change made brings the numerical result closer to the experimental data, this is still not sufficient for the correct prediction of heat fluxes reaching the effusion-cooled plate. In particular, by focusing on the temperature map obtained by the LES approach part of the gap with the experimental result is further reduced. This result allows to conclude that part of the underestimation was due to the modeling of sub-grid turbulence. The SBES simulations adopt a kω-SST RANS turbulence model for the near-wall region which seems to be not the most suitable for predicting the proper behavior of an effusion cooling system. This RANS model leads to an excessive underestimation of vortex structures that should be generated near the wall by all the effusion jets entering the chamber and consequently limits the turbulent mixing between the combustion gases and the coolant air, thus generating too thick a layer of coolant air on the wall and, finally, holding the plate at a lower temperature than it should be at.

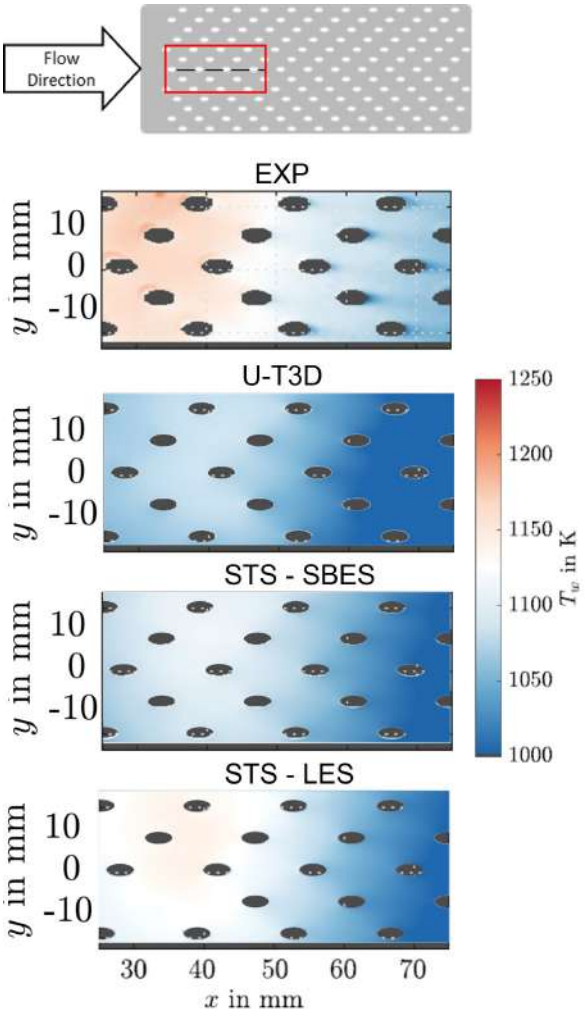

Figure 3.32: Wall temperature distributions on the highlighted portion of the effusion-cooled liner. The experimental maps is adapted from [99]

As it can be seen from the one-dimensional wall temperature profiles in Figure 3.33, the difference between numerical results and experimental

measurements is greatly reduced for the STS-LES simulation. The data in the graph have discontinuities where the plate symmetry plane cuts the effusion cooling holes. The beginning of the measurement portion of the effusion-cooled plate is located near the outer recirculation zone (ORZ). From what is seen in Figure 3.25, the vortex reproduced by the LES simulation is the one closest to the experimental. The higher vortex intensity brings greater recirculation of burned gas and consequently an increase in local temperature. The temperature peak reached near 40mm is well predicted by the LES simulation which presents the greatest swirling flow-cooling air interaction that leads to a significant impingement on the cooled wall. In this portion of the plate, the results differ from experimental results by 15K. On the contrary, SBES simulations, present the

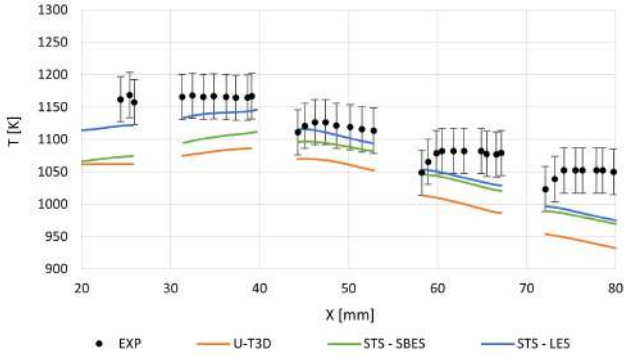

Figure 3.33: One-dimensional wall temperature profiles along the centerline of the analyzed portion of the effusion-cooled plate

same temperature level at the beginning of the plate, which is lower with respect to the one computed by the STS-LES calcualtion. However, the simulation with STS has a more pronounced thermal gradient due to the higher reactivity in the primary zone generated by the faster mixing of the fuel pilot jet. As seen from Figure 3.29, the STS simulations have higher temperature zones near the walls propagating from the high reactivity region of the IRZ. This once again confirms how complex the flow and

thermal fields of this academic combustor are, and how the pilot fuel jet modeling is a key aspect for correctly predicting not only the velocity and temperature of the gas phase inside the combustion chamber but also the thermal flux reaching the walls.

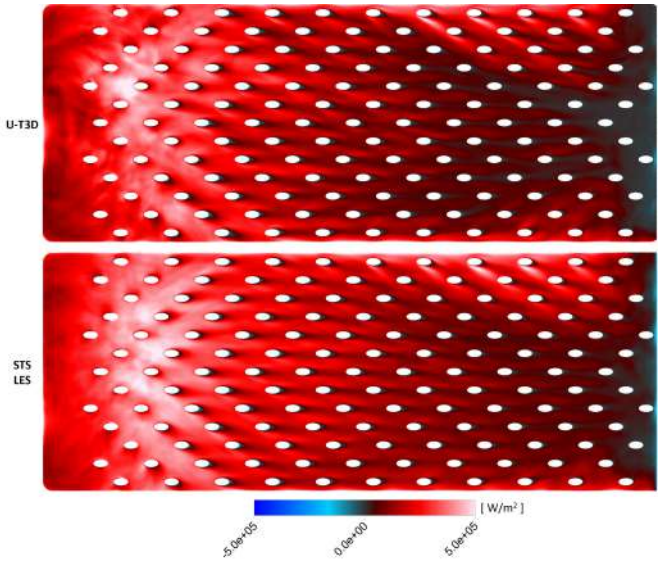

Figure 3.34: Time-averaged heat flux comparison between the simplified U-THERM3D (top) and the STS carried out with LES approach (bottom) on the effusion-cooled plate

These aspects can be confirmed by Figure 3.34, which shows the comparison of the heat flux investing the effusion-cooled plate wall between the simplified U-THERM3D simulation and the STS simulation with LES approach. The figure only shows the comparison between these two simulations to highlight the differences between the two numerical methods adopted since the simulation conducted with STS-SBES does not vary significantly from the map obtained with U-THERM3D shown. The maps not only justify the one-dimensional trends shown in Figure

3.33 but also verify what was stated in Section 3.4.1 , namely that the LES approach allows for more accurate prediction of wall flow because it does not underestimate the turbulent mixing that occurs outside the boundary layer between the coolant and the hot gases as SBES methods does. This conjecture is verified by noting that the heat fluxes predicted by the LES simulation tend to be higher, a result that comes closest to the experimental data. Although this occurs throughout the cooled-plate showing less cohesive and more diffusive effusion jets, it is clearly seen in the swirl flow impact zone, where the maximum heat flux is reached, and at the beginning of the plate, in the ORZ, where recirculation vortices dominates mass and heat transport. This behavior allows the conclusion that the underestimation of turbulent structures in simulations with effusion cooling has a strong impact on the determination of heat fluxes. Furthermore, it is possible to add that outside the boundary layer, this underestimate can be partially compensated with an LES approach compared to that established with a wall RANS modelling characteristic of hybrid approaches.

The same conclusions can also be visualized in term of total cooling effectiveness η_{TOT} defined as in [99] and according to Equation 3.7. T_∞ represents the temperature of the burned gas that is not affected by the cooling system. This term is defined as the temperature along the combustor centerline in the post-flame zone. Given the good agreement of the simulations with the experimental data in the considered combustor zone, shown in Figure 3.31, it was decided to take the same value used in [99] and equal to $T_\infty = 1775K$. The other two terms appearing in the equation are the wall temperature, obtained by multiphysics and multiscale simulations, denoted with T_w, and the cooling inlet temperature, T_c, set constant and equal to what is shown in Table 3.2 as in the experimental work [99]. Due to the definition used for total cooling effectiveness, the trend obtained is nothing more than a scaled function of the wall temperature and therefore the agreement between the numerical and

experimental data is the same to that shown in Figure 3.33.

$$\eta_{TOT} = \frac{T_\infty - T_w}{T_\infty - T_c} \tag{3.7}$$

In CFD simulations conducted with the STS method, a passive scalar

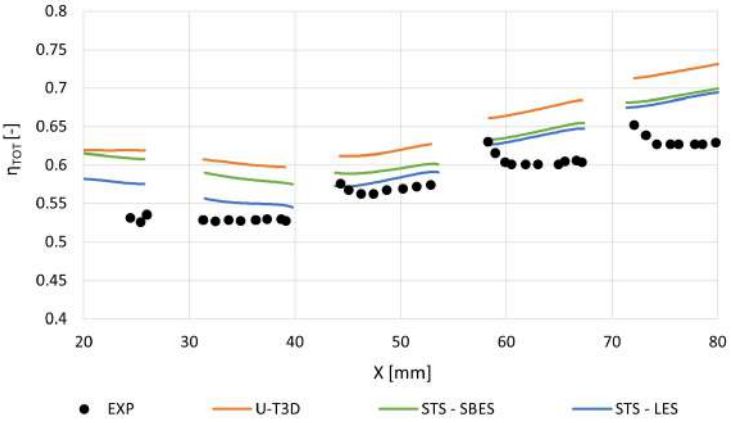

Figure 3.35: One-dimensional total cooling effectiveness profiles along the centerline of the analyzed portion of the effusion-cooled plate

was injected at the cooling system inlet. Its gives an indication of how the coolant is distributed over the effusion-cooled surface. Furthermore, this quantity can be interpreted as an adiabatic cooling effectiveness, η_{AD}, in analogy to Pressure Sensitive Paint (PSP) experimental techniques conducted under truly adiabatic conditions [14, 15, 16, 17, 18].

Figure 3.36 shows the adiabatic effectiveness maps obtained by CFD simulations. For both are superimposed also the respective total cooling effectiveness isolines, defined in Equation 3.7. The minimum value of this quantity is set limited to the lowest measured value, visible in Figure 3.35, to simplify visualization of the isolines. From the maps, it is possible to visualize the distribution of the effusion coolant flow over the plate. In the central portion at the beginning of the plate, the typical effect of

swirling flow on an effusion-cooled plate, identified by the low-efficiency zone, can be seen. Minimum coverage is achieved where the interaction of the swirling flow with the plate occurs leads to the inevitable washout effect that destroys all the coverage provided by the coolant.

These maps allow further justification for what has already been

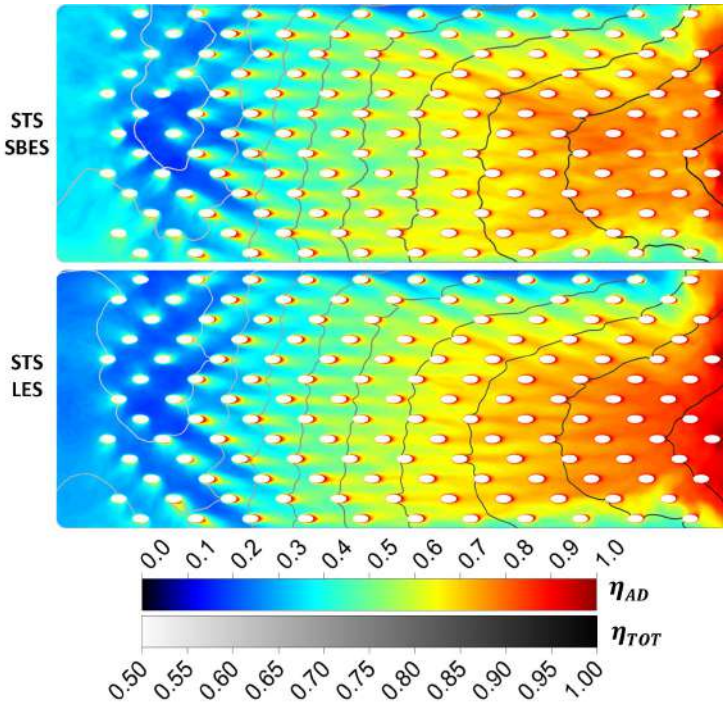

Figure 3.36: Contours of adiabatic cooling effectiveness obtained with the Solid Time-Step method for SBES approach (top) and LES (bottom) with total cooling effectiveness isolines superimposed.

discussed previously regarding the numerical approaches and for what have been stated for the velocity maps in Figure 3.25, as well as one-dimensional wall temperature profiles in Figure 3.33. In the initial portion of the cooled plate, near the first row of effusion holes, it can be noted

that the adiabatic effectiveness is lower for the simulation performed with LES approach. This is due to the greater intensity of the vortex structure present in the ORZ, which promotes mixing and tends to bring more hot gas flows near the plate. While no particular differences are evident in the central portions of the cooled plate, the situation changes at the end of the plate where there is a high accumulation of coolant, even more present in the LES simulation. Again, the results are in agreement with what has already been stated in the discussion of velocity profiles at 170mm (Figure 3.27) regarding the near-wall region flow.

By comparing axial and radial velocity maps near the second and third central rows of effusion holes in Figure 3.37, it is possible to have further verification of what was previously stated. In fact, it can be observed that the swirled flow tends to interact more with the effusion-cooled plate in simulations with STS, especially for the LES approach pointing out once again how near-wall region RANS modeling has no negligible impact on the prediction of turbulent structures. Regarding this, it is possible to see how the velocity distributions of the two SBES approaches are similar to each other. The same trend can also be observed from the radial velocity distributions in which less penetrating effusion jets can be observed for simulations carried out with the STS-LES approach.

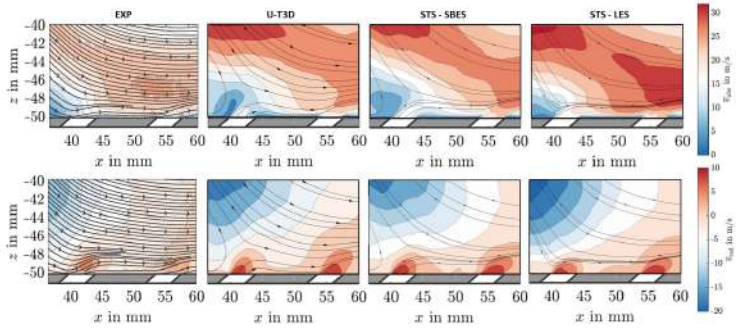

Figure 3.37: Near-wall region magnitude (top) and radial (bottom) velocity maps comparison. The experimental maps are adapted from [99].

Despite the agreement with the experimental data being increased in the STS-LES calculation, it is quite clear how all numerical approaches underestimate the blocking effect of the swirled flow on the first rows of effusion holes. These maps highlight even better what emerged from the analysis of the velocity profiles regarding the position of the swirled jet in Figure 3.27 and better contextualize the underestimation of the plate wall temperature in its initial zone in Figure 3.33. Another important aspect to be careful about when analyzing the radial velocity maps is that Greifenstein et al. in [99] showed two operating configurations for the cooling system during experimental tests. The author refers to two working conditions, the first in which there is an effective coverage contribution made by the holes where the radial velocity is positive, shown effectively in Figure 3.37 and a second in which instead the holes are affected by a negative radial velocity that minimizes the entry of coolant into the combustion chamber. For the chosen test point, the experimental behavior shown in Figure 3.37 is recorded on 66% of the measured samples. Such detailed evaluation was not conducted numerically, but in light of the results obtained a deeper investigation of the behavior of the effusion cooling system is necessary to better understand the discrepancies between simulations and experimental results. In fact, a more stable behavior of the cooling system in terms of the flow rate released from the numerically predicted effusion holes could lead to a higher coolant presence and thus an excessive lowering of wall temperatures.

3.4.5 Computational cost analysis

Before entering into the discussion regarding computation times, it seems proper to give a brief description of the super-computing center used to carry out the entire numerical campaign presented. The computing infrastructure used is the cluster named Karolina owned by IT4Innovations National Supercomputing Center within the Technical University of Ostrava in the Czech Republic. The petascale system employed consists of 831 computing nodes of which 720 are CPUs. Since CFD simulations with the ANSYS Fluent solver were conducted exclusively on CPUs their

main characteristics are summarized in Table 3.3.

Table 3.3: Characteristics of the CPU compute nodes of the IT4I Karolina cluster.

Processors	2x AMD ZEN 2 EPYC 7H12 2.6GHz
Number of Cores per Compute Node	128
RAM per Compute Node	256 GB
Max Memory Bandwidth	190.7 GiB/s
Interconnection	Infiniband HDR 200Gb/s

Figure 3.38 shows the scalability performance of the CFD solver tested with the numerical RSM combustor reactive test case running on the Karolina cluster. Due to the high number of computational grid elements, performance could not be tested on a single node of the cluster due a minimum memory requirements. As it can be noted from the graphs, the ANSYS Fluent solver for LES simulation performs very well up to eight computational nodes, a range in which it has an almost ideal efficiency and a linear speedup. The RSM combustor simulations were performed

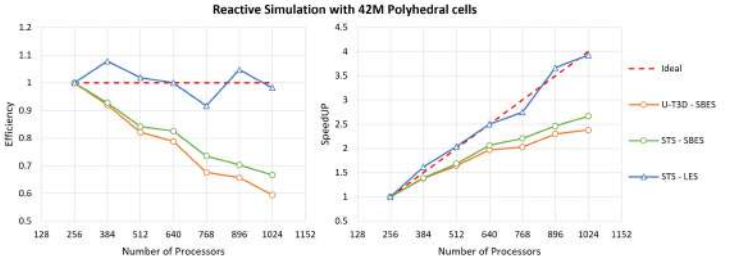

Figure 3.38: Performance of ANSYS Fluent simulation on IT4I Karolina Supercomputer.

by fixing the number of time-steps to be simulated, ensuring a minimum physical time of two flow-through times for the fluid domain. To obtain a statistically independent first moment, two additional flow-through times were performed to average all quantities of interest, for a total of four

flow-through times. To perform a detailed comparison of the calculation times of each proposed numerical method, it is therefore convenient to refer to the time required to perform a single fluid time-step.

Regarding the simulations carried out with the STS method, there is no difficulty in monitoring the calculation time of a single time-step and neither for the U-THERM3D simulation but it is worth mentioning that the latter is composed of several simulations carried out in parallel that exchange data with each other to update the coupled boundary conditions every ten fluid time-step. Therefore, part of the work focused on quantifying the time required for input/output operations between the two coupled simulations.

For the RSM combustor there are three coupled surfaces, consisting of the hot surface of the plate, i.e., facing the flametube, the cold surface facing the coolant air supply plenum, and the set of wet surfaces of the effusion holes through which coolant flows into the combustion chamber. Exchanged temperatures and heat fluxes are written for each node of the calculation grid belonging to the indicated surfaces. The summary of the number of points for which quantities have to be written is given in Table 3.4. It is worth to highlight that through the use of the methodology for effective effusion hole resolution [20, 81], with which U-THERM3D has already been used [21, 78], part of the data to be exchanged would itself be eliminated. In particular, all the part of the data exchanged concerning the effusion holes would be avoided. Although the number of data exchanged might be smaller than the treatment used in the manuscript it should be pointed out that the number of values to be written and read from the simulation is extremely case-dependent. It is worth to remember that the combustor under consideration is an academic type with simplified geometry compared to an industrial combustor, so it is evident how much these operations can impact on the overall computation time regardless of whether the effusion holes are actually discretized or modeled within the computational domain.

The times to perform the write and read operations required to update the coupled boundary conditions between the two solvers of the

Table 3.4: Number of point values written by the U-THERM3D procedure for each solver coupling.

Hot side effusion-cooled plate	500k
Effusion-cooled holes	635k
Cold side effusion-cooled plate	500k

U-THERM3D tool are shown in Figure 3.39. As illustrated in the figure, the time required for coupling operations is not affected by the number of nodes on which the simulation is performed and is always in the order of 60 seconds.

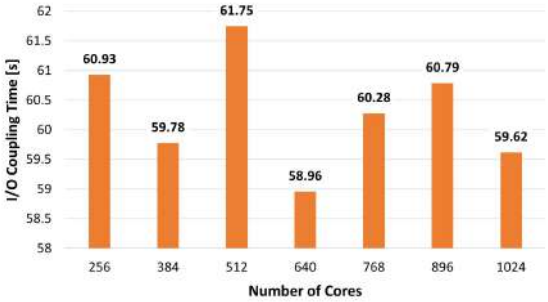

Figure 3.39: Coupling time of U-THERM3D tool for the RSM combustor performed on IT4I Karolina supercomputer.

At this point, keeping in mind that for the U-THERM3D simulation, the coupling is performed every 10 fluid time-steps, it is possible to calculate an equivalent time for the performance of a single time-step that also includes the time required to execute the coupling between the different solvers. The scalability performance of the 3 methods considered for solving conjugate heat transfer problems with a loosely-coupled approach is shown in Figure 3.40. Also shown in the figure there is the curve for the ideal U-THERM3D case, meaning excluding boundary condition update times, which in other words, coincides with the simulation of the gas phase alone. This curve allows the full appreciation of the power of

loosely coupled methods for solving conjugate heat transfer problems: these methodologies allow multiphysics problems to be solved with a little more computational cost, for the same numerical approach used, than a gas phase simulation alone. In particular, it can be noted that the inclusion of the solid domain within the fluid one for the STS method, does not result in any kind of computational cost increase, although it has been discretized with a large number of elements, about half of the number of the fluid domain.

Another important outcome that can be drawn from the present study is that the LES approach takes about 10 seconds less time to perform a single time-step on the same computational domain compared to the corresponding SBES simulation. This aspect should not be surprising since turbulence is not modeled in this numerical approach, so compared with the SBES simulation two fewer equations are solved, those of the kω-SST model. It should be specified, however, that in this case, it was possible to use the same computational grid of the SBES simulation as the criterion for the correct solution of the LES simulation was satisfied, otherwise, it would have been necessary to use a finer calculation grid with a consequent increase in computational cost. The same results are

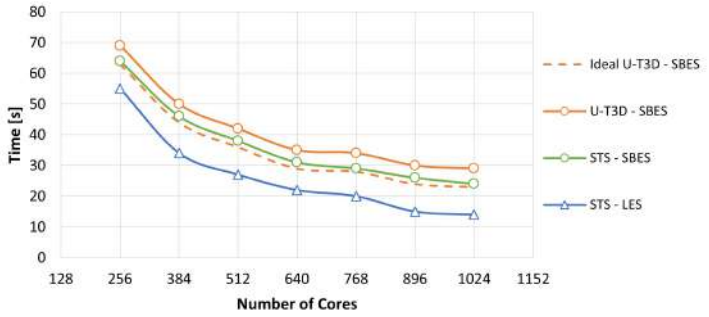

Figure 3.40: Comparison of single time-step execution times for the 3 loosely-coupled approaches considered for the RSM combustor simulations performed on IT4I Karolina supercomputer.

reported in terms of computational cost expressed in the number of cores

per computation hour in Figure 3.41. In these terms, the savings, given the same SBES numerical approach, with the use of the STS method alone is 7% by simulating on two nodes of the HPC infrastructure up to 18% on eight nodes. Using a numerical LES approach, on the other hand, savings are up to 50%. Indeed, by increasing the computational resources, the actual computation time decreases but since the execution time of the operations for updating the boundary conditions of the U-THERM3D simulation remains almost unchanged the specific weight of these on the overall computational cost increases. Looking at the data shown in the Figure 3.41, the comparison with a strongly-coupled CHT simulation would be even more striking, as the latter would require a computational cost in terms of cores per hour three orders of magnitude higher.

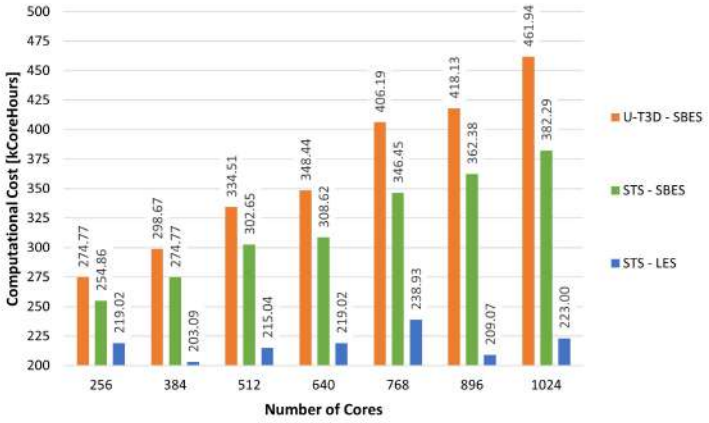

Figure 3.41: Comparison of computational cost for the 3 loosely-coupled approaches considered for the RSM combustor simulations performed on IT4I Karolina supercomputer.

3.4.6 Final considerations

In this chapter, the first application of the simplified version of the optimized workflow of the loosely coupled U-THERM3D tool for the accurated evaluation of heat flux and wall temperature was proposed. In particular, the new handling was applied for the interaction between the convective phenomena generated in the fluid phase and the conduction in the solid parts. The new methodology based on the built-in feature of the ANSYS Fluent solver called Solid Time-Step enables the resolution of convective and conductive phenomena in a single simulation by allowing the use of a different time-advancement for fluid and solid domains. The RSM combustor, developed and tested within the University of Darmstadt, was the academic test case chosen to stress the proposed workflow. Since the chosen test case had never been simulated by CFD analysis in the literature, part of the effort was focused on the development and validation of the numerical model, which led to the first multiphysics and multiscale simulation conducted using the simplified U-THERM3D tool for the prediction of the wall temperature. This simplified approach is characterised by the interaction of only the fluid and solid domains by means of the combined action of convective and conductive heat fluxes. For this first study, in fact, it was decided to neglect thermal radiation on the basis of the reduced brightness of the lean methane-air flames under which the combustor works. The heat flux exiting the combustion chamber was modelled with appropriate boundary conditions, delineated through a preliminary sensitivity analysis given the absence of useful data for closing the numerical problem. Despite a not negligible underestimation of the wall temperature distribution, preliminary results showed the capabilities of the multiphysics approach to predict a similar distribution compared with steady state and gas phase-only simulations justifying the purpose of the work.

Specifically, the behavior of the combustion chamber, being affected by a partially premixed flame, proved to be extremely sensitive to pilot fuel ignition. Therefore, exploiting the full validation of the proposed model on the simplified test case, it was decided to modify the boundary

condition related to the turbulent magnitudes of the pilot fuel jet, by moving from an integral value to the imposition of specific turbulent profiles obtained from the preliminary simulation to carry out the new simulation with the Solid Time-Step method.

In particular, the last part of numerical activity is composed by two simulations were carried out by applying the Solid Time-Step method. The first simulation performed was conducted with the same numerical approach for turbulence modeling used in the U-THERM3D simulation, a hybrid RANS/LES approach. While the second one was carried out with a full-LES approach to quantify the impact of RANS turbulence wall-treatment of the hybrid approach in estimating heat fluxes.

The Solid Time-Step method has proven capable of predicting the correct thermal fluxes and wall temperatures improving the agreement with reference experimental data. The work performed revealed all the critical issues related to numerical modeling of combustors. The strong impact of the pilot fuel jet on the whole behavior of the combustion chamber and the presence of the effusion cooling system makes the estimation of metal wall temperature extremely challenging. The LES simulation allowed good prediction of the vortex structures in the Outer Recirculation Zone and consequently the correct swirling flow-cooled plate interaction. In the investigated portion of the effusion-cooled plate, a wall temperature within the uncertainty of the experimental measurement was obtained highlighting the limitations of the RANS turbulence model used by the hybrid approach simulation. In particular, a large part of the results have been used to highlight and justify the underestimation of the turbulent mixing that is created immediately outside the boundary layer due to the previous underestimation of the vortex structures that are generated inside the effusion holes by the RANS/LES hybrid approach, mitigated instead by full LES modeling. Despite this new analysis, further verification will be conducted on the RSM combustor to understand the origin of the differences in numerical results from experimental data.

During this part of the work, a careful analysis of computational times was carried out to quantify the savings achieved by the Solid Time-Step

method for handling the thermal interaction between fluid and structure. The results show that for a test case that is not too complex in terms of cooling system as the one discussed, the amount of data to be written and read from simulations for updating the coupling interfaces of the U-THERM3D procedure is high and strongly impacts the overall computation time. By using the Solid-Time Step and thus eliminating execution times for input/output operations, the savings in computational cost, given the same numerical approach, start from 7% up to 17%. Whereas, for the same computational grid, switching to an LES approach saves up to 50 percent. As covered in the previous sections in the change of numerical approach, verification of the criteria for the correct resolution of turbulent structures is mandatory to obtain spendable results that are not affected by possible numerical problems due to the use of calculation grids that are not fine enough.

In conclusion, the Solid Time-Step method proved to be robust in predicting wall heat fluxes and at the same time flexible since it allows, like the U-THERM3D tool, the desired models to be used for both combustion and turbulence. It also proved to be cost-effective compared with the original tool by allowing the elimination of execution time for updating the boundary conditions of the coupled surfaces, reasons why it is believed that the proposed Solid Time-Step method can effectively replace the current convection-conduction interaction management of the U-THERM3D tool. For the purpose of the work, further investigation have to be conducted to understand whether the methodology validated in this sections can properly interact with the management currently in use in the U-THERM3D tool for radiative heat transfer modeling and, eventually, with mass source models for effusion cooling systems, reason why the next chapter will focus on validating the entire optimized workflow.

Chapter 4

DLR combustor model

This chapter will present the first application of the optimised full version of the oU-THERM3D tool with the aim to validate it on a challenging test case. In particular, the new workflow of the multiphysics and multiscale procedure defined in Section 2.4 will be used to predict the wall temperatures of an academic combustor operating with a non-premixed sooting flame. The test case considered for this second part of the work is the *FIRST* gas turbine combustor model developed and tested at the Deutsches Zentrum für Luft-und Raumfahrt (DLR) [119, 120], characterized by an extensive experimental measurement campaign for the study of an aeroengine RQL combustor model.

This gas turbine combustor model, operating with an ethylene-air flame, is characterised by the soot formation during the combustion reaction, a black particulate consisting essentially of unburnt carbon, which is therefore mainly formed in rich mixtures and high-carbon fuels [121]. This distinctive aspect makes the test case particularly interesting for the purposes of this work: soot in fact has a strong impact on the radiative heat transfer as it increases the brightness of the flame [122, 123] and the application of the proposed loosely coupled CHT procedure would be tested on a particularly challenging test case.

Although soot has a considerable impact on the thermal stress of

the combustor flametube walls, this will not be analysed in detail as the purpose of the work is to validate the optimised oU-THERM3D full procedure both from a wall temperature prediction and savings in computational cost point of view. Moreover, the gas turbine combustor model has already been studied in terms of soot numerical modelling in the literature and already validated numerical models will be exploited to conduct the present multiphysics simulation.

From this point of view, the FIRST combustor has already been extensively studied through numerical models: the reactive aerothermal fields developed within the combustor were analysed in adiabatic conditions in several papers [124, 125, 126]. In [127, 128, 129] the heat removed from the combustion chamber was taken into account by imposing the experimentally obtained temperatures on the boundary conditions of the numerical problem. As already anticipated, the combustor is characterized by the formation of soot as a combustion product, moreover, the presence of detailed measurements has made it quite famous in the numerical community for the development and application of various soot modeling. In [124, 128, 129, 130] a two equation model have been employed, meanwhile more complex models have been applied in [125, 126, 131].

Although the test case has been studied numerically by several authors the papers focusing on heat transfer are few. In this sense, Rodriguez in [132] performed on the estimation of heat fluxes on the walls of the gas turbine combustor model and how these are affected by thermal radiation and soot. The only other numerical works focused on heat transfer are those carried out by Paccati et al. in [79] with the baseline procedure of the U-THERM3D tool after a preliminary application of the steady-state version in [96, 133].

The aim of this chapter is to carry out the first simulation with the proposed optimised workflow of the U-THERM3D multiphysics and multiscale tool, then to validate the numerical procedure by comparing the results with those of the actual procedure and experimental reference data. As carried out in the previous Chapter 3, the reference simulation will be conducted with SBES approach while the simulation with the

optimised tool will be performed with LES analysis. Also for this new analysis, the procedure was maintained to verify the consistency of the previously obtained results in terms of wall temperature prediction and calculation times.

The chapter is structured as follow, an initial description of the experimental test rig with the main measurements conducted will be carried out. Subsequently, the numerical details used to carry out the simulations will be presented, and finally the calculation times will be analysed to highlight the computational savings obtained with the optimised workflow.

4.1 Experimental test rig description

In this section a summary of the key aspects of the selected test case are described. As already introduced, the experimental model was developed within the DLR to study the behaviour of an RQL gas turbine combustor model for aeronautical applications. The burner operates under pressure with a non-premixed ethylene-air sooting flame stabilized with a dual radial swirler system. The system has the main features of an RQL combustor model since it has a dedicated supply line for oxidising air, the purpose of which is to quench the flame and considerably lean out the mixture in the combustion chamber. Several test points were experimentally analysed by Geigle et al. [119, 120, 134] in which great efforts have been made to measure the concentration of polycyclic aromatic hydrocarbons (PAH) with spectroscopy techniques. A large part of the work focused on studying the soot formation at varying primary to secondary air ratios. In addition to the measurements carried out with Laser-Induced Incandescence (LII) and Laser-Induced Fluorescence (LIF) for,respectively, soot and OH concentrations also measurements with Particle Image Velocimetry (PIV) and Shifted Vibrational Coherent anti-Stokes Raman Scattering (SV-CARS) were also carried out, for the complete characterisation of aerothermal quantities. For a full description of the experimental techniques adopted, the interested reader is guided

to the above-mentioned publications.

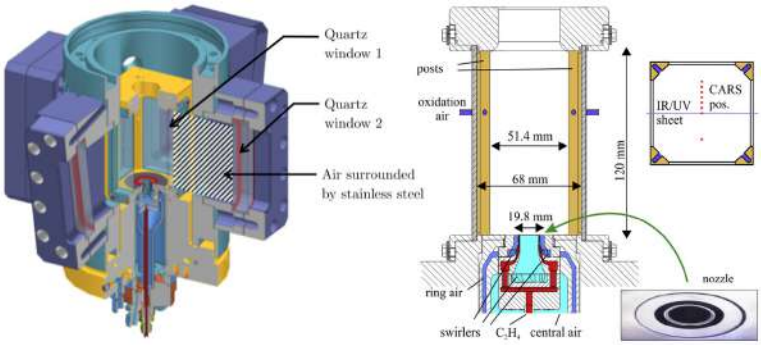

Figure 4.1: DLR - FIRST gas turbine combustor model adapted from [134, 135].

The main structural and geometrical features of the test rig highlighted in Figure 4.1. The experimental bench is cased in stainless-steel to ensure tightness under operating pressure. The combustion chamber has four optical accesses to collect experimental data, one on each side of the chamber itself and has a square cross-section of 68x68 mm^2 with an axial development of 120mm. The metal parts of the outer casing are water-cooled to ensure the safe operation of the experimental rig.

Moving inside the combustion chamber, this is equipped with a double radial swirl system through which primary air is fed. The two swirlers are characterized by a different swirl number (SN): the inner one has 8 vanes with SN = 0.82 meanwhile the outer one has 12 vanes and a swirl number of 0.78. Ethylene (C_2H_4) used as fuel is injected through a concentric ring, located between the two air inlets, with 60 different supply channels, all equally spaced.

4.2 Numerical features

Most of the numerical models used for this part of the work have been previously described within the manuscript. Regarding turbulence modeling, two simulations were carried out. The first simulation, employing the baseline version of the U-THERM3D tool, was conducted with SBES hybrid approach [35], meanwhile the second simulation for the application of the the optimized workflow was conducted with LES method, both approaches have been alredy described in Section 3.2.1.

As in the previous chapter, Section 3.2.2, also for these new reactive simulations the FGM tabulated approach was used to model the combustion reaction [107, 108]. The model has proved to be well validated for applications within high-fidelity simulations such as SBES or LES [27, 28, 78, 79, 106, 118]. In this case the Wang and Laskin mechanism [136] is employed to describe the chemical kinetics of ethylene-air combustion based on 75 species and 529 reactions. This chemical kinetic mechanism is necessary to have a correct prediction of soot [96, 133], which is fundamental later in the prediction of heat fluxes given the high impact it has on the radiative heat flux. Specifically, a proper model has been used for soot prediction, which will be described in the following dedicated section.

Regarding the radiative heat transfer solution, also in this numerical work the Discrete Ordinate model is employed with a 4x4 angular discretization and a 3x3 pixelation for each directions. The current model have been already described in Section 2.4.1.

4.2.1 Soot modeling

In this section the soot modeling employed for the reactive simulation of the FIRST burner will be described. The Moss-Brookes model is used in this numerical activity to take into account the soot presence. The process of soot formation is characterized by 3 basic stages: nucleation, surface growth, and coagulation. For more details on the formation and effects of soot the interested reader can consult the following sources

[121, 137, 138, 139]. This method need to solve two transport equations to model the soot formation. The first equation contains the number of particles of soot N and is shown below:

$$\frac{\delta\left(\rho b^*_{nuc}\right)}{\delta t} + \bigtriangledown \cdot \left(\rho \overrightarrow{v} b^*_{nuc}\right) = \bigtriangledown \cdot \left(\frac{\mu_t}{\sigma_{nuc}} \bigtriangledown b^*_{nuc}\right) + \frac{1}{N_{norm}} \frac{dN}{dt} \tag{4.1}$$

In which the instantaneous production rate of soot particles is given by the opposite contribution of nucleation in the gas phase and coagulation in the molecular regime.

$$\begin{aligned} \frac{dN}{dt} = & \underbrace{C_\alpha N_A \left(\frac{X_{prec} P}{RT}\right)^l exp\left\{-\frac{T_\alpha}{T}\right\}}_{\text{Nucleation}} \\ & \underbrace{- C_\beta \left(\frac{24RT}{\rho_{soot} N_A}\right)^{1/2} d_p^{1/2} N^2}_{\text{Coagulation}} \end{aligned} \tag{4.2}$$

The second transport equation is that of the soot mass concentration M:

$$\frac{\delta\left(\rho Y_{soot}\right)}{\delta t} + \bigtriangledown \cdot \left(\rho \overrightarrow{v} Y_{soot}\right) = \bigtriangledown \cdot \left(\frac{\mu_t}{\sigma_{nuc}} \bigtriangledown Y_{soot}\right) + \frac{dM}{dt} \tag{4.3}$$

This term depends on all three stages that characterize the soot production as shown as follow.

$$\begin{aligned} \frac{dM}{dt} = & \underbrace{M_P C_\alpha \left(\frac{X_{prec} P}{RT}\right)^l exp\left\{-\frac{T_\alpha}{T}\right\}}_{\text{Nucleation}} \\ & \underbrace{+ C_\gamma \left(\frac{X_{sgs} P}{RT}\right)^m exp\left\{-\frac{T_\gamma}{T}\right\} \left[(\pi N)^{1/3} \left(\frac{6M}{\rho_{soot}}\right)^{2/3}\right]^n}_{\text{Surface Growth}} \\ & \underbrace{- C_{oxid} C_\omega \eta_{coll} \left(\frac{X_{OH} P}{RT}\right) \sqrt{T} (\pi N)^{1/3} \left(\frac{6M}{\rho_{soot}}\right)^{2/3}}_{\text{Coagulation}} \end{aligned} \tag{4.4}$$

All the values for the constants of the model are the same adopted by

Paccati et al. in [79].

It should be specified that modeling of soot is a critical aspect within reactive CFD simulations and in this case the purpose of the work is not to assess the goodness of the model employed but only to take into account the soot contribution in term of radiative heat transfer. For this reason results in terms of soot concentration will not be analyzed in the manuscript.

4.2.2 Setup

All the simulations here reported were carried out with the commercial code ANSYS Fluent 2019R1 [42]. In this section the calculation domain and the boundary conditions will be described.

Table 4.1: Investigated operating conditions.

Operating pressure	3	[bar]
Equivalence ratio Φ	1.2	[-]
Q_{air}	140.8	[slm]
T_{air}	300	[K]
Q_{fuel}	39.3	[slm]
T_{fuel}	300	[K]
Fuel composition	C_2H_4	[-]

Compared with the simulations conducted by Paccati et al. in [79], in this numerical task a different test point was analyzed. The operating point without any secondary air injection was chosen, and the detailed values of mass flow rates and temperatures used for the simulations are provided in Table 4.1. This operating point was selected since it has never been studied numerically and because the condition of globally rich mixture without adduction of secondary air does not allow for a complete combustion reaction. This condition that is established inside the combustion chamber increases the concentration of soot with a relative increase of the overall radiative heat load on the walls.

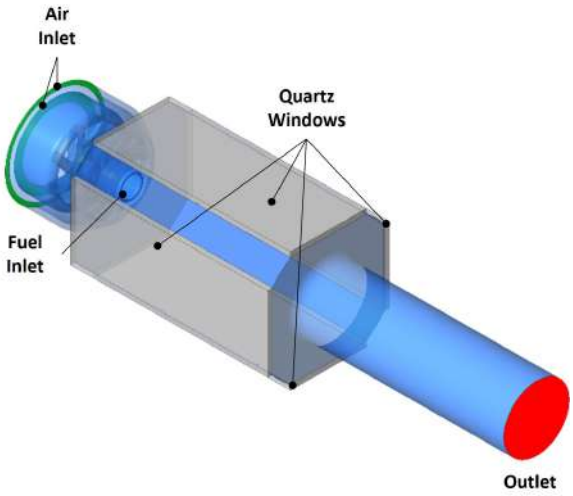

Figure 4.2: Calculation domain

As can be seen from Figure 4.2, the computational domain consists of the injector and the flametube, the final portion of which was extruded by 2.5 outlet diameters to avoid numerical distortions. The corresponding mass flow rates and temperatures shown in Table 4.1 were imposed on all the domain inlets, meanwhile a pressure condition is imposed at the outlet. With respect to the gas turbine combustor model the cooling system outside the quartz windows is not present. The heat removed from the cooling system is modeled with an imposed convective heat flow boundary condition, obtained from the reference work of Rofrigues et al. [135], as shown in Figure 4.3. In particular a reference temperature of 313 K and a heat transfer coefficient of 121 W/m^2K has been set. The optical accesses have been treated as fully transparent to radiation, whereas the hot sides of quartz surfaces are the coupled interfaces of the two fluid and solid domains, whose boundary conditions update at run time during the execution of the multiphysics simulation in accordance with what was already mentioned in Section 2.3. Also thermal properties

of quartz, defined as a temperature-dependent polynomial function are derived from [135]. The side surfaces of the quartz plates, which in the test rig is connected with the metal support structure, are not solved within the conjugate heat transfer problem, but are treated with a fixed temperature set equal to 800K according to [135]. All the other walls have been considered as grey surfaces with an emissivity of 0.8, meanwhile the no slip condition is imposed on all the domain walls.

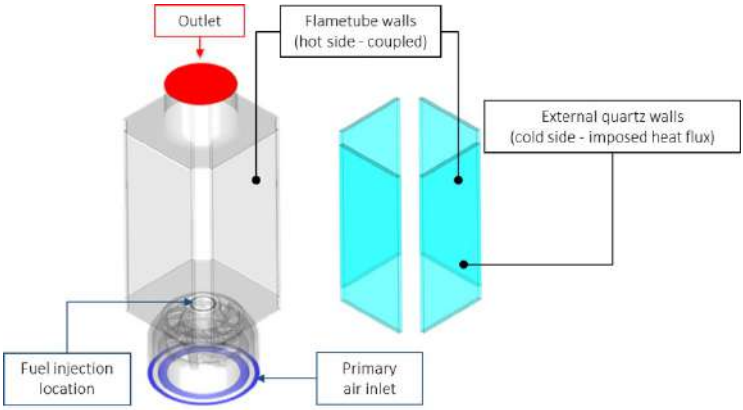

Figure 4.3: Details of the boundary conditions imposed on the coupled interfaces between the fluid domain and the quartz plates of the four optical accesses

Regarding the multiphysics simulations is important to remind that in the baseline U-THERM3D procedure needs to solve three simulations in parallel in continuous connection with each other for updating the coupled interfaces between the different domains present: the fluid domain (CFD) in which aerothermal fields and combustion are solved, the solid domain to take into account the conduction, and the simulation in which the RTE is solved. Meanwhile, the optimized procedure proposed solve directly the conduction in the same ANSYS Fluent session in which the CFD is solved by means of the Solid Time-Step (STS) method and takes the radiative

heat flux into account with another steady-state simulation by updating the coupling interfaces with an optimised frequency of 100 fluid time-steps. A sketch of the domains involved within the simulation with the optimized oU-THERM3D procedure and data exchange management can be seen in Figure 4.4. The STS method allows automatic interaction between the fluid and solid domains while solving them with an appropriate time step for each sub-domain. The interface with the radiative domain corresponds to the entire combustor flametube. The two parallel calculations exchange three-dimensional distributions of quantities of interest, in particular the fluid domain passes the gas-phase aerothermal information including pressure, temperature, enthalpy, species and the 2D wall temperatures distributions on the hot side solid interfaces, whereas it receives from the radiative domain the source term to be added to the energy equation to account the impact of the steady-state solved RTE in the radiative domain.

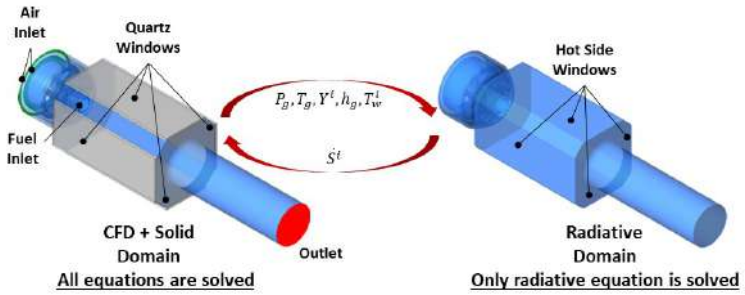

Figure 4.4: Details of the coupling management between the CFD simulation and the radiative domain for the optimized U-THERM3D framework

To carry out the multi-physics and multi-scale simulations 3 different calculation grids, respectively for the CFD, solid and radiative domains, were generated with the ANSYS Meshing software within the ANSYS Workbench suite, as ahown in Figure 4.5. The mesh employed for the simulation of the CFD domain is the one that required the most attention

in the generation phase. In fact, this calculation grid must allow the correct solution of the turbulent flow structures on which the chemical reaction also depends. For this reason several refinement with respect to the general sizing of 1mm have been adopted. In particular, in the swirler region as well as the first part of the primary zone where combustion takes place a size of 0.25mm is adopted, meanwhile the entire remaining portion of primary zone is discretized with a sizing of 0.4mm. A layer of five prismatic elements was generated for the correct discretization of the near-wall region, for a total of 58M of tetrahedral elements, then converted into more effective 12M of polyhedral elements [113].

Figure 4.5: Visualization of the three mesh grids employed to discretize the involved calculation domains: gas-phase (blue), solid plates (gray) and radiation (green)

The quartz plates have been discretized to ensure 5 tetrahedral elements in their thickness for a total of 1.5M of tetrahedral elements. It is worth mentioning that in the U-THERM3D baseline procedure, conduc-

tion is solved in a separate ANSYS Fluent session so that a computational domain is required only for solid parts. In the simulation with the optimized oU-THERM3D procedure (oU-T3D), the fluid-solid interaction is carried out by the Solid Time-Step method, which requires the simultaneous presence of the fluid and solid sub-domains. For this reason, a mesh including both parts was generated with the same characteristics already described.

Regarding the radiative domain a coarser mesh can be employed since that only the RTE in a steady-state manner has to be solved, for this reason 8M tetrahedral elements were used.

The meshes thus generated enabled full compliance with Pope's criterion [115] for SBES simulation with U-TEHRM3D baseline tool and that proposed by Celik [114] for LES simulation with the optimized multiphysics and multiscale workflow. As visible from Figure 4.6. The Shielding Function distribution is also shown for the SBES simulation. both criteria are well above 0.8 over all regions within the flametube, which allow the conclusion that more than 80% of the turbulent kinetic energy is correctly solved in the computational domains.

As extensively described earlier in the manuscript loosely coupled approaches allow temporal desynchronization of each heat transfer mechanism, dividing the conjugate heat transfer problem into several subdomains. In this case the fluid time-step is set equal to $5{\cdot}10^{-6}$s, equal to $0.25{\cdot}10^{-3}$ flow-trough times (FTT), whereas the solid solver advance in time with a larger step size equal to $5{\cdot}10^{-3}$s. The update of the coupled interfaces for the baseline U-THERM3D procedure occurs every 10 fluid time-steps, 30 solid time-steps, and 10 iterations of the radiative domain, meanwhile for the optimized workflow coupling between the fluid and solid domains is automatically handled by the Solid Time-Step method, and coupling with the radiative domain occurs every 100 fluid time-steps to still ensure compliance with the limits set by the characteristic time scales of each heat transfer mechanism, as already stated in Section 1.5.

Typically for this type of application, the simulations were carried out to ensure, at least, a simulated time equal to a total of four fluid domain

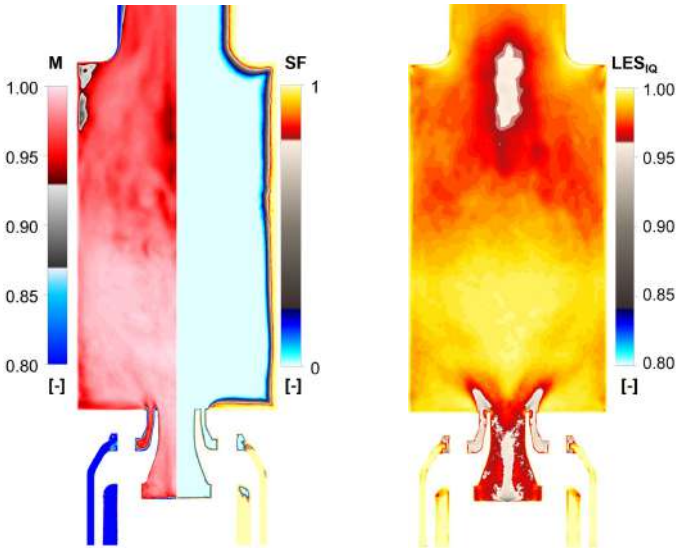

(a) *(b)*

Figure 4.6: (a) Pope criterion (left semi-plane) and Shielding Function (right semi-plane) for the SBES simulation, (b) Celik criterion for LES simulation.

flow-trough times, where the latter two have been employed to collect statistics on quantities of interest. For the flow-trough times estimation, the entire computational domain, including extrusion before outlet and visible in Figure 4.2, was considered so as to have a conservative assessment; in particular a FTT of 20ms was considered.

A bounded central difference scheme has been employed for the spatial discretization, meanwhile a second order implicit formulation has been used for time discretization. For both simulations, the Coupled algorithm was used to link velocity and pressure.

4.3 Results

This section will show the results obtained with the two multiphysics procedures for solving the conjugate heat transfer problem. First, the results of the aerothermal fields will be shown and compared with reference experimental data. After that, the analysis will focus on analyzing the wall temperatures of quartz optical accesses and finally the advantages of the new optimized procedure over the baseline in terms of computational savings will be shown.

Before moving to the analysis of the results, it should be noted that in addition to the two simulations introduced, a third preliminary simulation was carried out, in which the Solid Time-Step method was used for fluid-solid interaction and RTE is solved directly in the fluid domain with an unsteady SBES approach. This simulation will not be analyzed in detail as the results do not add anything to the discussion compared to those that will be shown with the other multiphysics simulations. This simulation will be recalled only in the final part to get an estimation on the computation time and the impact of the resolution of the RTE within the CFD simulation compared to a simulation dedicated to it.

4.3.1 Reactive flow fields discussion

From the velocity distributions shown in Figure 4.7, it is possible to see the typical flow field that occurs in a flametube with a swirl-stabilized system. The two Inner and Outer Recirculation Zones are well developed in the primary zone of the combustion chamber. The comparison of the two velocity maps does not reveal any particular differences other than a greater extension of the swirled jet wake of the U-THERM3D simulation, conducted with the hybrid SBES approach, after impacting the quartz wall. Since the zone in question develops in the area close to the wall, this could be due to RANS modelling of the turbulence.

From Figures 4.8 and 4.9, a more quantitative comparison can be made exploiting the radial velocity profiles at several axis locations of the

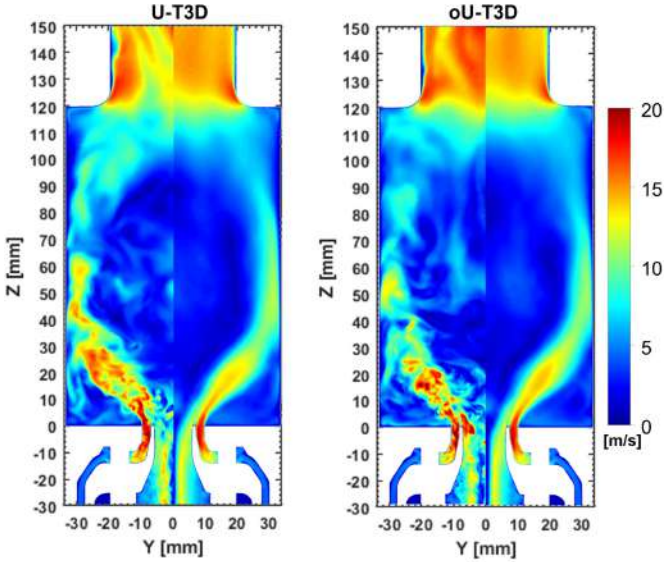

Figure 4.7: Instantaneous (left semi-plane) and time-averaged (right semi-plane) velocity comparison between the U-THERM3D and the optimized workflow (oU-THERM3D) in a midplane of the combustor

combustor. Starting from the first available section, i.e. 3mm from the start of the combustion chamber, it can be seen that the experimental profiles are smoother than the numerical ones. In fact, the numerical profiles predict a flow that is affected by the contribution of the double radial swirler. The two axial velocity peaks, even more visible from the tangential component graph are the distinct contributions of the inner and outer swirler. In this section, the maximum differences between numerical approaches and experimental data are reached but at the same time there is good prediction by CFD of minimum and maximum values. Given the good agreement reached in the following sections and keeping in mind that the experimental measurement is carried out close to the wall, only 3mm from the bluff body, it is possible that these data are characterised by a greater uncertainty.

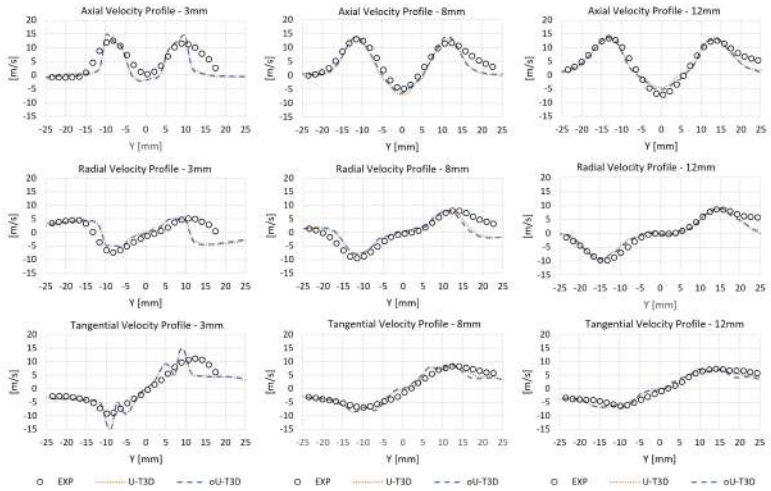

Figure 4.8: Radial distributions of time-averaged axial, radial and tangential velocity at Z = 3 mm (left), Z = 8 mm (middle) and Z = 12 mm (right)

Even at the available sections furthest from the injection system, that are shown in Figure 4.9, it can be seen that both simulations succeed in predicting a flow field well in agreement with the experimental data. Only in the central area of the combustion chamber there is a slight underestimation of the vortex formed within the inner recirculation zone between the wakes of the two swirl jets appreciable from the graphs of the axial velocity components. Starting from the axial section of 12mm to that at 24mm, the negative velocity axial component, which actually identifies a recirculation, is underestimated by the two simulations. In any case, the velocities involved in the portion discussed are low, and given the excellent agreement with the experimental data in all other portions of the combustion chamber for each of the different velocity components, it is concluded that both simulations are able to provide a good prediction of the swirling flow and the general velocity field formed within the

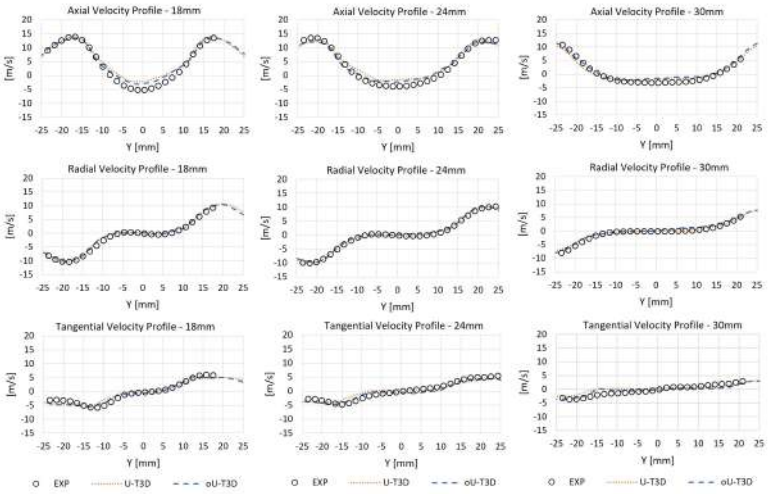

Figure 4.9: Radial distributions of time-averaged axial, radial and tangential velocity at Z = 18 mm (left), Z = 24 mm (middle) and Z = 30 mm (right)

flametube. Unfortunately, for the selected operating point, experimental radial RMS profiles are not available to quantify by how much the two simulations actually underestimate the turbulent components generated within the combustion chamber.

From the analysis of the axial velocity profile along the centerline of the combustor in Figure 4.10, it is possible to confirm what was said above. Although the recirculation velocities are low, the simulations underestimate the magnitude of the vortex in the area between 10mm and 30mm of the combustion chamber. From the graph, it can be seen that the vortex anchors within the swirler what leads to an underestimation of the axial velocity along the centerline in the first sections of the combustion chamber. Since the minimum axial velocity value is well predicted by the simulations the underestimation can be caused by a shift toward the burner of the vortex compared to that measured experimentally. It is im-

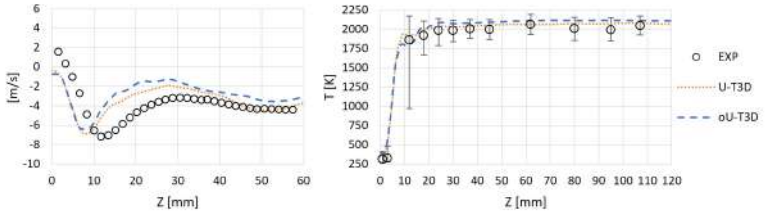

Figure 4.10: Time-averaged axial velocity (left) and gas-phase temperature (right) profiles comparison along the centerline of the combustor

portant to emphasize how this area very close to the inlets of the numerical problem can be affected by the boundary conditions used. Again, given the absence of experimental data for a complete flow characterization, the same flow rate conditions as in the experimental test were chosen (Table 4.1). In any case, the differences obtained with the two numerical approaches are limited to the inner recirculation zone and have values that are not significantly different from those measured, which is why the boundary conditions are considered suitable for modeling the problem.

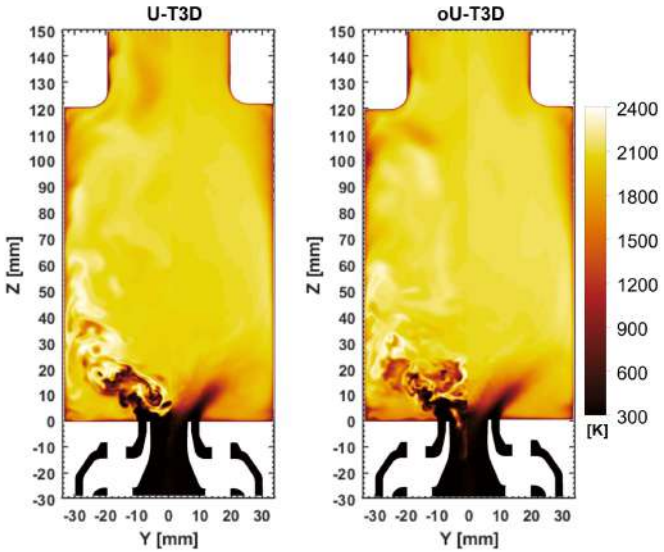

Figure 4.11: Instantaneous (left semi-plane) and time-averaged (right semi-plane) temperature comparison between the U-THERM3D and the optimized workflow (oU-THERM3D) in a midplane of the combustor

Moving the discussion to the analysis of gas-phase temperatures the good prediction of thermal levels along the combustor centerline can be appreciated. In this case, the minimum and maximum temperature values acquired during the measurement are also given for the experimental data. Given the maximum variability around 10mm from the bluff body, it is possible to state that it is at this height that the vortex related to the highly unsteady IRZ is established. The strong mass and heat transport generated by the vortex also causes the measurement to be extremely variable.

From the graph, it can be seen that the LES simulation conducted with the optimized version of the oU-THERM3D tool provides a slightly higher temperature value than the SBES simulation conducted with the baseline tool and the experimental data, while remaining within the vari-

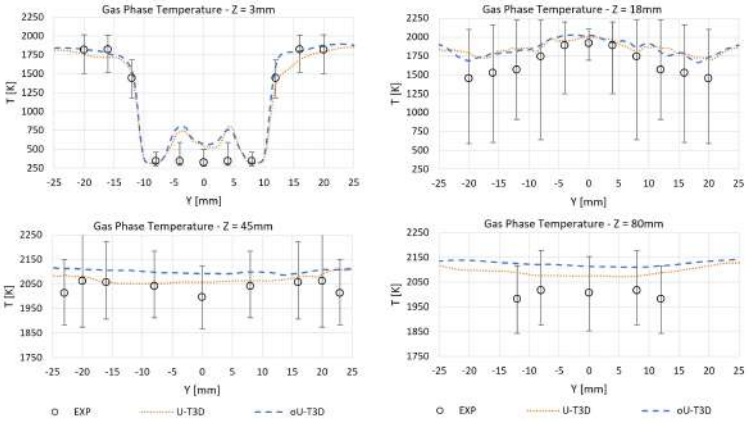

Figure 4.12: Radial distributions of time-averaged temperature at four axial sections

ability band of the measurement itself. This trend is also confirmed by the temperature maps shown in Figure 4.11 from which it can be seen that the oU-THERM3D simulation predicts a generally higher average temperature level than the other.

To better appreciate the differences between the two multiphysics simulations performed, the radial profiles of the time-averaged temperature for 4 sections of interest are shown in Figure 4.12. In the first available section, at 3mm from the bluff body, the oU-THERM3D simulation allows improved temperature estimation in the ORZ zones while in the central combustor zone there is a general overestimation by both simulations, perhaps due to the shift toward the burner of the vortex in the IRZ leading to greater hot gas transport than experimentally measured. Moving to higher Z dimensions, it can be seen that within the primary zone the two simulations give the same result (Z=18mm) while at even greater distances what was previously stated is confirmed, that is, that the simulation carried out with the optimized oU-THERM3D approach tends to predict a generally higher temperature than the simulation conducted

with the baseline U-THERM3D tool, but still within the range of acquired measurements.

4.3.2 Quartz temperature

From the previous section, it was found that both of the procedures analyzed succeed in performing an accurate prediction of the aerothermal fields developing inside the combustion chamber under investigation. In this section, the objective is to show whether multiphysics procedures can correctly predict the wall temperatures of quartz facing the flametube and thus be able to correctly model all the interactions that occur between the heat transfer mechanisms involved. Although the DLR gas turbine combustor model is less complex in terms of wall behavior than the RSM test case analyzed in the previous Chapter 3, given the absence of the cooling system, the new test case presents a non-negligible radiative contribution to the estimation of wall heat fluxes. However, it should be reminded that in the present work the quartz were treated as completely transparent bodies as it has been confirmed by Rodrigues et al. [135], that these have an absorber behavior only for low temperature levels while for high temperatures their behavior is almost that of a fully-transparent body.

Figure 4.13 shows the time-averaged wall temperatures distribution along the centerline of the hot and cold side of the quartz windows.
The wall region that faces to the burner primary zone has the highest thermal load. As one might reasonably expect, the highest heat fluxes are obtained on the side facing the flame. High-temperature zones are concentrated in the central areas of the optical accesses in accordance with what happens inside the combustion chamber, i.e. that the strong interaction between swirl flow and walls leads to an impact of hot gases on the surfaces reaching peak temperature. Heat transfer in this zone is therefore dominated by convective phenomena that bring hot gases at high temperature up to near the walls. The portions closest to the ends of the quartz are affected by the boundary conditions imposed on the lateral surfaces, but given the low conductivity of the quartz itself, these

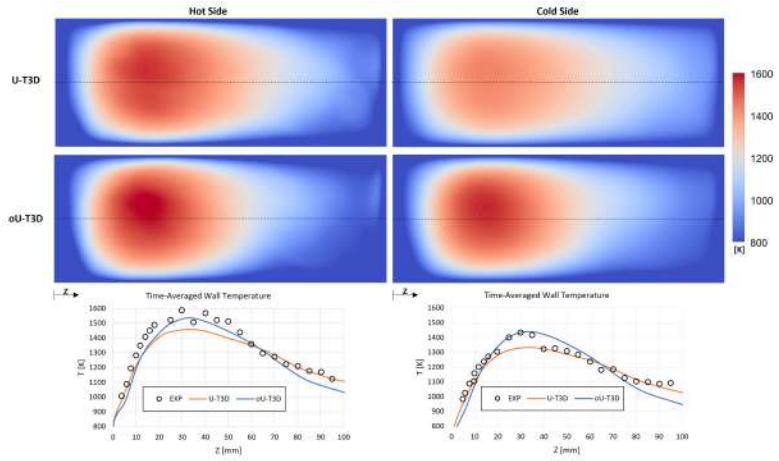

Figure 4.13: Quartz windows time-averaged wall temperatures comparison with experiments from [140]

affect only a few millimetres of the windows and do not influence the core regions where the comparison with the experimental data takes place.

The temperature profiles on the quartz centerline provide better evidence that the simulation performed with the optimized oU-THERM3D workflow, in which an LES approach was used, shows higher temperature values overall than the simulation performed with the original instrument using an SBES approach. In particular, the temperature profiles show how only the optimised approach can predict the correct value of temperature peaks both on hot and cold sides of the optical accesses, that it is a key aspect in the definition and design of cooling systems within gas turbine combustors. As already mentioned, in fact, temperature peaks are closely dependent on convective phenomena occurring within the combustion chamber. Again, a similar behaviour to that already seen on the RSM gas turbine combustor model was achieved. Namely, that the hybrid RANS/LES methodology for turbulence modeling, the current state-of-the-art for CFD applications on conjugate heat transfer problems within industrial applications, does not appear to be the best model since it

underestimates the heat flux that invests the solid wall. In [96] the author running the fully RANS multiphysics simulation obtained an even flatter solution of the temperature profile on the quartz with an underestimate greater than 200K. In this case, the SBES simulation, while showing a trend consistent with the experimental measurement, underestimates the temperature peak, i.e., where turbulent mixing dominates heat transfer, due to the application of RANS modeling in the near-wall regions.

With the results obtained, the oU-THERM3D procedure is considered to be fully validated, both in terms of aerothermal fields and wall temperatures the procedure proved to be robust in predicting the quantities of interest. In addition, the switch from hybrid SBES to full LES approach for treating turbulence has improved agreement with experimental data for areas dominated by turbulent phenomena. It has been shown that a lower coupling frequency on the coupled interfaces between the fluid and radiative domains does not lead to any distortion in terms of numerical results, and the associated computational savings will be analyzed in the next section.

4.3.3 Computational savings

Similar to what has been done previously in Section 3.4.5, a detailed comparison on calculation times between the two different multiphysics procedures for solving conjugate heat transfer problems will be shown. Again, the effort will focus on defining the equivalent time for carrying out an elementary operation, which in unsteady simulations is equivalent with the time required for the resolution of a single time step. In this case for the U-THERM3D simulation, given the presence of the domain in which the RTE is solved, the elementary resolution time will have to be increased not by one contribution, but by two: the first, already analyzed in detail in the previous Chapter 3, related to the updating of the coupled fluid-solid interfaces for which 2D distributions of convective heat fluxes are written, and the second term related to the fluid-radiation coupled interfaces. The latter, as already described, is defined by the exchange of 3D quantities by means the aerothermal distributions and the source term relative to the RTE solution.

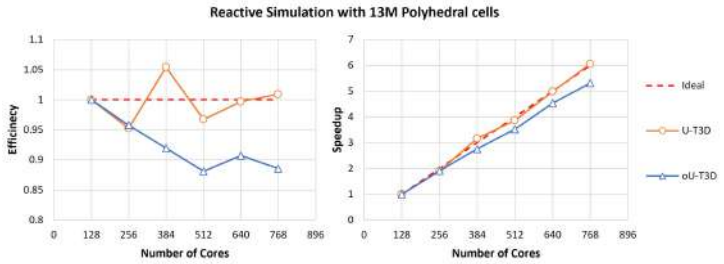

Figure 4.14: Performance of ANSYS Fluent solver on IT4Innovation Karolina Supercomputer for the FIRST gas turbine model simulation

The same calculation infrastructure was used for these new simulations, the information about the Karolina cluster of the IT4Innovations supercomputing center have been previously introduced in the Section 3.4.5. In Figure 4.14 the scalability performance of the ANSYS Fluent solver with new test case are shown. In this case, given the lower number

of the calculation grid, there was no error in the performance of the simulation on a single calculation node and also the number of tested nodes has been reduced compared to what was done in Section 3.4.5. Also in this case the behavior of the code in terms of scalability does not deviate much from the ideal for both numerical approaches.

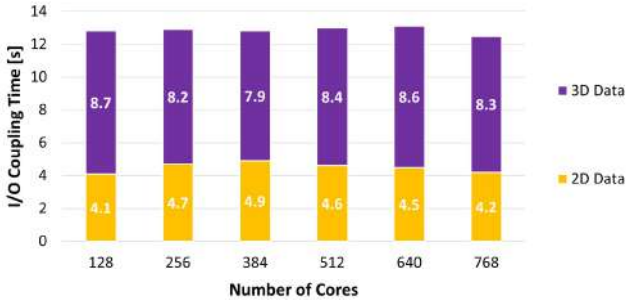

Figure 4.15: Coupling time of U-THERM3D for the FIRST burner performed on IT4I Karolina supercomputer

As mentioned earlier, the effort was focused on the definition of the equivalent time for the execution of a single time-step, thus the time to execute the operations for updating the boundary conditions of the coupled interfaces was monitored, and the results are shown in Figure 4.15. With respect to the RSM combustor the time required to update the coupled interfaces has a lower impact on the whole simulation time, but it's worth to remind that this kind of operation is extremely case-dependent. What emerges from the study is that even the operations performed on the three-dimensional data, to update the fluid-radiative coupled interfaces, have a time that does not depend on the number of cores on which the simulation is performed, holding more or less constant as the number of compute nodes employed varies. In addition, with respect to the fluid-solid coupled interfaces, given the absence of the cooling system they require fewer elements to be discretized. In fact, for the FIRST combustor, there are four coupled flat surfaces totaling about

45k elements, so an extremely small number compared with that for the RSM combustor interfaces (about 1.5M). What is interesting to point out is that despite the low number of elements the update of fluid-solid interfaces weighs about one-third of the total time to update interfaces, an interesting aspect, never previously evaluated on conjugate heat transfer simulations performed by means of the U-THERM3D tool.

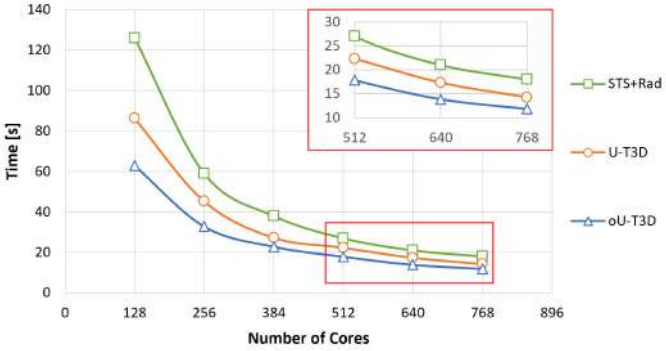

Figure 4.16: Single time-step execution time comparison for the 3 loosely coupled approaches employed for the FIRST burner simulations performed on IT4I Karolina supercomputer

Taking advantage of the data in Figure 4.15, it is possible to define the equivalent time to solve a single time step; in this context the scalability chart is shown in Figure 4.16. This graph also shows the timing data of the preliminary simulation in which the RTE have been solved within the CFD domain with the same SBES unsteady approach of the U-THERM3D baseline framework. The results of this preliminary simulation were intentionally not presented in the manuscript as they would not have added anything to the discussion as they were very similar to the results obtained with U-THERM3D approach. However, it turns out to be important to recall it in terms of computational cost to point out how much the RTE solution has a strong impact on computational time. These calculation times make it possible to justify why it is convenient

to increase the complexity of the procedure by solving the radiative heat transfer contribution in a separate domain rather than within the simulation in which the flow field and combustion are solved.

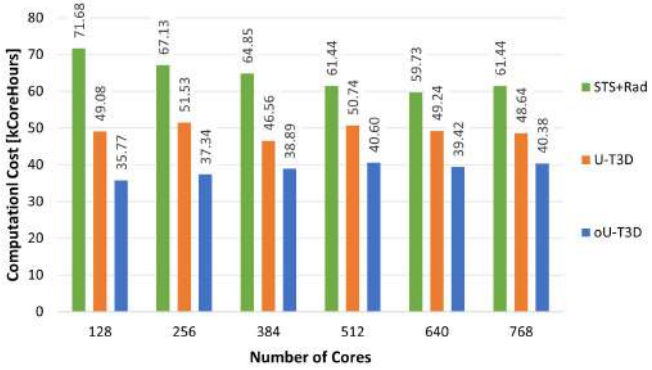

Figure 4.17: Comparison of computational cost for the 3 loosely-coupled approaches considered for the FIRST burner simulations performed on IT4I Karolina supercomputer

Moving to the comparison on the calculation time between the baseline U-THERM3D procedure and the optimized oU-THERM3D one, it is evident how the computational cost is reduced. The optimized procedure by carrying out the coupling between the CFD and radiative domains at a reduced frequency compared with the U-THERM3D approach results in non-negligible computational savings. In particular, the update occurs each 100 fluid time-steps and not even 10 as for the U-THERM3D approach. The computational costs expressed of core-hours are shown in Figure 4.17. Although the code does not have perfect linear scalability, in order to limit the overall calculation time and thus carry out simulations on as many computing resources as possible, the adoption of the optimised workflow oU-THERM3D tool for solving conjugated heat transfer problems with a loosely-coupled CFD approach leads to savings in the order of 17% compared to the original version.

4.4 Concluding remarks

In the present chapter the full optimized workflow of the oU-THERM3D tool for the solution of the conjugate heat transfer problem with a loosely coupled unsteady approach have been employed. The test case chosen to apply the numerical method is an academic gas turbine combustor model operating under pressure with a non-premixed ethylene/air sooting flame. The numerical approach is based on the simultaneous resolution of three different calculation domains to take into account all the main heat transfer mechanisms that are involved and interact with each other inside a gas turbine combustion chamber model. In particular three simulations are performed: one for the convective phenomena solution, one for the conduction in the solids and the last one for the radiative heat transfer contribution. The test case under study is particularly sensitive to radiative heat load due to the soot formation during the combustion reaction which increases the brightness of the flame and consequently the thermal loads on the walls of the combustion chamber.

The optimised procedure is based on the internalisation of the solid domain within the CFD domain, in which the turbulent structures and combustion reaction are resolved, and the use of an optimised coupling frequency for updating the boundary conditions at the coupled interfaces of the problem between the CFD and radiative domains. In particular, compared to the current U-THERM3D procedure, the optimised workflow performs the update of the coupling interfaces between the fluid and radiative domains every 100 fluid time steps and not every 10. Furthermore, the new procedure employs a full LES approach and not a hybrid one for the turbulence modelling. This makes the optimized procedure easier to use, more robust, requires less computational effort and capable of providing a more accurate estimate of wall temperatures.

During the numerical activity, it was verified that the results obtained from the two approaches were consistent with each other. As far as the aerothermal results of the gas phase inside the combustion chamber are concerned, the two approaches provide almost the same values and are

in excellent agreement with the experimental reference data. Regarding the wall temperature distributions only the simulation conducted with the oU-TEHRM3D approach can correctly predict the temperature peak reached in the primary zone, where the swirl flow impacts the quartz walls. This behaviour depends on the turbulence model used, in fact, the U-THERM3D simulation have been conducted with a hybrid SBES approach, that resolves the near-wall regions in a RANS manner that leads to an excessive underestimation of turbulent structures, thereby limiting the transport of mass and heat to the walls.

The last aspect covered in this chapter was the comparison of the computation times required by both loosely coupled methods. From the study regarding the time required to carry out update operations of coupled interfaces, it showed that although fluid-solid interfaces were not complicated they require one-third of the total time for data exchange. Despite the fact that the absolute times for the update operations are extremely case-dependent this result confirms what also emerged in the previous chapter, namely, that an internalization of the fluid-solid interfaces using the built-in feature of the ANSYS Fluent solver results in non-negligible computational savings. The main result of the activity relates to the management of data exchange between the fluid-radiation interfaces in that a decrease in the frequency with which simulations are coupled does not lead to any bias in the prediction of thermal loads and wall temperatures but at the same time reduces computational costs by 10%.

Conclusions

The design of gas turbine combustor cooling systems requires high efforts from both technical and economic perspectives. Given the prohibitive conditions that are established during the operation of a real gas turbine combustor experimental tests for complete understanding of the phenomena that occur within the flametube are rarely feasible. The correct estimation of heat fluxes and wall temperatures is critical for the proper design of the cooling systems for protection the metal components of gas turbine combustors. In this sense, the development of increasingly large and efficient computational infrastructures has enabled the massive use of CFD simulations to contain costs related to combustor design. Although technological development has provided the use of increasingly accurate numerical CFD methods, industrial activities needs increasingly accurate and rapid tools to obtain results. In this context, conjugate heat transfer problems have always required considerable computational effort to estimate heat loads, given and considering all the phenomena involved within a gas turbine combustor. Also because it has been well established that scale-resolving approaches are, at least, required for the proper estimation of wall temperatures. In particular, the simultaneous presence of all heat transfer mechanisms, all with their own characteristic time scales has led to the development of so-called *loosely coupled* approaches.

These numerical methods allows the desynchronization of different heat transfer mechanisms, such as combustion, convection, conduction, and radiation, but at the same time ensure that the mutual effect is taken into account. The possibility of being able to simulate any heat transfer

mechanism with the most suitable time step allows a large reduction in computational costs. Although these tools are extremely effective and customizable they are often not suitable to be used within industrial procedures since they are not easy to use or have particularly strict conditions that must be satisfied in order to properly work.

In this context, the research work was developed with the aim of optimizing the existing tool called U-THERM3D. This numerical framework has been developed within the ANSYS Fluent CFD solver for the accurate prediction of the wall temperatures of gas turbine combustor liner with a desynchronized loosely coupling methodology. This approach for solving the conjugate heat transfer problem is based on the division of the entire system into several sub-domains each dominated by a specific heat transfer mechanism. In this procedure, specifically, three solvers are used in parallel, so that a domain can be defined in which convective heat transfer is the main one and within combustion and turbulence are solved with the most suitable time step. Another sub-domain consists of the solid parts, which are dominated by conduction, and the last one is where only the radiative heat transfer is solved. This last phenomenon given the low characteristic time scale compared with the previous two is solved with a steady-state manner. The key aspect of the procedure is that the simulations interact with each other to exchange data and thus influence each other so that the final solution takes into account any mutual influence.

In this research activity, an optimized version for the wall temperatures estimation workflow was proposed to simplify the use of the tool and reduce the computational costs associated with multiphysics simulations. The proposed optimisation is based on a new data management for updating boundary conditions on coupled interfaces. In particular, the current version, based on write and read data operations, has been partially revised to reduce the time needed to update the coupled interfaces and thus reduce the overall computational cost. The new procedure is based on the internalisation of the fluid-solid interface, meanwhile the same handling has been maintained for the fluid-radiation interface, but with a

revision and optimisation of the coupling frequency. The new procedure for heat flux estimation was first developed and validated on a simplified case study, then, in order to obtain an extremely flexible tool, it was preferred to carry out a double validation on two different and challenging academic combustors.

In particular, in the first application only the new management for the convective and conductive interaction was taken into account. The parallel architecture is maintained but managed within a single session of the ANSYS Fluent CFD solver. This new approach is based on the built-in of the solver called *Solid Time-Step* method which allows the desynchronised solution of the two fluid and solid sub-domains directly in a single simulation. The proposed solution thus simplifies the tool and makes it more robust by relying on a single simulation and not two interconnected parallel simulations. In addition, as the write and read operations for updating the coupled interfaces are no longer required, a not negligible computational saving is achieved.

To carry out this validation, a simplified version of the tool has been developed which was then applied to a combustor operating with a swirl stabilized partially premixed lean methane-air flame and an effusion-cooled plate. The chosen test case made it possible to neglect the radiative contribution of heat transfer, allowing for a complete validation of the optimised simplified tool. The numerical work has shown how challenging it is to model a partially premixed flame operating with a pilot fuel jet given the strong impact of this on the whole combustion camber behaviour. Moreover It also brought out how hybrid approaches for turbulence modelling, the current state-of-the-art for industrial CFD applications fail to provide correct prediction of wall heat fluxes especially for the test case analysed, where the presence of an effusion cooling system made turbulent mixing in the near-wall region the most relevant effect.

The second part of the work focused on the application of the complete optimised workflow for heat flux and wall temperatures estimation, including radiative heat transfer. A second gas turbine combustor model was employed to carry out this part of the work. In particular, an academic

burner operating with an ethylene-air sooting flame was considered. The soot formation from the combustion reaction makes the contribution of radiative heat flux even more crucial. Here again, a comparison was made between the current tool and the one running with the optimised workflow. To further validate what was done in the first test case, a hybrid approach for turbulence modelling was used in the current tool, while a full LES approach was employed in the optimised one. Although the differences between the results in this case are smaller, further confirmation of what was previously obtained was nevertheless achieved, that is, only the full LES approach was able to predict the correct value of the temperature peak arising in the zone of maximum interaction between the flame and the wall region where the hybrid approach leads to an inevitable underestimation of turbulent mixing. The results showed also that a reduction, by a factor of ten, in the frequency with which the coupled interfaces between the CFD fluid and radiative domains are updated has no impact on wall temperature prediction but saves 10% in computational cost compared with the reference version of the U-THERM3D tool.

For both numerical tasks performed, reference experimental data were exploited to validate multiphysics and scale-resolving loosely-coupled procedures. Although the analysis of computational savings showed how much this varies according to the coupled interfaces and thus makes the evaluation extremely case-dependent, the study showed that especially the current management of updates of fluid-solid coupled interfaces based on writing and reading 2D data is not efficient. In particular, the analysis of calculation times showed that the data exchange between the different solvers leads to an increase in computational costs of up to 20%, thus underlining the goodness of the proposed optimisation, which does not require it.

Although the procedure defined in this manuscript is not limited to applications in gas turbine combustors but can be generalized to all conjugate heat transfer numerical problems, it is believed that the next step in the research effort is to apply the optimized oU-THERM3D tool to an industrial gas turbine combustor or an aeroengine combustor, which,

with its complex cooling systems, could provide a less indicative idea of how computationally efficient the use of this new tool is with respect to the original version.

List of Figures

List of Tables

Bibliography

[1] Han, Je-Chin, Dutta, Sandip, and Ekkad, Srinath. *Gas turbine heat transfer and cooling technology*. CRC press, 2012.

[2] Lefebvre, Arthur H and Ballal, Dilip R. *Gas turbine combustion: alternative fuels and emissions*. CRC press, 2010.

[3] Wurm, B, Schulz, A, Bauer, H-J, and Gerendas, M. Cooling efficiency for assessing the cooling performance of an effusion cooled combustor liner. In *Turbo Expo: Power for Land, Sea, and Air*, volume 55157, page V03BT13A010. American Society of Mechanical Engineers, 2013.

[4] McGuirk, JJ. "The aerodynamic challenges of aeroengine gas-turbine combustion systems." *The Aeronautical Journal*, 118(1204): 557–599, 2014.

[5] Ballal, Dilip R and Zelina, Joseph. "Progress in aeroengine technology (1939–2003)." *Journal of aircraft*, 41(1):43–50, 2004.

[6] ACARE. Flightpath 2050 europe's vision for aviation, 2011. URL `http://ec.europa.eu/transport/sites/transport/files/modes/air/doc/flightpath2050.pdf`.

[7] Levy, Yeshayahou, Sherbaum, Valery, and Arfi, Patric. "Basic thermodynamics of floxcom, the low-nox gas turbines adiabatic combustor." *Applied thermal engineering*, 24(11-12):1593–1605, 2004.

[8] Foust, Michael, Thomsen, Doug, Stickles, Richard, Cooper, Clayton, and Dodds, Will. Development of the ge aviation low emissions taps combustor for next generation aircraft engines. In *50th AIAA aerospace sciences meeting including the new horizons forum and aerospace exposition*, page 936, 2012.

[9] Moreno, V. Combustor liner durability analysis. Technical report, 1981.

[10] Wadia, Aspi R. "Advanced combustor liner cooling technology for gas turbines." *Defence Science Journal*, 38(4):363–380, 1988.

[11] Gustafsson, KM Bernhard and Johansson, T Gunnar. "An experimental study of surface temperature distribution on effusion-cooled plates." *J. Eng. Gas Turbines Power*, 123(2):308–316, 2001.

[12] Andrews, GE, Bazdidi-Tehrani, F, Hussain, CI, and Pearson, JP. Small diameter film cooling hole heat transfer: The influence of the hole length. In *Turbo Expo: Power for Land, Sea, and Air*, volume 79016, page V004T09A021. American Society of Mechanical Engineers, 1991.

[13] Andrews, GE, Khalifa, IM, Asere, AA, and Bazdidi-Tehrani, F. Full coverage effusion film cooling with inclined holes. In *Turbo Expo: Power for Land, Sea, and Air*, volume 78811, page V004T09A045. American Society of Mechanical Engineers, 1995.

[14] Andreini, Antonio, Becchi, Riccardo, Facchini, Bruno, Picchi, Alessio, and Peschiulli, Antonio. "The effect of effusion holes inclination angle on the adiabatic film cooling effectiveness in a three-sector gas turbine combustor rig with a realistic swirling flow." *International Journal of Thermal Sciences*, 121:75–88, 2017.

[15] Andreini, Antonio, Becchi, Riccardo, Facchini, Bruno, Mazzei, Lorenzo, Picchi, Alessio, and Turrini, Fabio. "Adiabatic effectiveness and flow field measurements in a realistic effusion

cooled lean burn combustor." *Journal of Engineering for Gas Turbines and Power*, 138(3), 2016.

[16] Lenzi, Tommaso, Palanti, Lorenzo, Picchi, Alessio, Bacci, Tommaso, Mazzei, Lorenzo, Andreini, Antonio, and Facchini, Bruno. "Time-resolved flow field analysis of effusion cooling system with representative swirling main flow." *Journal of Turbomachinery*, 142 (6), 2020.

[17] Lenzi, Tommaso, Picchi, Alessio, Bacci, Tommaso, Andreini, Antonio, and Facchini, Bruno. "Unsteady flow field characterization of effusion cooling systems with swirling main flow: Comparison between cylindrical and shaped holes." *Energies*, 13(19):4993, 2020.

[18] Lenzi, T, Picchi, A, Becchi, R, Andreini, A, and Facchini, B. "Swirling main flow effects on film cooling: Time resolved adiabatic effectiveness measurements in a gas turbine combustor model." *International Journal of Heat and Mass Transfer*, 200:123554, 2023.

[19] Mendez, Simon and Nicoud, Franck. "Adiabatic homogeneous model for flow around a multiperforated plate." *AIAA journal*, 46(10): 2623–2633, 2008.

[20] Andreini, Antonio, Da Soghe, Riccardo, Facchini, Bruno, Mazzei, Lorenzo, Colantuoni, Salvatore, and Turrini, Fabio. "Local source based cfd modeling of effusion cooling holes: Validation and application to an actual combustor test case." *Journal of engineering for gas turbines and power*, 136(1), 2014.

[21] Mazzei, Lorenzo, Andreini, A, Facchini, B, and Bellocci, L. A 3D coupled approach for the thermal design of aero-engine combustor liners. In *ASME Turbo Expo 2016: Turbomachinery Technical Conference and Exposition*, number A 3D coupled approach for the thermal design of aero-engine combustor liners, page V05BT17A009. American Society of Mechanical Engineers, 2016.

[22] Rida, Samir, Reynolds, Robert, Chakravorty, Saugata, and Gupta, Kapil. Imprinted effusion modeling and dynamic cd calculation in gas turbine combustors. In *Turbo Expo: Power for Land, Sea, and Air*, volume 44687, pages 589–599. American Society of Mechanical Engineers, 2012.

[23] Andrei, Luca, Innocenti, Luca, Andreini, Antonio, Facchini, Bruno, and Winchler, Lorenzo. "Film cooling modeling for gas turbine nozzles and blades: Validation and application." *Journal of Turbomachinery*, 139(1), 2017.

[24] Bizzari, R, Dauptain, A, Gicquel, L, and Nicoud, F. A thickened-hole model for les over multiperforated liners. In *4e Colloque du réseau d'INitiative en Combustion Avancée (INCA)*, page 46, 2017.

[25] Paccati, Simone, Mazzei, Lorenzo, Andreini, Antonio, and Facchini, Bruno. "Reduced-order models for effusion modeling in gas turbine combustors." *Journal of Turbomachinery*, 144(8):081013, 2022.

[26] Andreini, Antonio, Bertini, D, Facchini, B, and Puggelli, S. "Large-eddy simulation of a turbulent spray flame using the flamelet generated manifold approach." *Energy Procedia*, 82:395–401, 2015.

[27] Puggelli, S, Bertini, D, Mazzei, L, and Andreini, A. "Assessment of scale resolved cfd methods for the investigation of lean burn spray flames." *ASME J. Eng. Gas Turbines Power*, 2016.

[28] Puggelli, S, Bertini, D, Mazzei, L, and Andreini, A. "Modeling strategies for large eddy simulation of lean burn spray flames." *Journal of Engineering for Gas Turbines and Power*, 140(5), 2018.

[29] Mazzei, L, Puggelli, S, Bertini, D, Andreini, A, Facchini, B, Vitale, I, and Santoriello, A. "Numerical and experimental investigation on an effusion-cooled lean burn aeronautical combustor: Aerothermal field and emissions." *Journal of Engineering for Gas Turbines and Power*, 141(4), 2019.

[30] Bertini, D, Mazzei, L, Puggelli, S, Andreini, A, Facchini, B, Bellocci, L, and Santoriello, A. Numerical and experimental investigation on an effusion-cooled lean burn aeronautical combustor: aerothermal field and metal temperature. In *Turbo Expo: Power for Land, Sea, and Air*, volume 51104, page V05CT17A010. American Society of Mechanical Engineers, 2018.

[31] Oyarzun, Guillermo, Mira, Daniel, and Houzeaux, Guillaume. "Performance assessment of CUDA and OpenACC in large scale combustion simulations." jul 2021. URL `http://arxiv.org/abs/2107.11541`.

[32] Mira, Daniel, Pérez-Sánchez, Eduardo J., Borrell, Ricard, and Houzeaux, Guillaume. "HPC-enabling technologies for high-fidelity combustion simulations." *Proceedings of the Combustion Institute*, sep 2022. ISSN 1540-7489. doi: 10.1016/J.PROCI.2022.07.222.

[33] Spalart, Philippe R, Deck, Shur, Shur, Michael L, Squires, Kyle D, Strelets, M Kh, and Travin, Andrei. "A new version of detached-eddy simulation, resistant to ambiguous grid densities." *Theoretical and computational fluid dynamics*, 20(3):181–195, 2006.

[34] Spalart, Philippe R. "Detached-eddy simulation." *Annual review of fluid mechanics*, 41(1):181–202, 2009.

[35] Menter, F. Stress-blended eddy simulation (sbes)—a new paradigm in hybrid rans-les modeling. In *Symposium on Hybrid RANS-LES methods*, pages 27–37. Springer, 2016.

[36] He, L and Fadl, M. "Multi-scale time integration for transient conjugate heat transfer." *International Journal for Numerical Methods in Fluids*, 83(12):887–904, 2017.

[37] Fadl, M and He, L. On les based conjugate heat transfer procedure for transient natural convection. In *Turbo Expo: Power for Land, Sea, and Air*, volume 50879, page V05AT10A002. American Society of Mechanical Engineers, 2017.

[38] Berger, Sandrine, Richard, Stéphane, Staffelbach, Gabriel, Duchaine, Florent, and Gicquel, Laurent. Aerothermal prediction of an aeronautical combustion chamber based on the coupling of large eddy simulation, solid conduction and radiation solvers. In *Turbo Expo: Power for Land, Sea, and Air*, volume 56710, page V05AT10A007. American Society of Mechanical Engineers, 2015.

[39] Jaure, S, Duchaine, F, Staffelbach, G, and Gicquel, LYM. "Massively parallel conjugate heat transfer methods relying on large eddy simulation applied to an aeronautical combustor." *Computational Science & Discovery*, 6(1):015008, 2013.

[40] Koren, Chai, Vicquelin, Ronan, and Gicquel, Olivier. "Self-adaptive coupling frequency for unsteady coupled conjugate heat transfer simulations." *International Journal of Thermal Sciences*, 118:340–354, 2017.

[41] Bertini, Davide. *High-fidelity prediction of metal temperature in gas turbine combustors using a loosely coupled multiphysics approach.* PhD thesis, University of Florence, 2019.

[42] ANSYS. *Fluent 19.3 Theory Guide*, 2019.

[43] Rohsenow, Warren M, Hartnett, James P, Cho, Young I, et al. *Handbook of heat transfer*, volume 3. McGraw-Hill New York, 1998.

[44] Kreith, Frank, Manglik, Raj M, and Bohn, Mark S. *Principles of heat transfer.* Cengage learning, 2012.

[45] Cengel, YA. Termodinamica e trasmissione del calore. 1998.

[46] Heiss, John F and Coull, James. "Nomograph of dittus-boelter equation for heating and cooling liquids." *Industrial & Engineering Chemistry*, 43(5):1226–1229, 1951.

[47] Reynolds, HC, Swearingen, TB, and McEligot, DM. "Thermal entry for low reynolds number turbulent flow." 1969.

[48] Taylor, MF, Bauer, KE, and McEligot, DM. "Internal forced convection to low-prandtl-number gas mixtures." *International Journal of Heat and Mass Transfer*, 31(1):13–25, 1988.

[49] Xuan, Yimin and Li, Qiang. "Investigation on convective heat transfer and flow features of nanofluids." *J. Heat transfer*, 125(1): 151–155, 2003.

[50] Williams, Wesley, Buongiorno, Jacopo, and Hu, Lin-Wen. "Experimental investigation of turbulent convective heat transfer and pressure loss of alumina/water and zirconia/water nanoparticle colloids (nanofluids) in horizontal tubes." *Journal of heat transfer*, 130 (4), 2008.

[51] Taler, Dawid and Taler, Jan. Simple heat transfer correlations for turbulent tube flow. In *E3S Web of conferences*, volume 13, page 02008. EDP Sciences, 2017.

[52] Petrucci, Ralph H, Herring, F Geoffrey, and Madura, Jeffry D. *General chemistry: principles and modern applications*. Pearson Prentice Hall, 2010.

[53] Arrhenius, Svante. "Über die dissociationswärme und den einfluss der temperatur auf den dissociationsgrad der elektrolyte." *Zeitschrift für physikalische Chemie*, 4(1):96–116, 1889.

[54] Poinsot, Thierry and Veynante, Denis. *Theoretical and numerical combustion*. RT Edwards, Inc., 2005.

[55] Gülder, Ömer L. Turbulent premixed flame propagation models for different combustion regimes. In *Symposium (International) on Combustion*, volume 23, pages 743–750. Elsevier, 1991.

[56] Peters, Norbert. *Turbulent combustion*. Cambridge university press, 2000.

[57] Andreini, Antonio and Facchini, Bruno. *Sviluppo di Modelli Numerici per l'Analisi della Combustione Turbolenta Premiscelata nelle Turbine a Gas*. Ph. D. thesis, Università degli Studi di Firenze, Dipartimento di Energetica, 2004.

[58] Cintolesi, Carlo. *Large-eddy simulations of conjugate heat transfer with evaporation-condensation and thermal radiation*. PhD thesis, 04 2016.

[59] Modest, Michael F. *Radiative heat transfer*. Academic press, 2013.

[60] Kuznetsov, Anatoly, Melnikova, Irina, Pozdnyakov, Dmitriy, Seroukhova, Olga, and Vasilyev, Alexander. *Radiation in the Earth Atmosphere*, pages 1–18. Springer Berlin Heidelberg, Berlin, Heidelberg, 2012. ISBN 978-3-642-14899-6. doi: 10.1007/978-3-642-14899-6_1. URL `https://doi.org/10.1007/978-3-642-14899-6_1`.

[61] Duchaine, F., Corpron, A., Pons, L., Moureau, V., Nicoud, F., and Poinsot, T. "Development and assessment of a coupled strategy for conjugate heat transfer with large eddy simulation: application to a cooled turbine blade." *International Journal of Heat and Fluid Flow*, 30(6):1129–1141, 2009.

[62] John, Bibin, Senthilkumar, P, and Sadasivan, Sreeja. "Applied and theoretical aspects of conjugate heat transfer analysis: a review." *Archives of Computational Methods in Engineering*, 26(2):475–489, 2019.

[63] Alonso, Juan, Hahn, Seonghyeon, Ham, Frank, Herrmann, Marcus, Iaccarino, Gianluca, Kalitzin, Georgi, LeGresley, Patrick, Mattsson, Ken, Medic, Gorazd, Moin, Parviz, et al. Chimps: A high-performance scalable module for multi-physics simulations. In *42nd AIAA/ASME/SAE/ASEE Joint Propulsion Conference & Exhibit*, page 5274, 2006.

[64] Roe, B, Jaiman, R, Haselbacher, A, and Geubelle, Philippe H. "Combined interface boundary condition method for coupled thermal simulations." *International journal for numerical methods in fluids*, 57(3):329–354, 2008.

[65] Fadl, M, He, L, Stein, P, and Marinescu, G. "Assessment of unsteadiness modeling for transient natural convection." *Journal of Engineering for Gas Turbines and Power*, 140(1), 2018.

[66] Papanicolaou, E, Giebert, D, Koch, R, and Schulz, A. "A conservation-based discretization approach for conjugate heat transfer calculations in hot-gas ducting turbomachinery components." *International Journal of Heat and Mass Transfer*, 44(18):3413–3429, 2001.

[67] Bohn, Dieter, Ren, Jing, and Kusterer, Karsten. "Systematic investigation on conjugate heat transfer rates of film cooling configurations." *International Journal of Rotating Machinery*, 2005, 2005.

[68] Garg, Vijay K. "Heat transfer research on gas turbine airfoils at nasa grc." *International Journal of Heat and Fluid Flow*, 23(2): 109–136, 2002.

[69] Heselhaus, A and Vogel, D. Numerical simulation of turbine blade cooling with respect to blade heat conduction and inlet temperature profiles. In *31st Joint Propulsion Conference and Exhibit*, page 3041, 1995.

[70] Sondak, Douglas L and Dorney, Daniel J. "Simulation of coupled unsteady flow and heat conduction in turbine stage." *Journal of Propulsion and Power*, 16(6):1141–1148, 2000.

[71] He, L and Oldfield, MLG. "Unsteady conjugate heat transfer modeling." *Journal of turbomachinery*, 133(3), 2011.

[72] Gourdain, N, Gicquel, L, Montagnac, M, Vermorel, O, Gazaix, M, Staffelbach, G, Garcia, M, Boussuge, JF, and Poinsot, T. "High

performance parallel computing of flows in complex geometries: I. methods." *Computational Science & Discovery*, 2(1):015003, 2009.

[73] Buis, Samuel, Piacentini, Andrea, and Déclat, Damien. "Palm: a computational framework for assembling high-performance computing applications." *Concurrency and computation: practice and experience*, 18(2):231–245, 2006.

[74] Koren, Chai, Vicquelin, Ronan, and Gicquel, Olivier. "Multiphysics simulation combining large-eddy simulation, wall heat conduction and radiative energy transfer to predict wall temperature induced by a confined premixed swirling flame." *Flow, Turbulence and Combustion*, 101(1):77–102, 2018.

[75] Zhao, Xiaoli, Sun, Zhenxu, Tang, Longsheng, and Zheng, Gangtie. "Coupled flow-thermal-structural analysis of hypersonic aerodynamically heated cylindrical leading edge." *Engineering Applications of Computational Fluid Mechanics*, 5(2):170–179, 2011.

[76] Zhang, Shengtao, Chen, Fang, and Liu, Hong. "Time-adaptive, loosely coupled strategy for conjugate heat transfer problems in hypersonic flows." *Journal of Thermophysics and Heat Transfer*, 28 (4):635–646, 2014.

[77] Bertini, D, Mazzei, L, Andreini, A, and Facchini, B. Multiphysics numerical investigation of an aeronautical lean burn combustor. In *Turbo Expo: Power for Land, Sea, and Air*, volume 58653, page V05BT17A004. American Society of Mechanical Engineers, 2019.

[78] Bertini, Davide, Mazzei, Lorenzo, and Andreini, Antonio. "Prediction of liner metal temperature of an aeroengine combustor with multi-physics scale-resolving cfd." *Entropy*, 23(7):901, 2021.

[79] Paccati, Simone, Bertini, Davide, Mazzei, Lorenzo, Puggelli, Stefano, and Andreini, Antonio. "Large-eddy simulation of a model aero-engine sooting flame with a multiphysics approach." *Flow, Turbulence and Combustion*, 106(4):1329–1354, 2021.

[80] Andreini, A, Bonini, A, Caciolli, G, Facchini, B, and Taddei, S. "Numerical study of aerodynamic losses of effusion cooling holes in aero-engine combustor liners." *Journal of engineering for gas turbines and power*, 133(2), 2011.

[81] Da Soghe, Riccardo, Andreini, Antonio, Facchini, Bruno, and Mazzei, Lorenzo. "Heat transfer enhancement due to coolant extraction on the cold side of effusion cooling plates." *Journal of Engineering for Gas Turbines and Power*, 137(12), 2015.

[82] Paccati, Simone. *Development of advanced numerical tools for the prediction of wall temperature and heat fluxes for aeroengine combustors*. PhD thesis, University of Florence, 2020.

[83] Lienhard, IV and John, H. *A heat transfer textbook*. phlogiston press, 2005.

[84] Armaly, Bassem F, Durst, F, Pereira, JCF, and Schönung, B. "Experimental and theoretical investigation of backward-facing step flow." *Journal of fluid Mechanics*, 127:473–496, 1983.

[85] Lee, T and Mateescu, D. "Experimental and numerical investigation of 2-d backward-facing step flow." *Journal of Fluids and Structures*, 12(6):703–716, 1998.

[86] Barri, Mustafa, El Khoury, George K, Andersson, Helge I, and Pettersen, Bjørnar. "Dns of backward-facing step flow with fully turbulent inflow." *International Journal for Numerical Methods in Fluids*, 64(7):777–792, 2010.

[87] Wang, B., Zhang, H.Q., and Wang, X.L. "Large eddy simulation of particle response to turbulence along its trajectory in a backward-facing step turbulent flow." *International Journal of Heat and Mass Transfer*, 49(1):415–420, 2006. ISSN 0017-9310. doi: https://doi.org/10.1016/j.ijheatmasstransfer.2005.05.042. URL `https://www.sciencedirect.com/science/article/pii/S0017931005004746`.

[88] Spazzini, Pier Giorgio, Iuso, G, Onorato, M, Zurlo, N, and Di Cicca, GM. "Unsteady behavior of back-facing step flow." *Experiments in fluids*, 30(5):551–561, 2001.

[89] Velazquez, A, Arias, JR, and Mendez, B. "Laminar heat transfer enhancement downstream of a backward facing step by using a pulsating flow." *International Journal of Heat and Mass Transfer*, 51(7-8):2075–2089, 2008.

[90] Xu, JH, Zou, S, Inaoka, K, and Xi, GN. "Effect of reynolds number on flow and heat transfer in incompressible forced convection over a 3d backward-facing step." *International Journal of Refrigeration*, 79:164–175, 2017.

[91] Avancha, Ravikanth VR and Pletcher, Richard H. "Large eddy simulation of the turbulent flow past a backward-facing step with heat transfer and property variations." *International Journal of Heat and Fluid Flow*, 23(5):601–614, 2002.

[92] Chen, Lin, Asai, Keisuke, Nonomura, Taku, Xi, Guannan, and Liu, Tianshu. "A review of backward-facing step (bfs) flow mechanisms, heat transfer and control." *Thermal Science and Engineering Progress*, 6:194–216, 2018.

[93] Menter, FLORIANR. Zonal two equation kw turbulence models for aerodynamic flows. In *23rd fluid dynamics, plasmadynamics, and lasers conference*, page 2906, 1993.

[94] Menter, Florian R, Kuntz, Martin, and Langtry, Robin. "Ten years of industrial experience with the sst turbulence model." *Turbulence, heat and mass transfer*, 4(1):625–632, 2003.

[95] Mazzei, Lorenzo, Puggelli, Stefano, Bertini, Davide, Pampaloni, Daniele, and Andreini, Antonio. "Modelling soot production and thermal radiation for turbulent diffusion flames." *Energy Procedia*, 126:826–833, 2017.

[96] Paccati, Simone, Bertini, Davide, Puggelli, Stefano, Mazzei, Lorenzo, Andreini, Antonio, and Facchini, Bruno. "Numerical analyses of a high pressure sooting flame with multiphysics approach." *Energy Procedia*, 148:591–598, 2018.

[97] Moreno, Jose, Casado, Cintia, and Marugan, Javier. "Improved discrete ordinate method for accurate simulation radiation transport using solar and led light sources." *Chemical Engineering Science*, 205:151–164, 2019.

[98] Hermann, J, Greifenstein, M, Boehm, B, and Dreizler, A. "Experimental investigation of global combustion characteristics in an effusion cooled single sector model gas turbine combustor." *Flow, Turbulence and Combustion*, 102(4):1025–1052, 2019.

[99] Greifenstein, M, Hermann, J, Boehm, B, and Dreizler, A. "Flame–cooling air interaction in an effusion-cooled model gas turbine combustor at elevated pressure." *Experiments in Fluids*, 60(1):1–13, 2019.

[100] Al-Abdeli, Yasir M and Masri, Assaad R. "Review of laboratory swirl burners and experiments for model validation." *Experimental Thermal and Fluid Science*, 69:178–196, 2015.

[101] Heeger, C, Gordon, RL, Tummers, MJ, Sattelmayer, T, and Dreizler, A. "Experimental analysis of flashback in lean premixed swirling flames: upstream flame propagation." *Experiments in fluids*, 49(4): 853–863, 2010.

[102] Nassini, Pier Carlo, Pampaloni, Daniele, and Andreini, Antonio. Inclusion of flame stretch and heat loss in les combustion model. In *AIP Conference Proceedings*, volume 2191, page 020119. AIP Publishing LLC, 2019.

[103] Greifenstein, Max and Dreizler, Andreas. "Investigation of mixing processes of effusion cooling air and main flow in a single sector

model gas turbine combustor at elevated pressure." *International Journal of Heat and Fluid Flow*, 88, apr 2021. ISSN 0142727X. doi: 10.1016/j.ijheatfluidflow.2020.108768.

[104] ANSYS. *Fluent 21.1 Theory Guide*, 2021.

[105] Meneveau, Charles and Lund, Thomas S. "The dynamic smagorinsky model and scale-dependent coefficients in the viscous range of turbulence." *Physics of fluids*, 9(12):3932–3934, 1997.

[106] Both, Ambrus, Mira Martínez, Daniel, and Lehmkuhl Barba, Oriol. Assessment of tabulated chemistry models for the les of a model aeroengine combustor. In *Proceedings of Global Power and Propulsion Society, GPPS Chania22, 18th-20th September, 2022*. Global Power and Propulsion Society (GPPS), 2022.

[107] van Oijen, Jeroen. *Flamelet-generated manifolds: development and application to premixed laminar flames*. Technische Universiteit Eindhoven, 2002.

[108] Van Oijen, JA, Donini, A, Bastiaans, RJM, ten Thije Boonkkamp, JHM, and De Goey, LPH. "State-of-the-art in premixed combustion modeling using flamelet generated manifolds." *Progress in Energy and Combustion Science*, 57:30–74, 2016.

[109] Donini, A., Bastiaans, R., van Oijen, J., and de Goey, L. The implementation of five-dimensional fgm combustion model for the simulation of a gas turbine model combustor. In *ASME turbo expo 2015: turbine technical conference and exposition*, page V04AT04A007. American Society of Mechanical Engineers, 2015.

[110] Smith, Gregory P., Golden, David M., Frenklach, Michael, Moriarty, Nigel W., Eiteneer, Boris, Goldenberg, Mikhail, Bowman, C. Thomas, Hanson, Ronald K., Song, Soonho, Gardiner, William C. Jr., Lissianski, Vitali V., and Zhiwei, Qin. Gri3.0 mechanism.

[111] Chanson, Hubert. *Applied hydrodynamics: an introduction to ideal and real fluid flows*. CRC press, 2009.

[112] Goodwin, David G., Speth, Raymond L., Moffat, Harry K., and Weber, Bryan W. Cantera: An object-oriented software toolkit for chemical kinetics, thermodynamics, and transport processes. `https://www.cantera.org`, 2021. Version 2.5.1.

[113] Sosnowski, Marcin, Krzywanski, Jaroslaw, Grabowska, Karolina, and Gnatowska, Renata. Polyhedral meshing in numerical analysis of conjugate heat transfer. In *EPJ Web of Conferences*, volume 180, page 02096. EDP Sciences, 2018.

[114] Celik, IB, Cehreli, ZN, and Yavuz, I. "Index of resolution quality for large eddy simulations." 2005.

[115] Pope, Stephen B. "Ten questions concerning the large-eddy simulation of turbulent flows." *New journal of Physics*, 6(1):35, 2004.

[116] Boudier, G, Gicquel, LYM, and Poinsot, TJ. "Effects of mesh resolution on large eddy simulation of reacting flows in complex geometry combustors." *Combustion and Flame*, 155(1-2):196–214, 2008.

[117] Nassini, Pier Carlo, Pampaloni, Daniele, Meloni, Roberto, and Andreini, Antonio. "Lean blow-out prediction in an industrial gas turbine combustor through a les-based cfd analysis." *Combustion and Flame*, 229:111391, 2021.

[118] Amerini, A, Paccati, S, Mazzei, L, and Andreini, A. Assessment of a conjugate heat transfer method on an effusion cooled combustor operated with a swirl stabilized partially premixed flame. In *Turbo Expo: Power for Land, Sea, and Air*, volume 86038, page V06AT11A001. American Society of Mechanical Engineers, 2022.

[119] Geigle, K. P., Hadef, R., and Meier, W. "Soot formation and flame characterization of an aero-engine model combustor burning

ethylene at elevated pressure." *ASME J Eng Gas Turb Pwr*, 136 (2):021505, 2014.

[120] Geigle, K. P., O'Loughlin, W., Hadef, R., and Meier, W. "Visualization of soot inception in turbulent pressurized flames by simultaneous measurement of laser-induced fluorescence of polycyclic aromatic hydrocarbons and laser-induced incandescence, and correlation to oh distributions." *Applied Physics B*, 119(4):717–730, 2015.

[121] Glassman, Irvin. Soot formation in combustion processes. In *Symposium (international) on combustion*, volume 22, pages 295–311. Elsevier, 1989.

[122] Stöhr, M., Geigle, K. P., Hadef, R., Boxx, I., Carter, C. D., Grader, M., and Gerlinger, P. "Time-resolved study of transient soot formation in an aero-engine model combustor at elevated pressure." *Proceedings of the Combustion Institute*, 37(4):5421–5428, jan 2019. ISSN 1540-7489. doi: 10.1016/J.PROCI.2018.05.122.

[123] Çokuslu, Ömer Hakkı, Hasse, Christian, Geigle, Klaus Peter, and Ferraro, Federica. "Soot prediction in a Model Aero-Engine Combustor using a Quadrature-based method of moments." *AIAA Science and Technology Forum and Exposition, AIAA SciTech Forum 2022*, 2022. doi: 10.2514/6.2022-1446. URL `https://arc.aiaa.org/doi/10.2514/6.2022-1446`.

[124] Franzelli, B., Riber, E., Cuenot, B., and Ihme, M. Numerical modeling of soot production in aero-engine combustors using large eddy simulations. In *ASME Turbo Expo 2015: Turbine Technical Conference and Exposition*, number GT2015-43630, page V04BT04A049. American Society of Mechanical Engineers, 2015.

[125] Wick, Achim, Priesack, Frederic, and Pitsch, Heinz. Large-eddy simulation and detailed modeling of soot evolution in a model

aero engine combustor. In *ASME Turbo Expo 2017: Turbomachinery Technical Conference and Exposition*, pages V04AT04A020–V04AT04A020. American Society of Mechanical Engineers, 2017.

[126] Chong, Shao Teng, Hassanaly, Malik, Koo, Heeseok, Mueller, Michael E, Raman, Venkat, and Geigle, Klaus-Peter. "Large eddy simulation of pressure and dilution-jet effects on soot formation in a model aircraft swirl combustor." *Combustion and Flame*, 192:452–472, 2018.

[127] Eberle, C., Gerlinger, P., Geigle, K. P., and Aigner, M. "Numerical investigation of transient soot evolution processes in an aero-engine model combustor." *Combustion Science and Technology*, 187(12): 1841–1866, 2015.

[128] Eberle, Christian, Gerlinger, Peter, Geigle, Klaus Peter, and Aigner, Manfred. "Toward finite-rate chemistry large-eddy simulations of sooting swirl flames." *Combustion Science and Technology*, 190(7):1194–1217, 2018.

[129] Grader, Martin, Eberle, Christian, Gerlinger, Peter, and Aigner, Manfred. Les of a pressurized, sooting aero-engine model combustor at different equivalence ratios with a sectional approach for pahs and soot. In *ASME Turbo Expo 2018: Turbomachinery Technical Conference and Exposition*, pages V04AT04A012–V04AT04A012. American Society of Mechanical Engineers, 2018.

[130] García-Oliver, José M, Pastor Enguídanos, José Manuel, Olmeda-Ramiro, Iván, Both, A, and Mira, D. "Combustion modeling in a pressurized gas turbine burner using large-eddy simulations." *Proceedings 12CNIT 2022*, pages 690–699, 2022.

[131] Koo, Heeseok, Raman, Venkatramanan, Mueller, Michael E, and Geigle, Klaus-Peter. Les of a sooting flame in a pressurized swirl combustor. In *54th AIAA Aerospace Sciences Meeting*, page 2123, 2016.

[132] Rodrigues, Pedro. *Modélisation multiphysique de flammes turbulentes suitées avec la prise en compte des transferts radiatifs et des transferts de chaleur pariétaux.* PhD thesis, 06 2018.

[133] Paccati, S, Bertini, D, Puggelli, S, Mazzei, L, and Andreini, A. "Soot prediction in a model aero engine combustor with multiphysics approach."

[134] Geigle, Klaus Peter, Köhler, Markus, O'Loughlin, William, and Meier, Wolfgang. "Investigation of soot formation in pressurized swirl flames by laser measurements of temperature, flame structures and soot concentrations." *Proceedings of the Combustion Institute*, 35(3):3373–3380, 2015.

[135] Rodrigues, P, Gicquel, O, Darabiha, N, Geigle, KP, and Vicquelin, R. Assessment of external heat transfer modeling of a laboratory-scale combustor inside a pressure-housing environment. In *ASME Turbo Expo 2018: Turbomachinery Technical Conference and Exposition*, pages V05CT17A008–V05CT17A008. American Society of Mechanical Engineers, 2018.

[136] Wang, H. and Laskin, A. "A comprehensive kinetic model of ethylene and acetylene oxidation at high temperatures." *Progress Report for an AFOSR New World Vista Program*, 1998.

[137] Glassman, Irvin, Yetter, Richard A, and Glumac, Nick G. *Combustion.* Academic press, 2014.

[138] Lighty, Jo Ann Slama, Veranth, John M., and Sarofim, Adel F. "Combustion aerosols: Factors governing their size and composition and implications to human health." *Journal of the Air and Waste Management Association*, 50(9):1565–1618, 2000. ISSN 10473289. doi: 10.1080/10473289.2000.10464197.

[139] Ferraro, Federica, Gierth, Sandro, Salenbauch, Steffen, Han, Wang, and Hasse, Christian. "Soot particle size distribution recon-

struction in a turbulent sooting flame with the split-based extended quadrature method of moments." *Physics of Fluids*, 34 (7):075121, jul 2022. ISSN 1070-6631. doi: 10.1063/5.0098382. URL `https://aip.scitation.org/doi/abs/10.1063/5.0098382`.

[140] Nau, Patrick, Yin, Zhiyao, Geigle, Klaus Peter, and Meier, Wolfgang. "Wall temperature measurements at elevated pressures and high temperatures in sooting flames in a gas turbine model combustor." *Applied Physics B*, 123(12):279, 2017.